

Proposal for a  
**Solar, Anomalous, and Magnetospheric  
Particle Explorer  
(SAMPEX)**

Submitted to NASA in  
response to A.O. No. OSSA 2-88  
for the  
Small-Class Explorer Mission

**1. Investigation and Technical Plan**

University of Maryland  
Aerospace Corporation  
California Institute of Technology  
Goddard Space Flight Center  
Langley Research Center  
Max-Planck-Institut für extraterrestrische Physik

September 1988

Proposal for a  
**Solar, Anomalous, and Magnetospheric  
Particle Explorer  
(SAMPEX)**

Submitted to NASA in  
response to A.O. No. OSSA 2-88  
for the  
Small-Class Explorer Mission

**1. Investigation and Technical Plan**

**University of Maryland  
Aerospace Corporation  
California Institute of Technology  
Goddard Space Flight Center  
Langley Research Center  
Max-Planck-Institut für extraterrestrische Physik**

September 1988

**Solar, Anomalous, and Magnetospheric Particle Explorer  
(SAMPEX)**

**Principal Investigator**

G. M. Mason  
Department of Physics & Astronomy and I.P.S.T  
University of Maryland  
College Park, MD 20742  
(301) 454-2616

**Co-Investigators**

D. N. Baker  
Laboratory for Extraterrestrial Physics  
Code 690  
Goddard Space Flight Center  
Greenbelt, MD 20771  
(301) 386-8112

J. B. Blake  
Aerospace Corporation M2/259  
P.O. Box 92957  
Los Angeles, CA 90009  
(415) 336-7078

L. B. Callis  
Langley Research Center  
MS 401B  
Hampton, VA 23665-5225  
(804) 865-2985

D. C. Hamilton  
Department of Physics & Astronomy and I.P.S.T  
University of Maryland  
College Park, MD 20742  
(301) 454-7305

D. Hovestadt  
Max-Planck-Institut für extraterrestrische  
Physik  
D-8046 Garching, FRG  
49-89-3299817

B. Klecker  
Max-Planck-Institut für extraterrestrische  
Physik  
D-8046 Garching, FRG  
49-89-3299872

R. A. Mewaldt  
220-47 Downs Laboratory  
California Institute of Technology  
Pasadena, CA 91125  
(818) 356-6612

M. Scholer  
Max-Planck-Institut für extraterrestrische  
Physik  
D-8046 Garching, FRG  
49-89-3299821

E. C. Stone  
220-47 Downs Laboratory  
California Institute of Technology  
Pasadena, CA 91125  
(818) 356-4241

T. T. von Rosenvinge  
Laboratory for High Energy Astrophysics  
Code 661  
Goddard Space Flight Center  
Greenbelt, MD 20771  
(301) 286-6721

## Table of Contents

	Page
Abstract .....	i
Experiment Summary .....	ii
1. Introduction and Scientific Objectives .....	1
2. Scientific Rationale .....	2
A. Livetime and Charge State Determination .....	2
B. Solar Energetic Particles .....	4
C. Anomalous Cosmic Rays .....	9
D. Precipitating Relativistic Magnetospheric Electrons .....	12
E. Isotopic Composition of Galactic Cosmic Rays .....	15
3. Approach .....	16
4. Instrumentation/Technique/Status .....	17
A. MAST/PET - Mass Spectrometer Telescope/Proton Electron Telescope .....	17
B. LEICA - Low Energy Ion Composition Analyzer .....	20
C. HILT - Heavy Ion Large Telescope .....	23
D. DPU -Data Processing Unit .....	24
5. Instrument Integration .....	25
6. Ground and Flight Operations .....	25
7. Data Reduction and Analysis Plan .....	26

### Appendices

A. References .....	27
B. Collecting Power/Comparison to Planned Experiments .....	31
C. Instrumental Techniques and Performance .....	36
D. HILT Micrometeoroid Protection .....	48
E. Spacecraft Accomodations/Requirements .....	50
F. Spacecraft Orbital Lifetime, Inclination, and Radiation Dose Analysis .....	55
G. Biographical Information .....	66

### Abstract

We propose a Solar, Anomalous, and Magnetospheric Particle Explorer (SAMPEX) for the Small-Class Explorer mission (A.O. No. 2-88). SAMPEX would measure energetic particles for all elements from H to Ni ( $Z = 28$ ) over the energy range from  $\sim 0.4$  to several hundred MeV/nucleon, as well as electrons from 1 to 120 MeV with instruments of excellent charge and mass resolution and collecting power greatly exceeding previous instruments. By flying SAMPEX in a low altitude near-polar orbit, key information about the ionization state of solar energetic particles and anomalous cosmic rays, as well as local-time dependence of the precipitating magnetospheric particle fluxes can be obtained. The measurements made by SAMPEX would address a broad range of scientific objectives in such widely different areas as

- **Solar Studies:** the elemental and isotopic composition of the Sun; the temperatures of energetic particle acceleration sites in the corona; the mechanisms of solar energetic particle acceleration
- **Anomalous Component:** the ionization state and acceleration mechanism for the Anomalous Cosmic Ray Component; the elemental and isotopic composition of the Local Interstellar Medium
- **Magnetospheric/Middle Atmosphere:** physical mechanisms responsible for precipitating relativistic electron events; the effects of these particles on middle atmosphere production of  $NO_x$  and  $HO_x$  compounds which are important in the ozone depletion process
- **Galactic Cosmic Rays:** isotopic anomalies in the galactic cosmic ray sources, and the implications for galactic evolutionary processes and the origin of the solar system.

The instrument to carry out these measurements, SAMPEX, consists of a complementary set of four high resolution, high sensitivity particle detectors: the Low Energy Ion Composition Analyzer (LEICA), the Heavy Ion Large Telescope (HILT), the Mass Spectrometer Telescope (MAST), and the Proton/Electron Telescope (PET). These instruments are in an advanced state of development and can be readied for SAMPEX quickly and at moderate cost. LEICA and HILT have been constructed for flight on a Space Shuttle Get-Away-Special in 1988/1989. MAST and PET were originally approved and under construction for the (cancelled) U.S. spacecraft of the International Solar Polar Mission. We propose to modify LEICA and HILT, and to complete MAST and PET for the SAMPEX mission. We propose mounting these instruments on a NASA-supplied spacecraft such as the one described in Appendix A of the A.O. and launching them into a near-polar or polar orbit on a zenith-pointing, spinning spacecraft. Because of the advanced state of development of the SAMPEX payload, and modest spacecraft requirements, it is possible to launch by October 1, 1991 with a  $\geq 3$  year lifetime, thus giving coverage of part of the upcoming solar maximum and the declining phase of the solar activity cycle.

**Solar, Anomalous, and Magnetospheric Particle Explorer  
(SAMPEX)**

**Experiment Summary**

SAMPEX consists of a complementary set of four high resolution, high sensitivity particle detectors: the Low Energy Ion Composition Analyzer (LEICA), the Heavy Ion Large Telescope (HILT), the Mass Spectrometer Telescope (MAST), and the Proton/Electron Telescope (PET). Together they provide coverage of the elemental and isotopic composition from H to Ni ( $1 \leq Z \leq 28$ ) over a broad energy range, as well as measuring energetic electrons. They would be flown on a NASA-supplied "Small-Class Explorer" spacecraft.

**Instrument Performance and Resources**

	LEICA	HILT	MAST	PET
Energy range for electrons	—	—	—	1-120 MeV
H	0.75-8	—	7-15	18-350 MeV
He	0.4-8	3.9-90	7-91	18-500 MeV/nuc
C	0.35-12	7.2-160	12-210	
Si	0.26-18	9.6-177	19-345	54-195 MeV/nuc
Fe	0.16-25	11.0-90	24-470	
Charge range for elements	1-28	2-28	1-28	1-28
Charge range for isotopes	2-16	2	1-28	1-2
Geometry factor (cm <sup>2</sup> sr)	1.0	35-50	7-16	0.3-1.6
Field of View	24° × 20°	90° × 90°	101° cone	58° cone
Weight (kg)	7.7	24	7.1	(incl. with MAST)
Power (W)	5.4	7	4.3	(incl. with MAST)
Telemetry (kbps)	2	2	2	(incl. with MAST)

Total experiment weight: 38.8 kg (instruments above) + 10.0 kg isobutane and tanks

+ 5.7 kg mounting structure = 54.5 kg

Total experiment power: 16.7 W

Total bitrate: 6 kbps

**Mission Description**

Spacecraft: NASA-supplied

Orbit: Inclination ~82°- 90°

Launch Date: late 1991/early 1992

Attitude: spinning S/C, zenith-nadir pointing

Altitude: ≥580 km

Mission Duration: ≥3 years

## 1. INTRODUCTION AND SCIENTIFIC OBJECTIVES

The experiment proposed here, SAMPEX, will carry out energetic particle studies of outstanding scientific questions in the fields of space plasma physics, solar physics, heliospheric physics, cosmic ray physics, and middle atmospheric physics. We propose to measure the electron and ion composition of energetic particle populations from  $\sim 0.4$  MeV/nucleon to hundreds of MeV/nucleon from a zenith-pointing small satellite in near-polar orbit, using a coordinated set of detectors of excellent charge and mass resolution, and with higher sensitivity than previously flown instruments. While over the magnetic poles, the instrument will detect solar energetic particles, interplanetary particles, and galactic cosmic rays. At lower magnetic latitudes, geomagnetic cutoff effects will allow studies of the ionization state of these particles at energies much higher than can be studied from interplanetary spacecraft. At lower latitudes, we will also observe precipitating magnetospheric electrons, which then undergo important interactions with the middle atmosphere.

This broad range of studies can only be carried out on a low altitude near-polar orbiting spacecraft such as could be flown under the Small-Class Explorer Program. The advanced state of development of the proposed instruments means that the investigation could be quickly implemented for a late 1991 launch. This will allow important solar studies to be carried out near the peak of the solar activity maximum and continuing into the declining phase of the activity cycle. Such a time interval is not only ideal for the objectives discussed here but also would provide coverage of energetic particle fluxes in the period preceding the launch of the WIND spacecraft, as shown in Figure 1-1. SAMPEX would thus provide key particle data to complement the measurements of SMM, Solar-A, GOES and GRO during the solar maximum, as well as provide baseline coverage for Ulysses, Galileo, and the Pioneer and Voyager spacecraft. SAMPEX would also provide overlapping coverage for a number of regular and long duration balloon flights planned as part of the Max '91 program. SAMPEX precipitating particle measurements would be compared with observations on geostationary satellites and CRRES, and also with ozone measurements from UARS.

### *Solar Energetic Particles*

By observing large and small solar flare particle events with unprecedented precision during the upcoming solar maximum and beyond, SAMPEX will

- Provide significantly improved determinations of the solar elemental and isotopic composition based on *direct* sampling of solar material
- Probe the acceleration mechanisms in impulsive  $^3\text{He}$ -rich flares by improved composition and charge-state measurements
- Separate the Q/M dependence of the coronal shock acceleration process by measuring heavy ion spectra over an extremely broad energy range
- Determine the average charge-state of energetic solar particles, thereby characterizing the temperature of the acceleration site.

### *Anomalous Cosmic Rays*

By measuring the elemental and isotopic composition of anomalous cosmic rays in a polar orbit as a function of kinetic energy and geomagnetic-cutoff rigidity, SAMPEX will

- Determine the charge-state Q of anomalous cosmic rays and thereby verify if they are indeed singly charged and thus represent a sample of the neutral interstellar medium
- Search for evidence of galactic evolution effects on the isotopic composition of local galactic material accelerated in the heliosphere.

### *Magnetospheric Precipitating Electrons/Middle Atmosphere*

SAMPEX will measure electrons and protons from MeV energies upwards, scanning all local times and cutoffs, thus allowing

- Characterization of precipitating electrons during periods of declining solar activity
- Examination of whether middle atmospheric production of odd nitrogen and odd hydrogen molecules

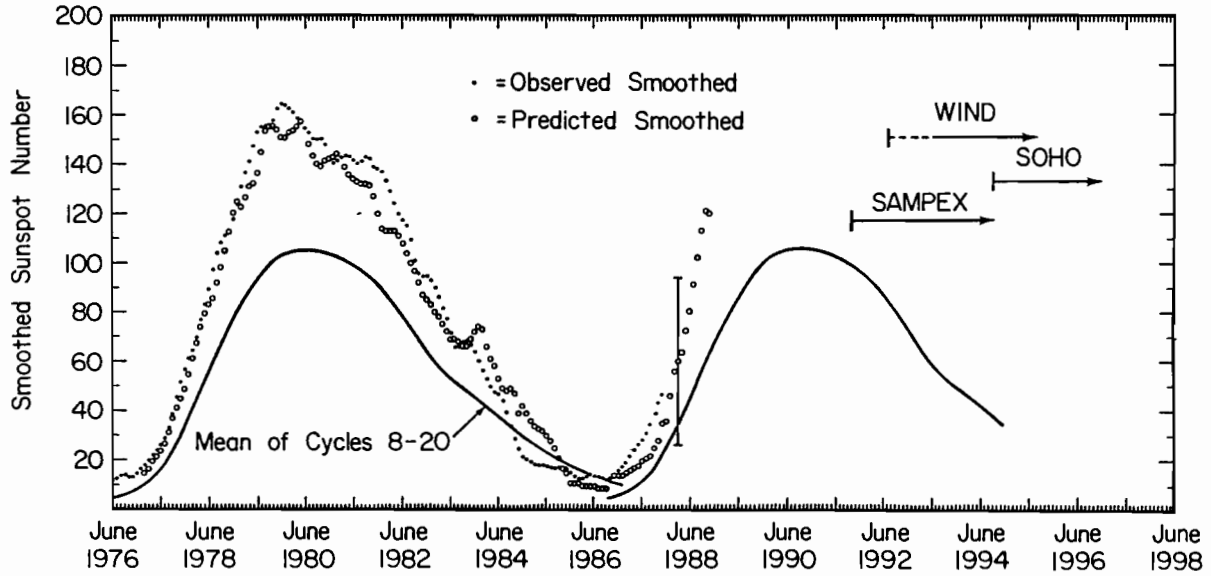


**Fig. 1-1** Smoothed sunspot numbers for the last solar cycle (from *Solar Geophysical Data*), along with the predicted future sunspot count. Time lines show nominal mission operation times of SAMPEX, WIND and SOHO.

by the precipitating electrons is at a sufficient rate to affect O<sub>3</sub> depletion.

#### *Galactic Cosmic Ray Isotopic Composition*

By providing improved measurements of galactic cosmic ray isotopes extending from H to Ni, SAMPEX will

- extend the search for isotopic differences between galactic and solar cosmic material to several additional key elements
- Determine the dominant nucleosynthesis processes contributing to cosmic ray source material.

## **2. SCIENTIFIC RATIONALE**

### **2.A Livetime and Charge State Determination**

The ability of charged particles to penetrate to a low altitude spacecraft is limited by the magnetic field of the earth. Particles with low rigidity (momentum per unit charge) are preferentially turned back by the field. At each point in the magnetosphere and for each arrival direction there exists a threshold value of magnetic rigidity, called the cutoff rigidity. Particles with rigidities below this cutoff value do not have access to the specified point from the specified direction. The cutoff depends on both the zenith and azimuth angles of arrival. In the vertical direction the cutoff rigidity has a value of 13 to 18 GV at the magnetic equator and is theoretically zero at the magnetic poles.

The geomagnetic transmission function gives the probability that a particle with rigidity  $R$  can reach the spacecraft. It is obtained by averaging the geomagnetic cutoff around the spacecraft orbit and thus will depend strongly on the inclination of the orbit. The transmission function can also be interpreted as an effective livetime of an experiment in a low altitude earth orbit.

In Figure 2-1 the relative livetime is calculated as a function of rigidity for two orbital inclinations, 75° and 90°, respectively. The calculation is based on the world wide grid of vertical cutoff rigidities computed by Shea and Smart (1983) for the epoch 1980. Figure 2-1 demonstrates that even in the very low rigidity range (100 MV) a relative livetime of 20 percent can be obtained in a high inclination (90°) orbit.



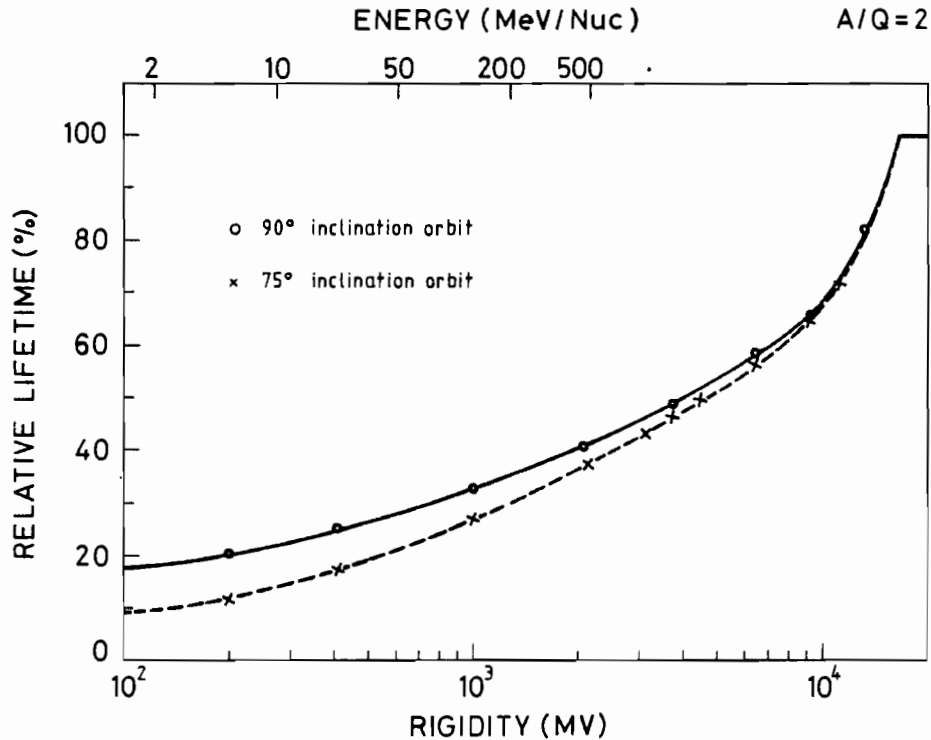


**Fig. 2-1** Relative livetime as a function of particle rigidity for two inclinations of the orbit (75° and 90°).

The energy scale at the top of Figure 2-1 is given for  $A/Q=2$  particles. For singly charged anomalous cosmic rays in the 5-50 MeV/nuc range ( $R = 1500-4900$  MV for  $O^+$ ,  $A/Q=16$ ), a duty cycle of 30-50 percent is possible.

The geomagnetic cutoff can be used to infer the ionic charge of heavy ions. For a specified point and specified direction the minimum rigidity for a particle to have access to this point is defined by  $R_{cutoff}$ . The rigidity depends on particle energy ( $E$ ), mass ( $A$ ) and ionic charge ( $Q$ ) as

$$R = 43.2 \cdot \sqrt{E/A} \cdot (A/Q) \quad (\text{for nonrelativistic particles}).$$

For a given value of  $R_{cutoff}$ , a measured particle spectrum will have a corresponding cutoff below some energy that depends on the charge state  $Q$ . If the species is primarily of one charge state, this break in the spectrum should be quite obvious. If several charge states are represented, the spectral cutoff will become smeared. The technique is thus most appropriate for distinguishing between significantly different values of  $Q$ . Many important issues involving the anomalous cosmic ray component and solar energetic particles can be resolved with this degree of charge resolution, as discussed below.

When a single charge state is involved, its value  $Q$  may be determined from the spectral cutoff energy and the geomagnetic cutoff.

$$Q = 43.2 \cdot \sqrt{(E/A)_{cutoff} \cdot A/R_{cutoff}}$$

$R_{cutoff}$  varies with position in the orbit so an application of this method requires that  $R_{cutoff}$  be known accurately as a function of time as the particles are detected. For the determination of  $R_{cutoff}$  basically two methods can be used:

**Table 2-1** Ionic Charge Determination Using the Geomagnetic Cutoff

Ion/technique:	Method 2 180 MV	Both Methods 400 MV	Method 1 2000 MV
Energy (MeV/nucleon)			
He <sup>+</sup>	1.1	5.4	130
He <sup>++</sup>	4.3	21	440
O <sup>+</sup>	0.07	0.3	8.4
O <sup>7+</sup>	3.3	16.4	350
Fe <sup>+</sup>	0.006	0.027	0.7
Fe <sup>14+</sup>	1.1	5.4	130
Fe <sup>20+</sup>	2.2	10.9	250

Method 1 – Computation of the local cutoff rigidity using a model of the Earth’s magnetic field and particle tracing techniques.

The accuracy of this method depends primarily on the accuracy of the model field, i.e., in particular on any disturbances of the actual field. In the rigidity range above a few GV, typical values of cutoff variations due to field disturbances are 0.1–0.3 GV, i.e., less than 10% (Flückiger *et al.* 1986). At lower rigidities (< 500 MV) field disturbances and any external sources not included in the standard field models could result in uncertainties of about 100 MV (e.g., Shea *et al.* 1976), i.e., about 20% in cutoff rigidity. At lower rigidities and high invariant latitude ( $\Lambda > 65^\circ$ ) the cutoff rigidity shows large diurnal variations and is significantly modified by time variable external sources (e.g., tail and magnetopause current, Smart *et al.* 1969). In this rigidity range the trajectory tracing technique using a model field is subject to large uncertainties and Method 2 is more accurate.

Method 2 – Determination of the cutoff rigidity using proton measurements.

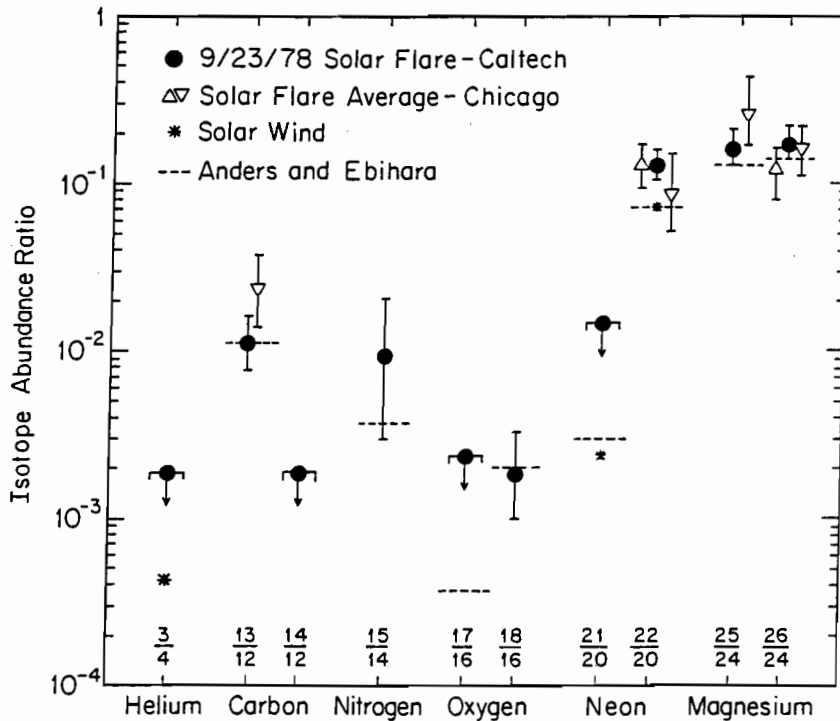
For low rigidities (< 400 MV) and high geomagnetic latitudes, where the trajectory tracing technique in a model field is subject to large uncertainties, the local cutoff can be derived directly by observing the cutoff in the proton spectrum since Q is known in this case. The Proton/Electron Telescope (PET) included in SAMPEX will provide proton measurements in the energy range of 18–120 MeV, corresponding to rigidities of 180–470 MV. Thus, PET completely covers the rigidity range appropriate to Method 2. This method is in particular applicable in large and medium intensity solar particle events, when the proton counting rate is of the order of a few hundred counts per second, i.e. the counting statistics are sufficient to determine the spectrum cutoff, and thus  $R_{cutoff}$ , in a short time interval.

Table 2-1 shows the energy of typical low and high ionic charge states of heavy ions, corresponding to the rigidity of 180, 400, and 2000 MV illustrating the energy ranges where either Method 1 or 2 will be applicable. Table 2-1 demonstrates that for most of the energy range of the proposed instrumentation it will be possible to determine the cutoff rigidity by either by Method 1 or 2.

## 2.B Solar Energetic Particles

### 2.B.1 Elemental and Isotopic Composition

Solar flares frequently inject large fluxes of energetic heavy nuclei into the interplanetary medium. Measurements of the composition of these particles provide a direct measure of the present solar elemental and isotopic makeup, providing crucial information for understanding the history of solar system material and adding new dimensions to the study of solar flare acceleration and propagation processes. In addition, such observations are particularly useful for interpreting the contribution of solar particle radiations to other solar system reservoirs, including planetary magnetospheres, the interplanetary medium, the lunar soil, and meteorites.



**Fig. 2-2** Comparison of the presently available measurements of the isotopic composition of solar flare nuclei [from a summary in Mewaldt and Stone 1989] with solar wind measurements (Geiss *et al.* 1972), and the Anders and Ebihara (1982) tabulation of "solar system" abundances.

Although the Sun contains >99% of solar system material, we have only limited direct knowledge of its elemental composition, and almost no *direct* knowledge of its isotopic composition. Spectroscopic measurements of solar isotopes are very difficult; there are isotope observations for only a few elements, and the uncertainties are large. Almost all of the *isotopic* abundances in the Cameron (1982) table of "solar system" abundances are based on measurements of terrestrial material, while meteoritic measurements are the standard source for solar system *elemental* abundances.

Solar energetic particles (SEP) represent a sample of solar material that can be used to make *direct* measurements of the Sun's isotopic makeup. Figure 2-2 summarizes the status of such measurements, and compares them with the few available measurements of the solar wind isotopic composition and with the Anders and Ebihara (1982) compilation of so-called "solar-system" abundances. The MAST and LEICA sensors on SAMPEX can make major advances in our knowledge of the Sun's isotopic composition. To illustrate the expected results that SAMPEX can achieve, we show in Figure 2-3 what the expected number of analyzed events per isotope would have been for the proposed MAST sensor during a large solar event in 1977 studied extensively by Voyager. For the first 7 large flares observed by Voyager in the first year after launch, the expected total number of  $Z > 2$  events that MAST would be expected to have seen is >10 times that in Figure 2-3, while at somewhat lower energies the proposed LEICA sensor would be expected to observe >100 times the yield shown for isotopes with  $Z \leq 16$  (e.g., see Figure C-6 in Appendix C). We describe below a few of the many problems that solar flare isotope measurements with SAMPEX can address.

Of the few elements studied to date, Ne is of particular interest because of the variety of Ne isotopic compositions that have been observed in the solar system, including solar wind, lunar, meteoritic, and planetary material. The SEP observations give a  $^{22}\text{Ne}/^{20}\text{Ne}$  ratio of  $\approx 0.12$ , significantly different from that measured in the solar wind ( $^{22}\text{Ne}/^{20}\text{Ne} = 0.073$ ). There is also evidence for such a difference from SEP and solar wind nuclei implanted in lunar and meteoritic samples (see, e.g., Black 1983; and Wieler, Baur,

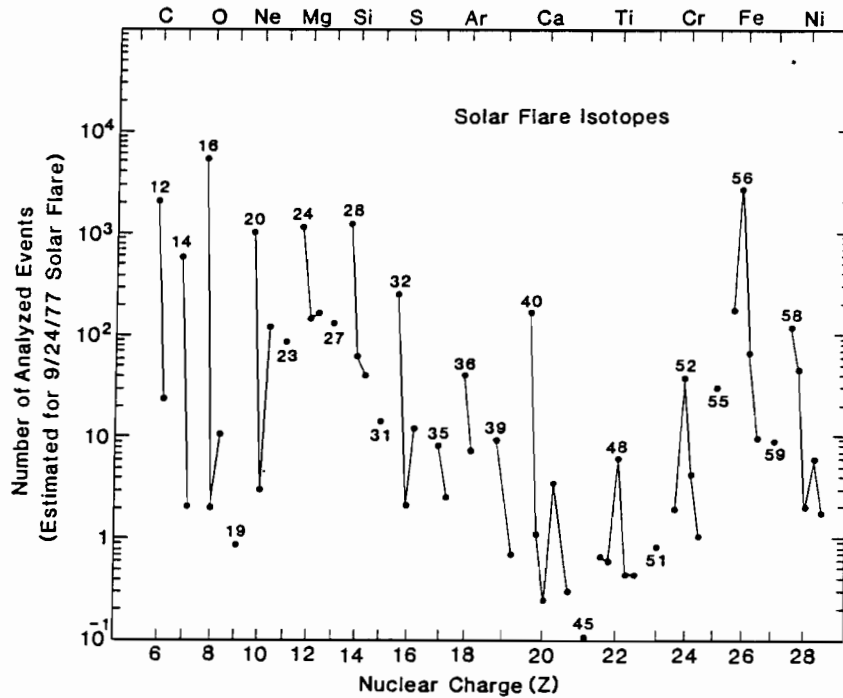


**Fig. 2-3** Estimated yield of solar flare isotope events that would have been observed by MAST during the 9/24/77 solar flare. The isotopes of each element are connected by a solid line with the mass of the dominant isotope labeled. This particular flare was relatively rich in heavy nuclei such as Fe; typical large flares would yield fewer Fe nuclei, but substantially more light nuclei such as C, N, and O.

and Signer 1986). Thus the composition of solar neon is a subject of controversy, with the Cameron and the Anders and Ebihara tables differing by a factor of  $\sim 1.7$  in their adopted standards. Fractionation effects occurring during the solar flare acceleration and/or propagation process have been corrected for in Figure 2-2, but measurements in additional flares are needed to confirm the SEP result. A remaining possibility to explain the SW-SEP difference is fractionation during solar wind acceleration. Measurements of  $^{38}\text{Ar}/^{36}\text{Ar}$ , where lunar and meteoritic data also suggest a SW-SEP difference of  $\sim 30\%$  (Black 1983), would provide additional insight into the relationship between the SEP and SW compositions.

Observations of N isotopes implanted in lunar soil seem to imply that the solar wind  $^{15}\text{N}/^{14}\text{N}$  ratio has increased by  $\sim 30\%$  over the life of the Moon (see, e.g., Geiss and Bochsler 1982). Suggested explanations for this surprising variation include: (1) continuing high-energy nuclear reactions on the Sun; (2) accretion of interstellar material, altering the solar composition; and (3) mixture of two separate components of solar system N with differing  $^{15}\text{N}/^{14}\text{N}$  ratios. For either (1) or (2) [and possibly (3)], effects on other isotope ratios would be expected. Indeed, there is also evidence for secular changes in  $^3\text{He}/^4\text{He}$  (Geiss 1973) and possibly  $^{13}\text{C}/^{12}\text{C}$  (Becker 1980), and evidence for radioactive  $^{14}\text{C}$  in the solar wind (Begemann *et al.* 1972). A measure of the SEP C and N isotopic composition would directly test the above models and provide a *current* benchmark for determining if the composition of the Sun is indeed evolving with time.

It is almost a decade since the first high-resolution measurements of heavy solar flare isotopes were provided by the Caltech instrument on *ISEE 3*. Since that time little progress has been made because no instruments with improved collecting power have been launched, and this field has therefore remained relatively unexplored. As Appendix B indicates, SAMPEX can improve on the collecting power of past and planned instruments by 1 to 2 orders of magnitude.

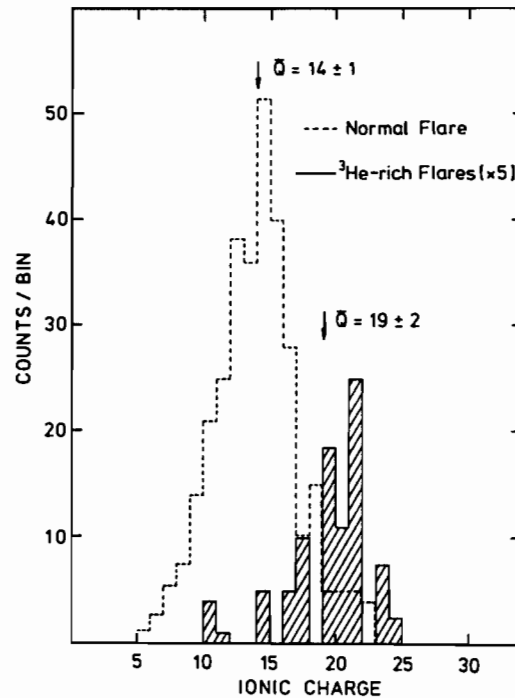


**Fig. 2-4** Charge distribution of iron in the energy range 0.3 to 1.0 MeV per nucleon obtained for  $^3\text{He}$ - and Fe-rich solar particle events (cross-hatched histogram) and for one event without compositional anomalies (1978 September 25-27), dashed line (Klecker *et al.* 1984).

### 2.B.2 Charge State Measurements

Solar energetic particles (SEP) provide a sample of ions from the source region deep in the solar atmosphere. Since the charge state distribution of SEPs is determined by the plasma conditions at the acceleration site, a detailed measurement of the charge state distribution of individual ionic species can be used as a diagnostic tool. In particular, the electron temperature at the acceleration site can be derived, in principle, from the charge state distribution. Recent measurements on *ISEE 3* provided mean charge states for several elements during individual flare events at energies  $<3$  MeV/nucleon. It has been found that during individual flares temperatures as derived from mean charge states are not compatible with a single equilibrium temperature of the source region (Luhn *et al.* 1984). With the large collecting power of the proposed instrumentation and using the geomagnetic cutoff method, SAMPEX will be able to extend the SEP ionic charge measurements to a higher energy range not previously accessible.

In recent years small scale solar energetic particle events with anomalies in the elemental, isotopic, and charge composition have been under intense investigation. A special class of events rich in  $^3\text{He}$  has been discovered and subsequently  $^3\text{He}/^4\text{He}$  ratios ranging from a few percent to greater than unity have been observed (e.g., Serlemitsos and Balasubramanyan 1975). These large  $^3\text{He}/^4\text{He}$  ratios imply an enrichment of  $10^3$ - $10^4$  over typical solar and solar wind values. Thus, such events represent one of the most extreme fractionation processes known to occur at astrophysical sites and may give important clues on conditions in the solar corona and on the mechanisms of particle acceleration in solar flares. These events are usually correlated with enhancements of heavy ions ( $\text{Fe}/\text{O} > 1$ , e.g., Gloeckler *et al.* 1975; Mason *et al.* 1986). In order to explain these anomalies of the elemental and isotopic composition a number of models have been developed (e.g., Fisk 1978). It is now generally thought that the enrichment process proceeds in two steps. The first step involves heating of the particles via plasma instabilities. In the second step the particles above a certain threshold in velocity or rigidity are further accelerated. As both steps in this process depend strongly on the ionic charge of the ions, the determination of ionic charge states is of vital importance for

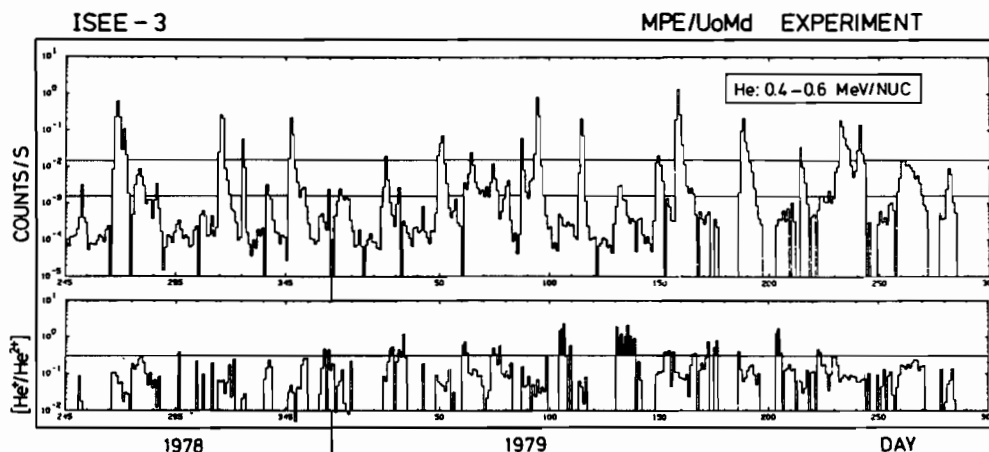


**Fig. 2-5** Daily averages of the interplanetary helium flux (upper panel) between 0.4 and 0.62 MeV per nucleon and of the  $He^+/He^{++}$  ratios (lower panel) from 1978 September 2 to 1979 October 27. Periods with  $He^+/He^{++} > 0.3$  are darkened. Data gaps are due to low He count rates ( $< 20$  counts per day) (Hovestadt *et al.* 1984).

the understanding of these events.

Previously, only two experiments (on *ISEE 1* and *ISEE 3*) have had the capability to determine energetic ion charge states, and they operated for only a relatively short period of time ( $< 1$  year). Due to the limited sensitivity and energy range of these experiments, SEP charge state measurements in the low intensity  $^3He$ -rich events have been made only in a small energy range near 1 MeV/nucleon and only for a few elements (He, Si, Fe) (Klecker *et al.* 1984; Luhn *et al.* 1985). These limited measurements have already revealed significant differences between the charge states of Si and Fe in  $^3He$ -rich events and those in events with normal composition (Fig. 2-4). Note that these differences are rather large ( $\sim 40\%$  for Fe) and thus can be measured using the geomagnetic cutoff technique discussed in §2.A. The high charge states of Si and Fe found in these events indicate that these ions may originate in rather hot ( $> 10^7$  K), localized regions at the sun. Furthermore, the high charge states seem to be incompatible with the selective resonant heating mechanism (Fisk 1978) and the non-resonant turbulent heating (Kocharov and Kocharov 1981), which were proposed to explain the enrichment of  $^3He$  and heavy ions. With the large collecting power of the SAMPEX sensors it will be possible to extend this investigation to more elements and to higher energies. The result should be new input for further theoretical investigation of these events.

Another unexpected finding in the initial SEP charge state studies was the large abundance of  $He^+$  frequently observed in low intensity solar particle events (Fig. 2-5). With ionization temperatures of  $2-4 \times 10^6$  K as derived from heavy ion mean charge states, a  $He^+/He^{++}$  ratio  $< 10^{-4}$  was expected. However, the first measurements in the energy range from 0.4-1.0 MeV/nuc showed much larger  $He^+/He^{++}$  ratios ranging from a few percent to greater than one (Hovestadt *et al.* 1984). Surprisingly, for time periods with large  $He^+/He^{++}$  ratios ( $> 0.3$ ) no low charge states of heavy ions (C, O, Fe) have been found. However, it is not known whether these differences between He and heavy ion charge states are due to selective injection and/or acceleration processes at the sun or due to the very limited energy range of the previous experiments. The large energy range and collecting power of SAMPEX and will enable us to investigate this question in detail.

While the geomagnetic cutoff technique on SAMPEX is not sufficiently sensitive to distinguish between adjacent heavy ion charge states (e.g.,  $O^{6+}$  from  $O^{7+}$ ), it is suitable to answer questions such as those we

have discussed which involve large percentage differences in charge state (e.g.  $\text{He}^+$  vs.  $\text{He}^{++}$  and  $\text{Fe}^{14+}$  vs.  $\text{Fe}^{20+}$ ).

### 2.B.3 Solar Flare Acceleration and Propagation Processes

Although it has long been known that the elemental composition of solar flare nuclei varies from flare to flare, it is only recently that the nature of these composition variations began to be understood, when a Voyager study of many flares by Breneman and Stone (1985) showed that, over a limited energy range, the ionic charge to mass ratio ( $Q/M$ ) is the principal organizing factor for determining spectral and composition variations in large solar flares. They found that composition variations showed a power law dependence on  $Q/M$ , and by correcting for such effects unfractionated coronal abundances for a wide range of elements were obtained. This approach has recently been extended to solar flare isotope measurements, in order to obtain unfractionated coronal isotopic abundances for a few elements (Mewaldt and Stone 1989).

SAMPEX will be able to provide simultaneous measurements of both the elemental and isotopic composition of a wide range of heavy elements (and of protons, alphas, and electrons) over an energy interval extending from  $<1$  to  $\sim 100$  MeV/nucleon. The HILT sensor will measure heavy ion spectra with unprecedented accuracy up to  $\sim 100$  MeV/nucleon and, in conjunction with LEICA, will be able to test whether the  $Q/M$  dependence of spectral forms found by Breneman and Stone (1985) extends to higher and lower energies. Such measurements in a number of large events, supplemented by charge-state determinations of SEPs extending to energies of tens of MeV/nucleon, may help separate and characterize the  $Q/M$ -dependent fractionation occurring during the acceleration process itself and that arising from rigidity-dependent propagation of the flare particles through the interplanetary medium.

$^3\text{He}$ -rich solar flares are generally small events that provide a sample of coronal material from more restricted high-temperature regions in which heavier nuclei are enriched as might be expected from thermal diffusion. Recent analysis by Mason *et al.* (1986) suggests that two separate enhancement mechanisms may be occurring. The enhancement of the  $^3\text{He}/^4\text{He}$  ratio by orders of magnitude over that of the solar wind may well arise from a plasma resonance mechanism which results in preferential acceleration of  $^3\text{He}$  and certain other isotopes such as  $^{13}\text{C}$  (Mason *et al.* 1980). However, the heavy element enhancements may well reflect the ambient abundances in restricted regions of the corona such as might result from thermal diffusion processes (Nakada 1969). Isotopic measurements of other heavy nuclei in  $^3\text{He}$ -rich flares, which should be possible for the first time with LEICA, should better characterize these two distinct processes.

Another class of impulsive solar flares is associated with nuclear gamma ray emission (e.g., review by Ramaty and Murphy 1987) which is caused by the interaction of accelerated protons with the solar atmosphere. In these events ion and electron acceleration can take place on time scales of seconds (Chupp 1984). The interplanetary particles associated with these events are rich in heavy elements (Van Hollebeke and McDonald 1985), and have large electron/proton ratios (Evenson *et al.* 1984). However, since only a small fraction of the accelerated particles escape into interplanetary space there have been only 4 known cases of gamma-ray *line* flares which produced measureable particle fluxes at Earth—all these occurred during the past solar maximum (1980-1982) (Ramaty and Murphy 1987). By flying during part of the upcoming solar maximum, SAMPEX should observe several more gamma ray line flares, thus greatly increasing the inventory of known events and helping constrain models for particle acceleration in these flares. SAMPEX's large geometrical factor instruments are ideally suited to detect both the heavy ions and electrons accelerated in gamma ray events.

## 2.C Anomalous Cosmic Rays

In the energy range below  $\sim 50$  MeV/nucleon, there are at least six elements (He, C, N, O, Ne, and Ar) whose energy spectra show anomalous increases in flux above the quiet time galactic cosmic ray spectrum (see, e.g., the review by Gloeckler 1979). Although there have been a number of models proposed to explain this so-called "anomalous" cosmic ray (ACR) component, it is now generally believed to represent neutral particles that drift into the heliosphere, become ionized by the solar wind or UV radiation, and then get

Galactic Cosmic Ray and "Anomalous" Oxygen Spectra

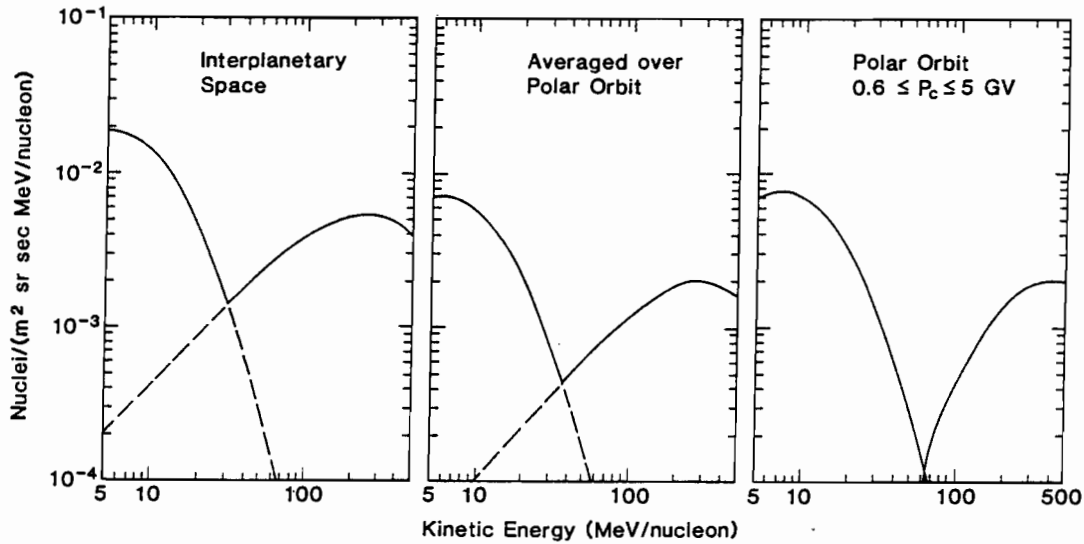


**Fig. 2-6** Galactic cosmic ray and anomalous cosmic ray oxygen spectra in (a) interplanetary space; (b) averaged over a polar orbit; (c) averaged over those portions of the orbit with geomagnetic cutoff  $R_{cutoff}$  in the interval 0.6 to 5 GV. Anomalous oxygen is assumed to be singly-charged and 1993 (based on 1971) flux levels are assumed. Note the uncontaminated sample of ACR oxygen that is obtained in the right hand panel.

accelerated to energies  $>10$  MeV/nucleon (Fisk, Koslovsky, and Ramaty 1974), possibly at the solar wind termination shock (Jokipii 1986). A unique prediction of the model of Fisk *et al.* is that the anomalous cosmic rays should be singly ionized, a generally accepted assertion for which there is as yet only indirect evidence (see, e.g., Cummings, Stone, and Webber 1984).

### 2.C.1 Charge State Measurements

It has long been realized that measurements in a polar orbit could test this prediction directly using the geomagnetic field as a magnetic spectrometer, since singly ionized ions have more efficient transmission through the field than their fully-stripped counterparts. However, previous attempts to use this approach on Spacelab (e.g., Adams *et al.* 1987) have not as yet turned out to be definitive tests of this model because: a) the flux of anomalous oxygen at 1 AU was very low due to large solar modulation effects at the time of the Shuttle flights; b) only limited ( $\sim 1$  week) exposure times were possible; and c) because the experiments lacked detailed resolution as to the time (and therefore cutoff) at which each particle was observed. Measurements with SAMPEX will overcome each of these difficulties and should give definitive measurements of the charge state of anomalous He and O, assuming that their flux during 1993 and 1994 has recovered as expected from solar maximum levels.

Figure 2-6 shows the estimated interplanetary spectra of ACR and GCR oxygen for 1993, based on measurements of anomalous He and O reported by von Rosenvinge *et al.* (1975) for the year 1971 (22 years earlier) since a variety of recent studies show that solar modulation effects recur on a 22-year time scale. To estimate the spectra observed by a polar orbiting experiment (averaged over the orbit) we use the geomagnetic transmission function shown in Figure 2-1, where we have assumed that ACR oxygen is singly-charged. Note that ACR oxygen nuclei can penetrate the Earth's magnetic field at much lower latitudes than GCR nuclei that have the same energy/nucleon since their rigidity is 8 times greater.

As an example, Figure 2-7 illustrates one method of determining the charge state of anomalous He and O. It shows the expected count rate of 14-20 MeV/nucleon He and O in MAST, as a function of the vertical cutoff rigidity, for various assumed charge states. The estimated uncertainties are based on one



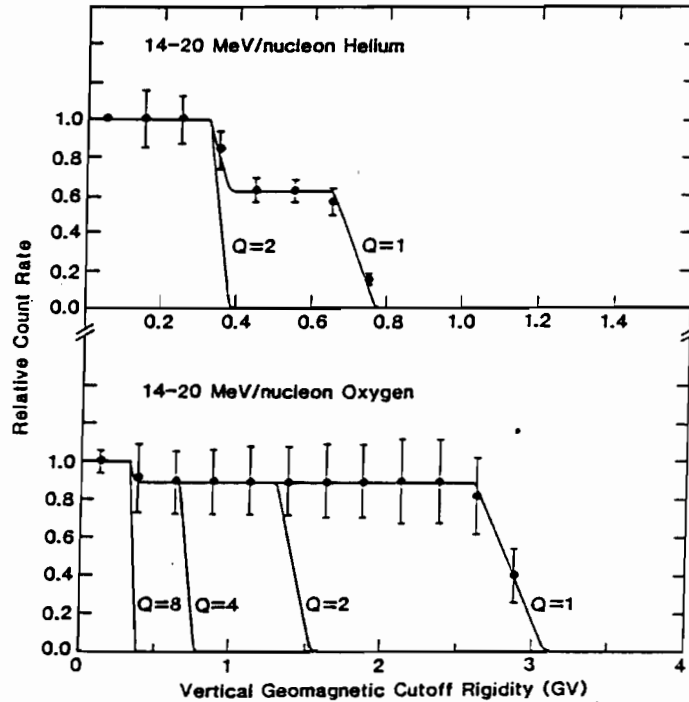


**Fig. 2-7** An illustration of the use of the geomagnetic field to determine the charge state of anomalous He and O nuclei. The expected relative count rates in various cutoff intervals are indicated for several assumed values of the charge state. The data points indicate the expected size of the statistical uncertainties that MAST could achieve in a polar orbit, assuming 1993 (1971) flux levels, and a 75% duty cycle and singly ionized ACR nuclei.

year's accumulation at 1993 (1971) flux levels. The HILT sensor extends to somewhat lower energies, and it will have approximately 5 times the counting rate of MAST for ACR particles. It can be seen that if the ACR component is indeed singly charged, its signature should be clear. The ability of SAMPEX to measure both the composition and energy spectra of all elements from H to Fe over a broad energy interval with good time (cutoff) resolution will provide numerous cross checks on this approach.

### 2.C.2 Isotopic Composition

If the ACR component is shown to be singly charged, proving the model of Fisk, Koslovsky, and Ramaty (1974) to be essentially correct, then this component represents a direct sample of the local interstellar medium that carries important information about galactic evolution in the solar neighborhood over the time interval since the formation of the solar nebula. This information can be obtained by comparing the isotopic composition of ACR nuclei with that of solar system nuclei, including those accelerated in solar flares. Radio and optical spectroscopy studies of interstellar matter show evidence that the interstellar abundances of isotopes such as  $^{13}\text{C}$ ,  $^{17}\text{O}$ ,  $^{18}\text{O}$ , and  $^{15}\text{N}$  differ by a typical factor of  $\sim 2$  to  $3$  from their solar system values (see, e.g., the reviews by Wannier (1980) and Penzias (1983)). The magnitude of these abundance variations is consistent with the predictions of some galactic evolution models.

An isotope spectrometer such as MAST in a polar orbit has a significant advantage in studying ACR isotopes because the Earth's field can be used as a magnetic filter to select a pure sample of ACR nuclei, uncontaminated by solar or galactic cosmic ray nuclei, which are highly ionized. Figure 2-6 illustrates an example of this "double-spectrometer" approach. By selecting events measured over the cutoff range from 0.6 to  $\sim 5$  GV, where (singly ionized)  $\sim 15$ - $40$  MeV/nucleon ACR nuclei can penetrate the Earth's field, but solar and galactic cosmic rays  $< 50$  MeV/nucleon are completely excluded, a pure sample of ACR oxygen

**Table 2-2** MAST Event Rates for "Anomalous" Cosmic Ray Isotopes

Element	Energy Range (MeV/nuc)	Estimated <sup>a</sup> Number of Events for 1993	Estimated <sup>b</sup> Number of Events for 1994
He	7-40	10,000	60,000
N	13-40	200	700
O	14-40	1100	3600
Ne	16-40	70	200

<sup>a</sup> Based on 1971 flux levels, a polar orbit and a 75% duty cycle.

<sup>b</sup> Same as (<sup>a</sup>), but for 1972 flux levels.

(and neon) is obtained, uncontaminated by solar and GCR oxygen and neon events. We emphasize that these measurements could not be carried out in interplanetary space.

Table 2-2 shows the number of ACR events per year estimated for 1993 and for 1994 flux levels. Of these, Ne should be the most interesting, since only relatively few Ne events are required to decide if ISM Ne has  $^{22}\text{Ne}/^{20}\text{Ne} \simeq 0.1$ , as found in solar system material, or has  $^{22}\text{Ne}/^{20}\text{Ne} \simeq 0.4$ , as in GCR source material. This would provide an important test of some recent theories that suggest that cosmic rays represent a sample of the ambient interstellar medium that has been accelerated to relativistic energies.

### 2.C.3 Elemental Composition and Energy Spectra

The large collecting power of the sensors on SAMPEX can also provide the first opportunity to extend ACR observations in the inner heliosphere into the solar minimum part of the solar cycle. Because of the small flux of ACR nuclei, the limited size of previous instrumentation, and competition with solar flare and galactic cosmic ray nuclei, observations of the anomalous component were not possible at 1 AU during the last solar maximum (1980). However, using the double spectrometer approach outlined above in combination with the large collecting power of SAMPEX, the low fluxes of ACR nuclei expected in 1991 can be separated from SEP and GCR nuclei with similar energies per nucleon. These measurements, in combination with those from the Voyager Pioneer, and Ulysses spacecraft in the outer heliosphere, can provide new insight into the acceleration and transport of these ions under solar maximum conditions.

Using the geomagnetic field to sweep away the lower rigidity SEP and GCR nuclei, this same double-spectrometer approach can also be used at higher flux levels to search for possible anomalous enhancements in the spectra of other elements, and it can provide a systematic study of the rare C and Ar elements recently discovered in the anomalous cosmic rays. Table 2-3 summarizes expected counting rates in HILT for four anomalous species for the years 1991 and 1993.

**Table 2-3** Event Rates of the Anomalous Component as Observed with HILT (Estimated counts/year)

Time Period	Helium	Carbon	Oxygen	Argon
1991	360	—	120	—
1993	84,000	200	18,000	25

## 2.D Precipitating Relativistic Magnetospheric Electrons

Only recently have instruments been flown to monitor long-term variations of highly relativistic electron fluxes in Earth's outer magnetosphere. It has been observed that  $\gtrsim 1$  MeV electron intensities increase

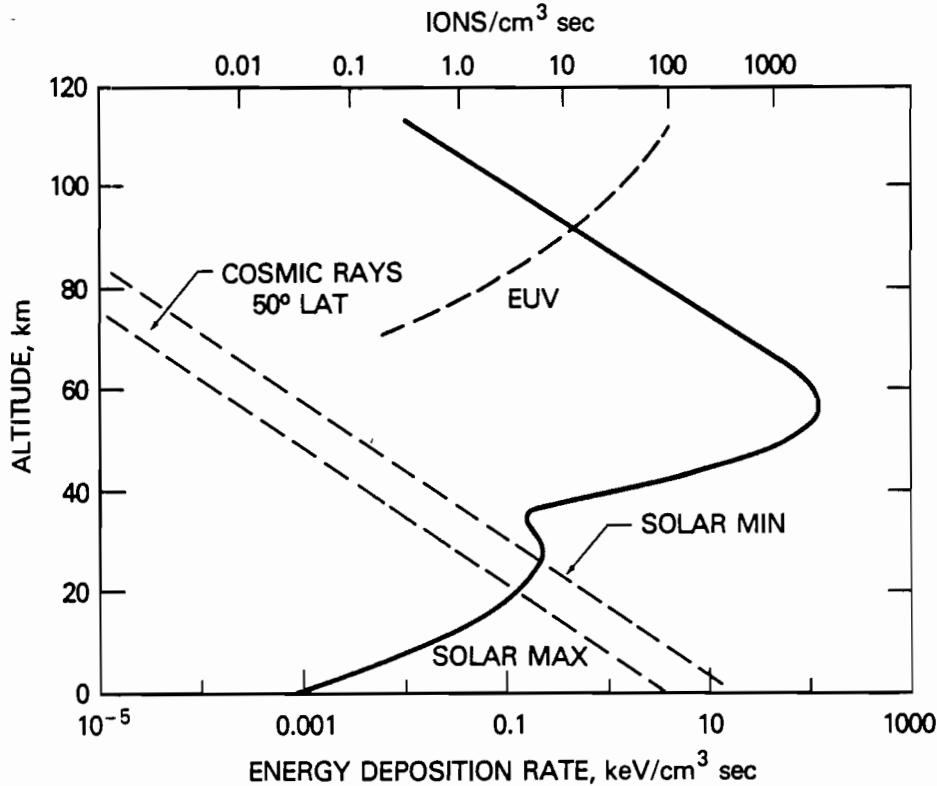


**Fig. 2-8** Atmospheric energy deposition rates at various altitudes for energetic electrons, galactic cosmic rays, and solar extreme ultraviolet (EUV) radiation determined from a numerical transport code.

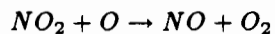
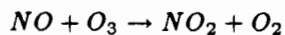
substantially for periods of a few days near the synchronous orbit often with a recurrence period of  $\sim 27$  days. This periodic enhancement in the relativistic electron flux is related to recurrent solar wind streams in the middle and outer heliosphere, which in turn are controlled by the solar rotation (Paulikas and Blake 1979; Baker *et al.* 1986). It is found that during a high-energy electron event period, the energy spectrum is very hard with significant flux enhancements extending to greater than 10 MeV. Multi-satellite studies (e.g., Higbie *et al.* 1987) suggest that these relativistic electron enhancements occur throughout the entire outer trapping region ( $3 \lesssim L \lesssim 8$ ).

Long-term observations (1979-present) of relativistic electrons show a strong solar cycle dependence. Such electrons were relatively absent near the last sunspot maximum (1979-80), but were prominently present in the approach to sunspot minimum (1984-85)—thus, paralleling the overall occurrence pattern of high-speed solar wind streams that emerge from solar coronal holes (Baker *et al.* 1987). Using numerical models and the observed equatorial energy spectra, it has been shown that the multi-MeV electrons—when they precipitate—can cause a large ( $10\text{-}100 \text{ keV/cm}^3\text{-s}$ ) energy deposition at 40-60 km altitude in the atmosphere. This could, therefore, dominate other ionization sources at these heights (such as cosmic rays and solar EUV) by several orders of magnitude (see Figure 2-8).

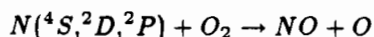
Recent modeling and data analysis efforts focused upon the upper stratosphere and lower mesosphere (Callis *et al.* 1988) suggest that the precipitating relativistic electrons may indeed lead to substantial long-term increases in the odd nitrogen levels at these heights with an attendant impact on local ozone levels. To establish more thoroughly these preliminary results, more detailed knowledge of these precipitating electrons is required. We have provisionally concluded that this electron population could play an important role in coupling solar wind and magnetospheric variability (on 27-day and 11-year cycles) to the middle atmosphere

through a modulating effect on lower D-region ionization and on upper level ozone chemistry (Baker *et al.* 1987).

The importance of energetic particle precipitation on the chemical composition of the middle atmosphere has been reviewed by Thorne (1980). High energy particles have a significant effect on the chemistry of the stratosphere, mesosphere, and thermosphere through the production and subsequent transport of odd nitrogen ( $NO_x$ ) and odd hydrogen ( $HO_x$ ) species. (cf. Rees and Roble, 1979; Rees and Romick, 1985). The  $NO_x$ , for example, governs the rate at which ozone is destroyed by the reactions



The primary high energy particles produce an intense flux of secondary electrons that can lead to the formation of atomic nitrogen in the  $^4S$ ,  $^2D$ , and  $^2P$  states,  $N(^4S, ^2D, ^2P)$ . The atomic nitrogen can recombine with  $O_2$  to yield NO and atomic oxygen,



The rate of the above reaction is particularly rapid for nitrogen atoms in the excited  $^2D$  and  $^2P$  states.

Auroral electron precipitation is confined to a narrow latitudinal band (Inv. latitude  $\Lambda \sim 68^\circ - 72^\circ$ ), i.e., the auroral oval itself, and auroral electrons penetrate only down to  $\sim 100$  km altitude before stopping. Unlike the auroral electrons, multi-MeV electrons are capable of penetrating down to the lower D-region and into the upper stratosphere over a broader latitudinal range. The bremsstrahlung X-rays that such electrons produce when interacting with atmospheric constituents can penetrate even more deeply; hence the primary electrons and the secondary photons can be significant ionization sources. It follows from chemistry models and from results as shown in Figure 2-8 that there may be a decrease in ozone concentrations caused by the increased concentrations of  $HO_x$  and  $NO_x$ . It is conceivable that these chemical perturbations could lead to substantial temperature changes in the mesosphere and consequent changes in eddy mixing rates and atmospheric gravity wave propagation.

A critical problem, therefore, is to determine the actual nature of relativistic electron precipitation. With the PET sensor on a low-altitude, high-inclination spacecraft, we will be able to specify the longitude, latitude, and local time precipitation characteristics. The PET energy range of optimum electron resolution (1-14 MeV) closely matches that required for these studies. These precipitation data, in turn, can be utilized in our atmospheric deposition codes to provide a much more accurate and realistic picture of the middle atmospheric source function of  $NO_x$  and  $HO_x$ . The requirement is for a systematic and accurate assessment of the intensity and energy spectrum of the precipitating electrons on a world-wide basis. Within this framework, the outstanding problem is to realistically model the middle atmospheric energy deposition and the subsequent chemistry and transport based upon actual particle input functions. The theoretical tools required for this are being developed right now.

We would propose as part of the SAMPEX project to help bring together the normally disparate disciplines of magnetospheric physics, atmospheric chemistry, and lower ionospheric electrodynamics. The goals would be, by direct low-altitude measurements, to understand

- The long-term and continuing variability of relativistic electrons in the middle magnetosphere
- How rapidly and efficiently the magnetospheric electrons are precipitated into the atmosphere
- Where (in a detailed sense) the electrons are precipitated in longitude, latitude, and local time
- The detailed  $NO_x$  and  $HO_x$  source function (suitable for photochemical-transport calculations) due to relativistic electron precipitation events as a function of season and phase of the solar cycle
- Modifications of lower D region conductivity patterns as may affect global ELF wave (i.e., Schumann resonance) propagation and the global atmospheric electrical circuit.

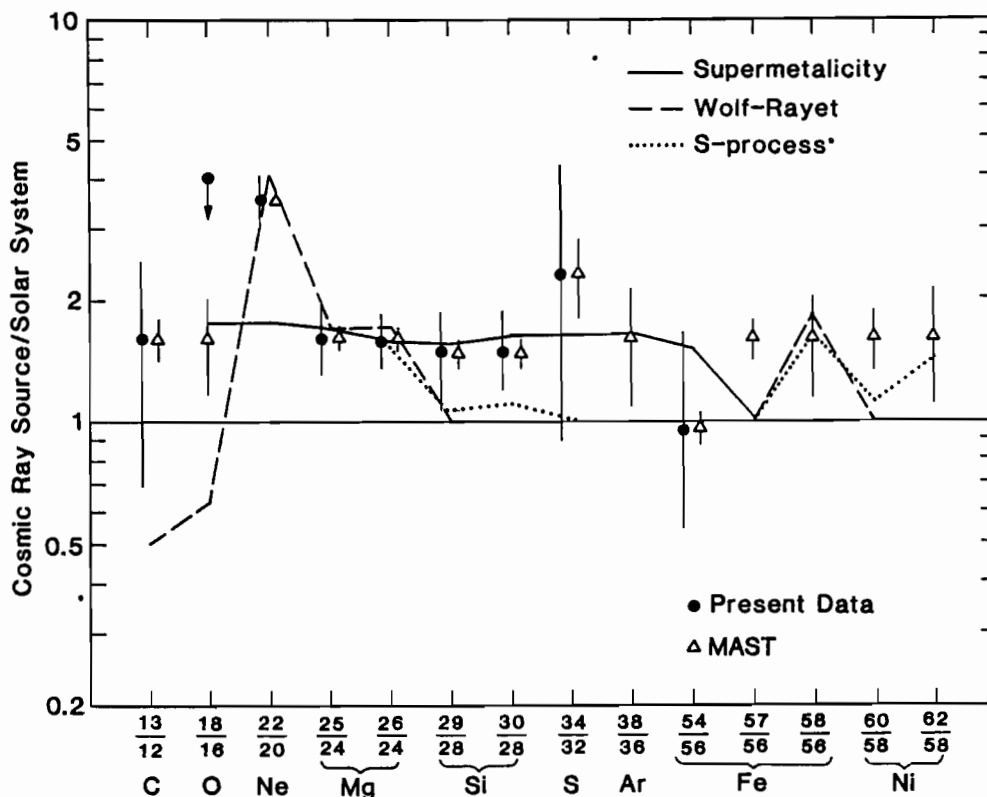


**Fig. 2-9** Composition of cosmic ray source material normalized to the solar system composition tabulated by Cameron (1982). Predictions are shown for three theoretical models (Woosley and Weaver 1981; Prantzos *et al.* 1985) that have attempted to explain the observed excess of neutron-rich Ne, Mg, and Si isotopes. A comparison of the size of the error bars expected for MAST with those of presently available measurements indicates the improved precision that MAST could achieve in three years (taking into account solar modulation level for the years 1991 to 1993, and assumed duty cycle of 75%, and assumed fragmentation cross-section uncertainties of 5%). Note that the MAST estimates have been made at an assumed ratio of 1.5 for those isotopes where there is presently no measured value.

We should note that energetic solar protons with energies in excess of  $\sim 30$  MeV can also cause significant energy deposition in the stratosphere over the entire polar cap region down to  $60^\circ$  magnetic latitude with accompanying production of  $NO_x$  and  $HO_x$ . A depletion of stratospheric ozone was observed by satellite-borne instruments following the great August 1972 solar flares (Reagan *et al.* 1981). SAMPEX, and in particular the PET sensor, will monitor these energetic solar protons during the period of maximum solar activity.

### 2.E Isotopic Composition of Galactic Cosmic Rays

Galactic cosmic rays represent a directly accessible sample of matter from outside the solar system. The isotopic composition of this sample of high energy matter contains a record of the nuclear history of cosmic rays including their synthesis in stars and subsequent nuclear interactions with the interstellar gas. Cosmic ray isotope observations have already revolutionized our views of both cosmic ray origin and propagation. As an example, measurements by a number of groups have shown that  $^{22}\text{Ne}$  is a factor of at least 3 times more abundant in cosmic ray source material than in the solar system, while the abundances of  $^{25}\text{Mg}$ ,  $^{26}\text{Mg}$ ,  $^{29}\text{Si}$ , and  $^{30}\text{Si}$  are all enhanced by a factor of  $\sim 1.5$ . These and other estimates of the source composition,

based on a compilation of recent measurements, are shown in Figure 2-9.

The discovery of isotopic abundance anomalies in cosmic rays has led to a number of suggestions as to how the nucleosynthesis of cosmic ray and solar system matter may have differed. They include: 1) the possibility that cosmic rays represent a sample of more evolved material, possibly from supernova explosions in metal-rich regions of the galaxy (Woosley and Weaver 1981); 2) the possibility that cosmic rays come from a restricted class of objects such as Wolf-Rayet stars (Casse and Paul 1982), and 3) the possibility that the *solar system* composition is "anomalous" with respect to the rest of the galaxy as a result of its peculiar history of formation (Olive and Schramm 1982). The source compositions predicted by three such models are indicated in Figure 2-9. To test the predictions of these models will require accurate measurements of a range of other cosmic ray isotopes including  $^{13}\text{C}$ ,  $^{18}\text{O}$ ,  $^{54}\text{Fe}$ ,  $^{58}\text{Fe}$ , and the neutron-rich isotopes of S, A, Ca, and Ni. With the direct evidence of nucleosynthesis differences that has been discovered to date, it would be remarkable if the cosmic ray abundances of some of these other isotopes were not also different.

In Figure 2-9 we indicate the expected accuracy that MAST could achieve for several key isotope ratios, taking into account both statistical and propagation uncertainties. Note that in a number of cases measurements with MAST should provide significant tests of existing models, and they may, of course, also discover surprising new results.

In addition to providing information on the nature and possible location of cosmic ray nucleosynthesis, isotope measurements can reveal the time scale between nucleosynthesis and acceleration, and the time scale of cosmic ray storage in the galaxy. Thus measurements of radioactive nuclei that decay only by electron capture, such as  $^{60}\text{Ni}$ ,  $^{57}\text{Co}$ ,  $^{56}\text{Fe}$ , and  $^{59}\text{Ni}$  can address the important question of whether cosmic rays represent a sample of the interstellar medium, or whether they represent newly synthesized material, possibly from supernovae (Soutoul, Casse, and Juliusson 1978). The abundances of radioactive clocks such as  $^{26}\text{Al}$ ,  $^{36}\text{Cl}$ ,  $^{41}\text{Ca}$ ,  $^{53,54}\text{Mn}$ , and  $^{60}\text{Fe}$  can provide information on the galactic confinement time of heavy nuclei, which can be compared with that for medium nuclei ( $6 \leq Z \leq 8$ ) as measured by  $^{10}\text{Be}$ . The event rates expected for MAST for cosmic ray clocks such as  $^{10}\text{Be}$ , and  $^{26}\text{Al}$  are  $\sim 3$  times those observed by the UCB *ISEE 3* experiment (Wiedenbeck 1983), the best measurements to date. MAST should also have significantly improved mass resolution.

### 3. APPROACH

The preceding discussion has shown that key progress in a broad range of scientific questions in studies of solar energetic particles (SEP), anomalous cosmic rays, magnetospheric/middle atmosphere studies, and galactic cosmic rays can be accomplished using high resolution measurements of energetic particle fluxes observed over a broad energy range from a low altitude near polar orbiting satellite beginning at the upcoming solar maximum. The four sensors that comprise SAMPEX each address a subset of the required measurements with enough overlap in energy range and response to allow intercalibration and partial redundancy. LEICA will return information on SEP and the lower energy part of the anomalous cosmic ray spectrum; in the energy range above LEICA, HILT will provide ultra-high sensitivity composition and spectral information on the anomalous component and SEP; MAST will study the composition of SEP, the anomalous component and galactic cosmic rays with lower sensitivity than HILT, but with isotopic resolution; PET will provide proton and electron measurements. The low polar orbit of SAMPEX is essential in allowing the precipitating particle observations and the charge state studies of the anomalous component and solar energetic particles.

All the SAMPEX instruments are in an advanced state of development, allowing launch into the late 1991 solar maximum period. Two of them, LEICA and HILT, are sensors designed and constructed for Space Shuttle flight together in the Get-Away-Special program. LEICA and HILT development began in 1984 as an experiment named HIENLO that was designed to study the anomalous component and solar energetic particles. It was originally scheduled for an initial launch in late 1986 from Cape Kennedy, with a series of subsequent launches into polar orbit (provided by the Air Force) to have followed from Vandenberg Air Force Base. With the delay in the shuttle program, the flight was postponed and is now scheduled for the

1988/1989 time frame (payload G-0335); however, with the indefinite postponement of Vandenberg AFB launches, the crucial polar orbit exposure for HIENLO was lost. The Small-Class Explorer program provides a perfect flight opportunity with exactly the near polar orbit for which LEICA and HILT were designed, with the substantial additional benefit of greatly improved scientific returns because of the much longer exposure time achievable with a satellite vs. the Shuttle. Both instruments are new designs and represent the latest technology for covering a broad energy range with very high sensitivity and excellent resolution.

The two other instruments, MAST and PET, comprise a single instrument package that was designed to fly on the U.S. spacecraft of the International Solar Polar Mission (ISPM, now called Ulysses). At the time the ISPM spacecraft was terminated, MAST and PET were designed and well under construction. Because of the exploratory nature of the ISPM mission, MAST and PET are versatile instrument designs that can provide isotope measurements over a broad energy range with outstanding mass resolution. Thus, although the characteristics of the Small-Class Explorer mission are somewhat different from ISPM, the versatility of these instruments ensures that MAST and PET can achieve important objectives at all phases of the solar cycle. In spite of the lower duty cycle that polar orbits offer for studies of solar and galactic particles, MAST in all cases exceeds the collecting power of past or presently operating instruments (see discussion in Appendix B).

Thus, all the components of SAMPEX offer the benefit of an extensive design and development effort, sponsored by NASA, the Air Force, and the German government, as highly reliable spaceflight instruments. It is this heritage that makes possible the quick implementation of SAMPEX in the Small-Class Explorer program, without resorting to obsolete instrumentation. We propose to modify LEICA and HILT, and to complete the construction of MAST and PET for the SAMPEX mission. Below, the instruments are described in more detail.

#### 4. INSTRUMENTATION/TECHNIQUE/STATUS

##### 4.A The MAST/PET Sensors

###### 4.A.1 The Mass Spectrometer Telescope - MAST

MAST is designed to measure the isotopic composition of elements from Li ( $Z=3$ ) to Ni ( $Z=28$ ) in the range from  $\sim 10$  MeV/nucleon to several hundred MeV/nucleon. MAST consists of a combination of surface barrier and lithium-drifted solid-state detectors, as shown in Figure 4-1 (see also Table 4-1). The first four detectors, M1 through M4, which define the acceptance aperture, are identical one-dimensional position-sensitive detectors (PSDs) lined with 92 parallel strips on one surface of each (0.5 mm pitch), which together form an X-Y hodoscope for determining the position of incident particles. The combined M1 through M4 positions determine the particle trajectories, allowing accurate corrections to be made for the pathlength variation with angle and detector response non-uniformities. Detectors D1 and D2 are conventional surface barrier detectors, while D3 through D7 are lithium-drifted detectors of graduated thickness. The lithium-drifted devices have integral guard rings (G) that are used as anticoincidence devices. All detectors except D7 are pulse-height analyzed.

Isotope identification in MAST is accomplished by the standard  $dE/dx$  vs  $E$  technique, using the energy lost in the last detector triggered as  $E$ , and the outputs of the previous detectors as redundant measurements of  $dE/dx$ . The use of position-sensitive detectors, combined with an all solid-state telescope optimized for isotope resolution, was pioneered in the Caltech HIST instrument for *ISEE 3*, which has provided the best mass resolution yet achieved for either solar or galactic cosmic ray isotopes (see Appendix C). Based on the proven mass resolution techniques of HIST, the MAST design should achieve a mass resolution  $\leq 0.3$  amu for all elements with  $3 \leq Z \leq 28$ , as discussed in Appendix C. At the same time, the geometry factor of MAST will be  $\sim 20$  times greater than HIST (see Appendix B), allowing statistically significant studies of relatively rare isotopes.

Table 4-1 summarizes the energy intervals covered by MAST for two representative elements. Note in particular that the use of relatively thin detectors at the front of the MAST stack extends isotope

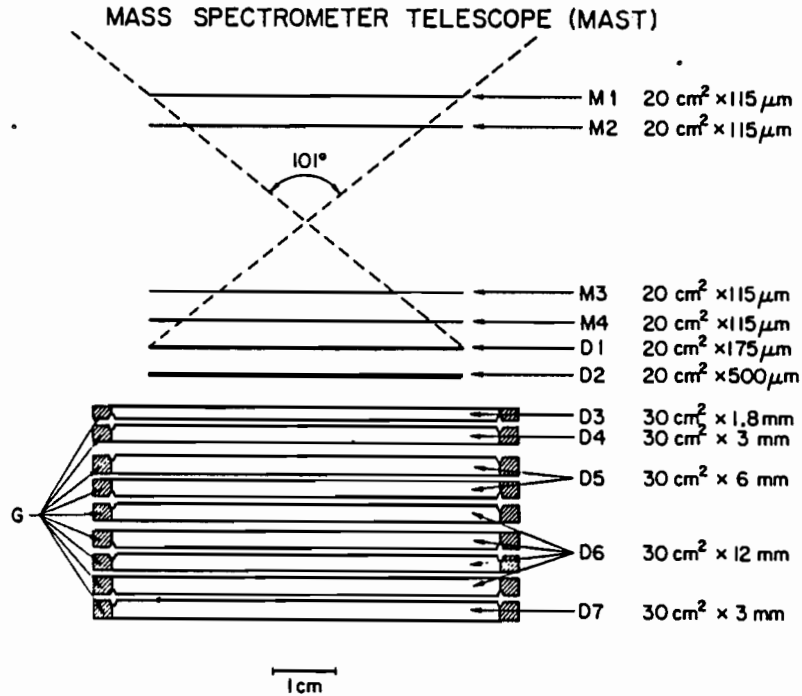


**Fig. 4-1** A schematic of the Mass Spectrometer Telescope (MAST) with the detector areas and thicknesses indicated. The shaded rings (G) are integral guard rings used in anticoincidence.

**Table 4-1** MAST Detectors, Geometry Factors, and Energy Ranges

Detector	Nominal Thickness (mm)	Area (cm <sup>2</sup> )	Geometry Factor (cm <sup>2</sup> sr) <sup>a</sup>	Threshold Energies <sup>a</sup> (MeV/nucleon)	
				<sup>16</sup> O	<sup>56</sup> Fe
M1	0.115	20			
M2	0.115	20			
M3	0.115	20			
M4	0.115	20	16.1	14.2	24.0
D1	0.175	20	14.1	16.9	29.0
D2	0.50	20	12.5	20.4	35.5
D3	1.7	30	12.4	29.4	50.6
D4	3.0	30	12.0	49.0	89.5
D5	6.0	30	10.6	73.6	136.5
D6	12.0	30	8.3	109.8	207.0
D7	3.0	30	6.6	164.3	316.0

<sup>a</sup> M1 · M2 · M3 · M4 coincidence required for analysis

identification down to ~15 MeV/nucleon. This, along with its large geometry factor makes MAST very suitable for isotopic analysis of solar energetic particles, the anomalous cosmic ray component, as well as galactic cosmic rays.

Although optimized for isotopic analysis of the elements Li to Ni, MAST will also perform measurements of stopping He isotopes from ~7 to ~60 MeV/nuc, and H isotopes from ~7 to ~15 MeV/nuc. In addition, MAST will analyze particles that trigger D7 and thus penetrate the entire stack, providing differential energy spectra of the more abundant elements to well beyond the endpoint energy for stopping particles,



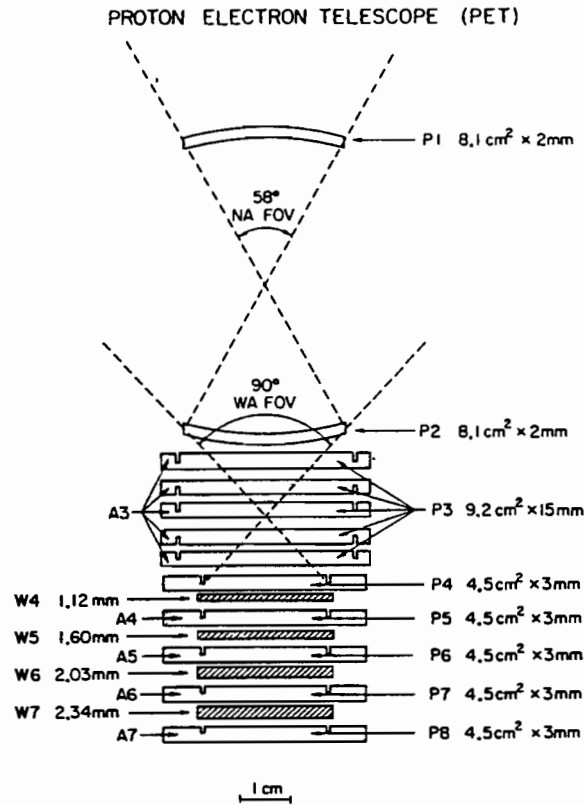


**Fig. 4-2** Schematic of the PET telescope with the areas and thicknesses of the detectors indicated. In the back of the telescope, inactive tungsten absorbers (W4 to W7) are used to extend the energy range for high energy electrons, protons, and helium nuclei.

and integral flux measurements at higher energies. A priority system will ensure that the most interesting events are selected for readout, with stopping  $Z \geq 3$  events given highest priority. However, since MAST will be assigned a bit rate of 2 kbps on the SAMPEX mission, the pulse heights from essentially all stopping  $Z \geq 3$  nuclei can be transmitted, even in very large flares.

Given sufficient event statistics, the MAST resolution should be sufficient to resolve all isotopes with  $Z < 30$ . For example, a mass resolution  $\sigma_m = 0.25$  amu is sufficient to resolve two adjacent isotopes whose relative abundance differs by a factor of  $\sim 100$  to 1. Examples of the excellent MAST resolution are given in Appendix C.

#### 4.A.2 The Proton/Electron Telescope - PET

The PET system is designed to complement MAST by measuring the energy spectra and relative composition of protons (18-350 MeV) and helium nuclei (18-500 MeV/nuc) of solar, magnetospheric, interplanetary, and galactic origins, and the energy spectra of solar flare and precipitating electrons from  $\sim 1$  to 100 MeV. In addition, it provides isotope resolution for  $^2\text{H}$  up to higher energies than MAST. The PET system can also duplicate in a limited way some measurement capabilities of MAST by providing energy spectra and elemental composition of nuclei from Li through Fe, and some isotopic information on nuclei from H to Ne. PET uses solid state components exclusively, and is derived from detector systems proven on previous NASA missions, particularly on OGO 6, Pioneers 10 & 11, IMPs 7 & 8, Helios, and Voyagers 1 & 2.

Figure 4-2 represents a schematic cross section of the PET telescope. It consists of two curved (spherical) aperture detectors (P1, P2), and eight flat detectors (P3 - P8) with integral guard-ring elements (A3 - A8), separated by tungsten absorbers (W4 to W7). All solid state detectors are of lithium-drifted design. The

**Table 4-2** Pet Response

Particle	Energy Interval (MeV or MeV/nuc)	Geometry Factor (cm <sup>2</sup> sr)	Detector Combination
Electrons	1 - 14	1.6 - 1.0	P1 · P2 · $\overline{P4}$
	14 - 130	1.0 - 0.3	P1 · P2 · P4 · $\overline{P8}$
	> 13	0.3	P1 · P2 · P8
H,He	18 - 64	1.6 - 1.0	P1 · P2 · $\overline{P4}$
	64 - 120	1.0 - 0.3	P1 · P2 · P4 · $\overline{P8}$
	> 120	0.3	P1 · P2 · $\overline{P8}$
Nuclei <sup>a</sup> ( $Z \geq 3$ )	54 - 195	1.6 - 1.0	P1 · P2 · $\overline{P4}$

<sup>a</sup> Commandable HI-Z mode, energy range is for <sup>28</sup>Si.

detectors P1 through P3 feed into individual 4095-channel pulse height analyzers with two commandable discriminator thresholds. Their amplifiers have a high and low gain mode each. Another PHA is provided for the sum of signals from P4 through P7. P8 and the guards A3 through A8 feed into 2-level discriminators. The chief capabilities of PET are summarized in Table 4-2.

In both the LO-Z and HI-Z modes, particles enter through the telescope aperture (P1 and P2). The PET LO-Z mode provides the differential energy spectra of electrons and H and He nuclei over the ranges listed in Table 4-2, and includes H and He isotope resolution for nuclei stopping before P4. The signals from P1, P2, P3 and the sum of P4 to P7 are pulse-height analyzed so that the techniques of multiple differential-energy loss  $dE/dx$ , total energy  $E$ , and range  $R$  measurements can be utilized. Based on experience with Voyager, the quadruple  $dE/dx$  measurements for penetrating particles should allow the extension of the proton differential energy spectrum to at least 350 MeV and the He spectrum to >500 MeV/nuc, with integral flux measurements beyond. The HI-Z mode allows the measurement of the energy spectra of elements from Li through Fe, with limited isotope resolution through neon.

The primary driver in the detailed design of PET is the objective to measure electron spectra from ~1 MeV to beyond 100 MeV. This led to the combination of a [ $dE/dx - E$ ] detector arrangement (principally P1 through P3) for 1-14 MeV electrons, with a [ $dE/dx - R(ange)$ ] arrangement using P1 through P8 with tungsten absorbers for electron energies through 120 MeV.

#### 4.B The Low Energy Ion Composition Analyzer - LEICA

The Low Energy Ion Composition Analyzer (LEICA) measures ion fluxes over the charge range from He through Ni from about 0.35 to 10 MeV/nucleon. Exploratory measurements of ultra-heavy species (mass range above Ni) will also be performed in a more limited energy range near 0.8 MeV/nucleon. A schematic cross section of the LEICA telescope is shown in Figure 4-3. LEICA is virtually identical to the Solar Energetic Particle composition instrument developed at the University of Maryland for flight on a Space Shuttle Get-Away-Special mission in 1988/1989. LEICA thus benefits from a four-year design and development effort at Maryland, which has produced a flight instrument. The basic time-of-flight versus energy technologies used in LEICA have been flight proven in University of Maryland experiments on the AMPTE - CCE spacecraft, and on instruments built and flight qualified for the Ulysses mission.

The instrument is a time-of-flight mass spectrometer that identifies incident ion mass  $M$  and energy by simultaneously measuring the time-of-flight  $t$  and residual kinetic energy  $E$  of particles that enter the telescope and stop in one of the array of four Si solid state detectors in the telescope. The time-of-flight is determined by START and STOP pulses from chevron microchannel plate (MCP) assemblies that detect secondary electrons that are emitted from the entrance foil and the front surface of the solid state detec-

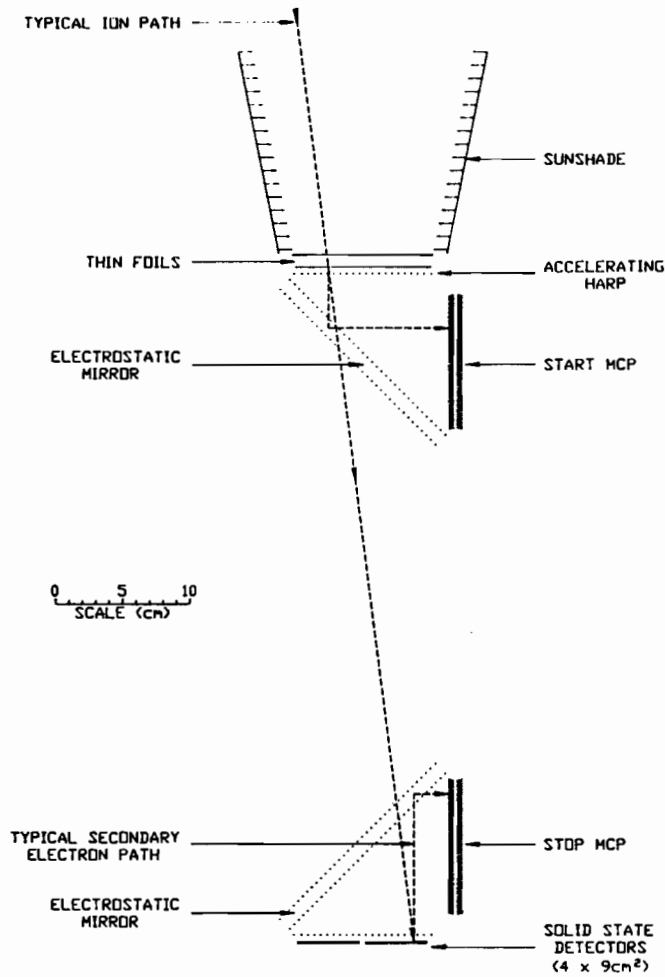


**Fig. 4-3** The LEICA telescope schematic cross section.

tor, respectively, when the ion passes through them. These secondary electrons are accelerated to  $\sim 1$  kV and deflected onto the MCPs by electrostatic mirrors. The design of the secondary electron optics yields isochronous flight paths for all secondary electrons emitted normally from the foils or detector surface. The measured energy  $E = 1/2MV^2$ , and the velocity  $V = L/t$  (where  $L$  is the path length in the telescope) are combined to yield the mass of the ion  $M = 2E(t/L)^2$ , and the energy per nucleon  $E/M$  inside the telescope. The ion incident energy is obtained after correcting for the energy loss in the entrance foils.

LEICA's low energy threshold is achieved by using the time-of-flight technique with thin entrance foils on the telescope. The high mass resolution is attained by combining time-of-flight measurements of high accuracy ( $\sim 650$  psec FWHM as shown for the prototype in Appendix C) with a long (about 50 cm) flight path whose length is determined accurately by measuring the entrance position of the ion on the foil and the position struck by the ion in the array of solid state detectors. Finally, the large geometrical factor is obtained by using large area microchannel plates ( $8 \text{ cm} \times 10 \text{ cm}$ ) and solid state detectors (array of four circular detectors, each with  $900 \text{ mm}^2$  active area), thereby achieving a geometrical factor of  $1.0 \text{ cm}^2\text{-sr}$ . Table 4-3 shows typical LEICA energy intervals and event totals for moderately large flares,  $^3\text{He}$ -rich solar flares, and interplanetary shock events, with the energy range restricted to the region of high mass resolution.

Immunity to solar UV and visible radiation is achieved by using two  $0.75 \mu$  Ni entrance foils. A double foil prevents single pinholes from allowing sunlight to enter the telescope. The thin foils are protected by an acoustic cover that is opened after launch. The acoustic cover is mounted on a sunshade that serves an additional role of preventing particles incident from outside the  $24^\circ \times 20^\circ$  instrument view cone from striking the front foil, thereby preventing excessive START rates in large solar flare events.

**Table 4-3** LEICA Energy Intervals and Typical Event Collection

Element	Energy Interval (MeV/nuc)	Moderately Large Flare <sup>a</sup>	<sup>3</sup> He-rich Flare <sup>b</sup>	Interplanetary Shock <sup>c</sup>
He	0.4 - 8	1.9 x 10 <sup>6</sup>	22,000	500,000
C	0.35 - 12	14,000	240	5,000
O	0.4 - 11	27,000	720	13,000
Si	0.4 - 4	3,200	350	?
Fe	0.5 - 4	3,700	970	1,100

Geometrical factor: 1.0 cm<sup>2</sup>-sr; event numbers in the table represent particles triggering LEICA and counted by the LEICA species rates

<sup>a</sup> based on November 22, 1977 solar particle event; telemetry allows PHA events to be telemetered for all  $Z \geq 6$  events and for 150,000 He events

<sup>b</sup> average of 30 <sup>3</sup>He-rich flares, 1978-80, and spectral slope of 2.6

<sup>c</sup> average of 24 shocks, 1978-80, spectral slope of 2.0, and composition based on observations above 0.5 MeV/nucleon

For each ion triggering the instrument, a measurement is made of the time-of-flight, the energy signal in the solid state detector, and the pulse sizes from three-collector wedge-and-strip anodes (WSA) in back of both the start and stop MCPs. A triple coincidence requirement (START-STOP-Si detector) with a short (300 nsec) time window gives high background immunity for all analyzed events. The locations at which the ion struck the foil and the solid state detector array are easily determined from the WSA information and the fact that the electrostatic mirrors produce accurate images on the MCPs. From these two positions an accurate calculation of the particle trajectory can be made, a requirement for high mass resolution analysis. All events triggering the system have their digitized time-of-flight and Si detector energy deposit measurements converted into pseudo-logarithmic form by fast gate logic. The  $\log(t)$  and  $\log(E)$  are used to determine whether each particle is a proton, He nucleus, or heavier than He. Events triggering LEICA that are identified by the pseudo-log lookup system to be protons are counted in several energy bins. He and heavier nuclei are passed along to an on-board microprocessor for further processing.

Because of the very high event rates observed by LEICA in large flares, it is not possible to transmit all particle information within available telemetry allocations. Two types of information are therefore returned: first, detailed pulse-height-analysis (PHA) data at a rate of 5 events/sec, and second, "species rates", which are counting rate data that cover H, He, O, and Si and Fe groups with 12 energy intervals covering the full energy range of the instrument. Species rates are telemetered every 15 seconds. The on-board event microprocessor examines all heavy ions triggering the system, and in the case of PHA data makes a priority selection to prevent He nuclei from dominating the telemetry in active periods. The microprocessor also determines the species and energy of each event using look-up tables, and increments the proper species rate.

High mass resolution analysis is done on the ground using the ion trajectory information telemetered with the PHA data. Mass histograms are formed for selected energy ranges, with the relative abundance of each species determined from the population at the appropriate mass bin in the histogram. Since LEICA has multi-parameter analysis it is possible to identify and correct for residual background in the instrument, an essential feature for identifying a broad range of ions with widely differing abundances. Appendix C contains examples of the LEICA's excellent mass resolution.

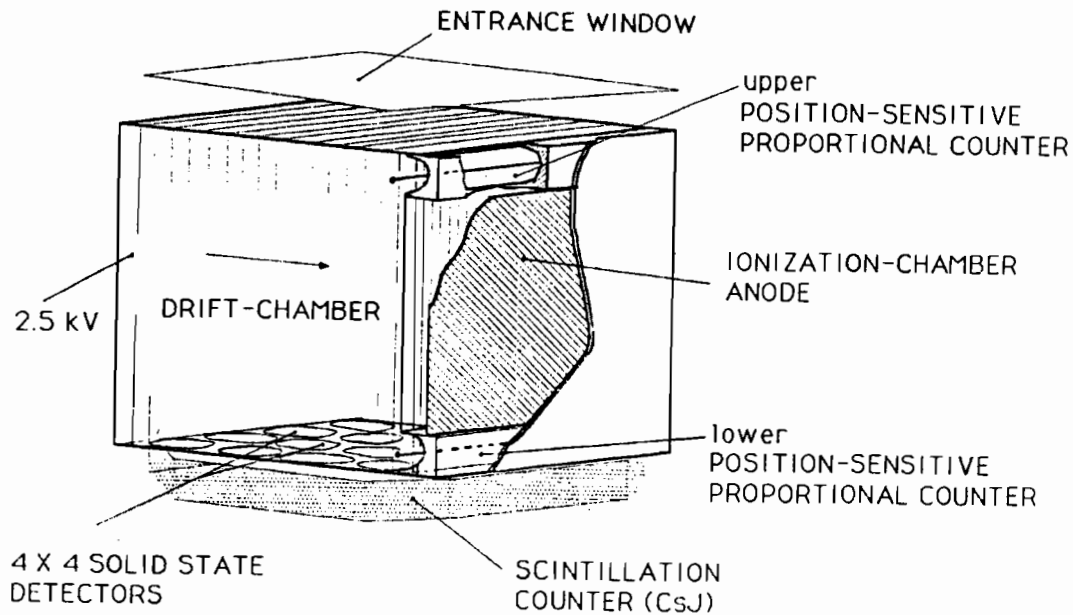


Fig. 4-4 HILT telescope cross section.

#### 4.C The Heavy Ion Large Telescope - HILT

The HILT sensor is designed to measure heavy ions from He to Fe in the energy range from 8 to 310 MeV/nucleon (for oxygen). It thus covers the energy range of medium energy solar energetic ions and the range of maximum intensity of the anomalous component of cosmic rays. Together with LEICA and MAST/PET a comprehensive measurement of the entire solar and anomalous particle population will be achieved.

To meet our scientific objectives in the multi MeV/nucleon range for statistically accurate heavy nuclei spectral and cutoff measurements, the sensor will have an unprecedented geometric factor, increased by a factor of about 20 compared to other instruments previously flown. The sensor combines the techniques of  $dE/dx$  measurement in a proportional counter and ion drift chamber with the measurement of residual energy in solid state detectors and in a CsI scintillator. The sensor also measures the particle trajectories. With the information of particle energy, mass, and direction in combination with the spacecraft position in the low altitude polar orbit, it will be possible for the first time to infer the ionic charge of ions in this energy range. Like LEICA, the HILT sensor is already fully developed and only some technical changes will be necessary to optimize the instrument for the long duration flight on the SAMPEX mission. The techniques are based on flight proven technology, which has been demonstrated on the IMP-7/8, S3-3, ISEE 1, and ISEE 3 missions.

A schematic diagram of HILT is shown in Figure 4-4. The sensor consists of a three element ion drift chamber with a thin multilayer entrance window ( $80 \mu$  Al total) followed by an array of 16 solid state detectors (SSD) and a CsI scintillation counter, which is viewed by 4 light sensitive diodes. The entrance foil serves as part of the gas enclosure and assures, in combination with a micrometeoroid bumper shield, a long lifetime against damage by micrometeoroids (see Appendix D).

*The Ion Drift Chamber - Proportional Counter System.* The first and third element of the drift chamber is sensed by two position sensitive proportional counters (PC1, PC2) with triangular shaped cathodes, the center element is operated as an ionization chamber (IC). The energy losses of ions in all 3 elements are pulse height analyzed and thus provide a triple  $dE/dx$  measurement. In addition, the signals from the triangular

**Table 4-4** Energy Range of HILT

Ion	Low Energy Range (MeV/nucleon)	High Energy Range (MeV/nucleon)
He	3.9-20.	20.-90.
C	7.2-35.	35.-160.
O	8.3-41.	41.-310.
Ne	9.1-45.	45.-250. <sup>a</sup>
Fe	11.0-72.	72.-90. <sup>a</sup>

<sup>a</sup> Top of energy range limited by amplifier dynamic range.

shaped cathodes of the two proportional counters are analyzed. These signals provide, in combination with the corresponding energy signal, information on the position along the proportional counter axis. In the first (upper) element the drift time (TOD) of electrons generated along the track of the incoming particle is also determined. The drift time is the time elapsed between the response of the SSDs and the anode of PC1. Drift time and position response of PC1 provide two coordinates for the incoming ion at the top plane of the sensor. At the bottom plane the position response of PC2 and the information on the detector row triggered by the incoming ion provide another two coordinates. From these 4 coordinates, the trajectories of the incoming ions can be derived. The accuracy of the determination of the incident angle is limited by the diameter of the detector and the position response of the PCs and is about 5° FWHM.

The ion drift chamber-proportional counter system operates with isobutane at a pressure of 75 torr (at 20°C). The density of the isobutane is actively controlled by a gas regulation system providing a continuous flow-through of isobutane, as successfully flown on the MPE instruments for the IMP-7/8, *ISEE 1*, and *ISEE 3* missions. The gas supply consists of 8.4 kg of liquid isobutane, sufficient for a lifetime of 3 years, stored in two tanks of TiAlV64 alloy.

*The Solid State Detector Array.* The detectors are arranged in an array of 4 × 4 detectors with 4 detectors in one row connected to one amplifier chain. In addition to the pulse height analyzed energy signal the information on the particular row triggered by the ion will be transmitted with the pulse height information. The triple  $dE/dx - E$  measurement combines high mass resolution with high background rejection. It allows the identification of all elements between He and O, and of all even Z elements up to Fe. At low Z (He - B) the resolution is sufficient to identify individual isotopes. An example of HILT heavy ion resolution measured during an accelerator calibration is shown in Appendix C.

In the present design for the GAS experiment detectors with 500 μ thickness and an effective area of 500 mm<sup>2</sup> are used. This results in a geometrical factor of 35 cm<sup>2</sup> sr. In order to extend the energy range of the high resolution system to higher energies we propose to replace the detector array by 2 mm detectors. If the new detectors are available with a larger effective area it might be possible to increase the geometrical factor to about 50 cm<sup>2</sup> sr.

*The CsI Crystal.* High energy ions penetrating the solid state detectors are stopped in a CsI crystal of 2 cm thickness. This extends the energy range of the sensor to 310 MeV/nucleon (for O). Due to limitations of the CsI resolution and the smaller  $dE/dx$  signals in the IC-PC system the directional and mass resolution in the high energy range is somewhat degraded and not sufficient to provide isotopic resolution. However, elemental resolution for the more abundant elements is still achieved. A summary of the energy ranges of the sensor for different ions is given in Table 4-4.

#### 4.D The Data Processing Unit - DPU

LEICA, HILT, MAST, and PET will be completed at the institutions where they were developed, and will be integrated with the overall experiment Data Processing Unit and central power supply (DPU) at the Aerospace Corporation for a system level test. After this integration is completed, the SAMPEX instruments will be integrated into the spacecraft. Because there is only a single electrical and data interface with the

SAMPEX BLOCK DIAGRAM

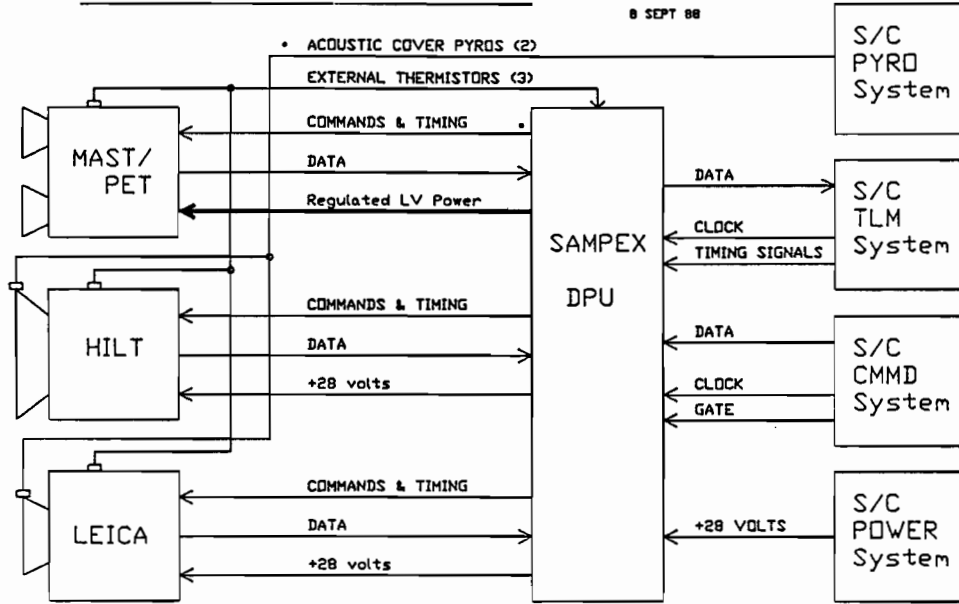


Fig. 4-5 SAMPEX Block Diagram

spacecraft, we anticipate that instrument integration with the spacecraft will be accomplished quickly. Figure 4-5 shows an overall block diagram of the SAMPEX experiment.

**5. INSTRUMENT INTEGRATION**

Because the SAMPEX experimental components are primarily existing hardware, the volumetric requirements are accurately known, and can be easily accommodated in the available space indicated in the A.O. (Fig. 6 of A.O. Appendix A). Appendix E.b shows a typical layout of SAMPEX in the available volume. Table 5-1 summarizes other SAMPEX instrument parameters relevant to spacecraft accommodation.

**Table 5-1 SAMPEX Resource Requirements**

Mass: 54.5 kg <sup>a</sup>
Power: 16.7 W
Bitrate: 6 kpbs
Operating temp: 0-20° C

<sup>a</sup> Instruments + isobutane tanks + mounting structure

**6. GROUND AND FLIGHT OPERATIONS**

SAMPEX requires a near polar orbit on a zenith-nadir pointing, spinning spacecraft. A scan in local time is part of the mission objectives, hence Sun synchronism is not desired. The orbital altitude has been selected to give a minimum lifetime of 3 years in order to be confident of observing several large solar particle events, to monitor the precipitating electron flux over a significant portion of a solar cycle, and to collect statistics on low intensity phenomena such as the anomalous component and galactic cosmic rays. Our detailed orbital lifetime analysis shows that with body mounted solar cells, a 3-year lifetime requires a 580 km altitude for solar maximum conditions (see Appendix F.a). In this low orbit, SAMPEX will receive a very low radiation exposure (see Appendix F.c) and the body mounted solar cells can provide ample power (see Appendix E.a).

The SAMPEX spacecraft is anticipated to be a NASA supplied spacecraft essentially similar to those described in Appendix A of the A.O., except that SAMPEX will not require as complex a spacecraft as the examples given in the A.O. For example, compared to the 132 kg zenith-nadir 3-axis stabilized spacecraft with solar paddles and 81 W available to the science instrument, the configuration needed for SAMPEX is considerably lighter since it does not need the pointing system, the paddles, or as large a power system. From informal discussions with Mr. R. Pincus (GSFC Code 740.2), it appears that the a Small-Class Explorer spacecraft configured to meet SAMPEX requirements would have a  $\approx 110$  kg mass.

A near polar orbit of  $82^\circ$  inclination is considered here for the nominal mission since it gives adequate coverage of different cutoff rigidities, and it increases the payload mass by about 7 kg compared to a  $90^\circ$  orbit (see Appendix F.b). Using the "payload mass" data in the A.O. for polar orbit, this results in a 168 kg payload for the  $82^\circ$  orbit at the required height. Thus, there is  $168 - 110 = 58$  kg available for SAMPEX, thus allowing some margin over the 54.5 kg mass of the instrument.

The SAMPEX experiment has a data rate of approximately 6000 bits/second. Currently available storage devices can store approximately 2 days of data before playback. No routine commanding is planned except for occasional operation of the experiment calibrators. Thus, we envision routine operations can consist of a single acquisition by the Wallops Island station every second day.

## 7. DATA REDUCTION AND ANALYSIS PLAN

Data processing and analysis will be performed at each of the participating institutions. The single copy of the spacecraft data stream sent to the University of Maryland will be processed to put data in proper time order and to remove overlaps. It then will be merged with attitude/ephemeris data supplied by NASA and sent to each of the Co-I institutions. Each Co-I group that has contributed hardware will take the lead in the processing of its own data to easily interpretable physical units. It is anticipated that different members of the team will collaborate as subgroups in scientific investigations, according to their scientific interests. Appendix G gives brief biographical sketches of all the investigators and examples of recent publications. We also anticipate the participation of several graduate students performing their Ph.D. thesis research using SAMPEX observations.

Reduced SAMPEX data will be submitted to the NSSDC. We recognize, however, that the time period near solar maximum will be of special interest to the solar physics community and in particular to members of the community carrying out observations on balloons, or with spacecraft. We plan to make SAMPEX data rapidly available to such groups in support of their work. We also anticipate carrying out correlative studies with other groups concerning, for example,

- modulation studies of galactic cosmic rays, done in collaboration with Pioneer, Voyager, Ulysses, and Galileo,
- examination of composition and spectra in gamma-ray line flares, in collaboration with SMM, GRO, Solar-A, and possible balloon experiments,
- comparison of precipitating electron observations with LANL experiments on geostationary satellites and CRRES; comparison with atmospheric ozone measurements by the SAGE II sensor system (LaRC, NASA) and UARS, and with balloon and rocket data (R. Holzworth, U. Wash., and R. Goldberg, GSFC), and ground based riometer and Schumann resonance monitoring stations, and
- studies of the acceleration and propagation of impulsive solar particles, in collaboration with Type III radio burst studies.



**Appendix A**

**References**

References

- Adams, J. H., A. J. Tylka, L. P. Beahm, C. H. Tsao, and B. Stiller 1987, *Proc. 20th Internat. Cosmic Ray Conf. (Moscow)*, **3**, 446.
- Althouse, W. E., A. C. Cummings, T. L. Garrard, R. A. Mewaldt, E. C. Stone, and R. E. Vogt 1978, *IEEE Trans. Geosci. Electron.*, **16**, 204.
- Anders, E. and M. Ebihara 1982, *Geochim. Cosmochim. Acta*, **46**, 2362.
- Baker, D. N., J. B. Blake, D. J. Gorney, P. R. Higbie, R. W. Klebesadel, and J. H. King 1987, *Geophys. Res. Lett.*, **14**, 1027.
- Baker, D. N., J. B. Blake, R. W. Klebesadel, and P. R. Higbie 1986, *J. Geophys. Res.*, **91**, 4265.
- Becker, R. H. 1980, *Earth and Planetary. Science Letters*, **50**, 189.
- Begemann, F., W. Born, W. Palme, E. Vilcek, and H. Wänke 1972, *Proc. Lunar Sci. Conf. 3rd*, 1693.
- Biswas, S., etal 1987, *Proc. 20th Internat. Cosmic Ray Conf. (Moscow)*, **3**, 451.
- Black, D. C. 1983, *Astrophys. J.*, **266**, 889.
- Breneman, H. H. and E. C. Stone 1985, *Astrophys. J. (Letters)*, **299**, L57.
- Cameron, A. G. W. 1982, in *Essays in Nuclear Astrophysics*, ed. C. A. Barnes, D. D. Clayton, and D. N. Schramm, (Cambridge University Press).
- Callis, L. B., D. N. Baker, J. B. Blake, R. W. Klebesadel, D. J. Gorney, and M. Natarajan 1988, *Trans. Am. Geophys. U.*, **69**, 310.
- Casse, M. and J. A. Paul 1982, *Astrophys. J.*, **258**, 860.
- Chupp, E. L. 1984, *Ann. Rev. Astron. Astrophys.*, **22**, 359.
- Cummings, A.C., and E. C. Stone 1987, *Proc. 20th Internat. Cosmic Ray Conf. (Moscow)*, **3**, 413.
- Cummings, A.C., E. C. Stone, and W. R. Webber 1984, *Astrophys. J. (Letters)*, **287**, L99.
- Evenson, P., P. Meyer, S. Yanagita, and D. J. Forrest 1984, *Astrophys. J.*, **283**, 439.
- Fanselow, J. L. and E. C. Stone 1972, *J. Geophys. Res.*, **77**, 3999.
- Fisk, L. A. 1978, *Astrophys. J.*, **224**, 1048.
- Fisk, L. A., B. Kozlovsky, and R. Ramaty 1974, *Astrophys. J. (Letters)*, **190**, L35.
- Flückiger, E.O., D. F. Smart, and M. A. Shea 1986, *J. Geophys. Res.*, **91**, 7925.
- Garcia-Muñoz, M. private communication, 1986.
- Garcia Muñoz, M., G. M. Mason, and J. A. Simpson 1973, *Astrophys. J. (Letters)*, **182**, L81.
- Geiss, J. 1973, *Proc. 13th Internat. Cosmic Ray Conf. (Denver)*, **5**, 3375.
- Geiss, J., F. Buehler, H. Cerutti, P. Eberhardt, and Ch. Filleux 1972, *Apollo 16 - Preliminary Science Report, NSDS SP-315*, p.14-1.
- Geiss, J. and P. Bochsler 1982, *Geochim. Cosmochim. Acta*, **46**, 529.
- Gloeckler, G. 1979, *Rev. Geophys. Space. Phys.*, **17**, 569.
- Gloeckler, G., D. Hovestadt, O. Vollmer, and C. Y. Fan 1975, *Astrophys. J. (Letters)*, **200**, L245.
- Grün, E., and Rauser, P., 1969, *Space Res.*, **IX**, 147.
- Higbie, P. R., R. W. Klebesadel, D. N. Baker, M. S. Gushoven, and J. B. Blake, 1987, *J. Geophys. Res.*, (submitted).
- Hovestadt, D., G. Gloeckler, B. Klecker, and M. Scholer 1984, *Astrophys. J.*, **281**, 463.
- Hovestadt, D., O. Vollmer, G. Gloeckler, and C. Y. Fan, 1973, *Phys. Rev. Letters*, **31**, 650.
- Imhof, W. L., J. B. Reagan, and E. E. Gaines 1971, *J. Geophys. Res.*, **76**, 4276.

- Jokipii, J. R. 1986, *J. Geophys. Res.*, **91**, 2929.
- Klecker, B., D. Hovestadt, G. Gloeckler, and C. Y. Fan, 1980, *Geophys. Res. Lett.*, **7**, 1033.
- Klecker, B. *et al.* 1984, *Astrophys. J.*, **281**, 458.
- Kocharov, L. G., and G. E. Kocharov 1981, Ioffe Physico-Technical Institute, Leningrad, preprint No. 722.
- Luhn, A., B. Klecker, D. Hovestadt, G. Gloeckler, F. M. Ipavich, M. Scholer, C. Y. Fan, and L. A. Fisk 1984, *Adv. Space Res.*, **4**, No. 2-3, 161.
- Luhn, A., D. Hovestadt, B. Klecker, M. Scholer, G. Gloeckler, F. M. Ipavich, A. B. Galvin, C. Y. Fan, and L. A. Fisk 1985, *Proc. 19th Internat. Cosmic Ray Conf. (La Jolla)*, **4**, 241.
- Mason, G. M., L. A. Fisk, D. Hovestadt, and G. Gloeckler 1980, *Astrophys. J.*, **239**, 1070.
- Mason, G. M., D. V. Reames, B. Klecker, D. Hovestadt, and T. T. von Rosenvinge 1986, *Astrophys. J.*, **303**, 849.
- McDonald, F. B., B. J. Teegarden, J. H. Trainor, and W. R. Webber 1974, *Astrophys. J. (Letters)*, **187**, L105.
- McDonnell, J. A. M., 1971, *Space Res.*, **XI**, 415.
- Mc Kibben, R.B. 1977, *Astrophys. J. (Letters)*, **217**, L113.
- Mewaldt, R. A. 1983, *Rev. Geophys. Space. Phys.*, **21**, 295.
- Mewaldt, R. A., J. D. Spalding, and E. C. Stone 1984, *Astrophys. J.*, **280**, 892.
- Mewaldt, R. A. and E. C. Stone 1987, *Proc. 20th Internat. Cosmic Ray Conf. (Moscow)*, **3**, 255.
- Mewaldt, R. A., and E. C. Stone 1989, *Astrophys. J.*, in press.
- Meyer, Jean-Paul 1985, *Proc. 19th Internat. Cosmic Ray Conf. (La Jolla)*, **9**, 141.
- Nakada, M. P. 1969, *Solar Phys.*, **7**, 302.
- Olive, K. A. and D. N. Schramm 1982, *Astrophys. J.*, **257**, 276.
- Pailer, N., and Grün, E., 1980, *Planet. Space Sci.*, **28**, 321.
- Paulikas, G. A., and J. B. Blake 1979, in *Quantitative Modeling of Magnetospheric Processes, Geophys. Monogr. Ser.*, **21**, ed. W. P. Olson, (Washington: AGU), p. 180.
- Penzias, Arno. A. 1983, *Science*, **208**, 663.
- Prantzos, N., M. Arnould, J. P. Arcoragi, and M. Casse 1985, *Proc. 19th Internat. Cosmic Ray Conf. (La Jolla)*, **3**, 167.
- Ramaty, R., and R. J. Murphy 1987, *Space Sci. Rev.*, **45**, 213.
- Reagan, J. B., R. E. Meyerott, R. W. Nightingale, R. C. Gunton, R. G. Johnson, J. E. Evans, and W. L. Imhof 1981, *J. Geophys. Res.*, **86**, 1473.
- Rees, M. H. and R. G. Roble 1979, *Planet. Space Sci.*, **27**, 453.
- Rees., M. H. and G. J. Romick 1985, *J. Geophys. Res.*, **10**, 9871.
- Sentman, D. D. 1983, *J. Atmos. Terr. Phys.*, **45**, 55.
- Sentman, D. D. and D. N. Baker 1987, *Abstracts IUGG XIX General Assembly, Vancouver, B. C.*, p 523.
- Serlemitsos, A. T. and V. K. Balasubrahmanyam 1975, *Astrophys. J.*, **198**, 195.
- Shea, M. A., and D. F. Smart 1983, *Proc. 18th Internat. Cosmic Ray Conf. (Bangalore)*, **3**, 415.
- Shea, M. A., D. F. Smart, and H. Carmichael 1976, AFGL-TR-76-0115.
- Simpson, J. A. 1983, *Ann. Rev. Nuc. Part. Sci.*, **33**, 323/
- Simpson, J. A., J. P. Wefel, and R. Zamow 1983, *Proc. 18th Internat. Cosmic Ray Conf. (Bangalore)*, **10**, 332.
- Smart, D. F., M. A. Shea, and Gall, R. 1969, *J. Geophys. Res.*, **74**, 4731.

- Shea, M. A., D. F. Smart, and J. R. McCall 1967 *Canad. Jour. Phys.*, **46**, S1098.
- Soutoul, A., M. Casse, and E. Juliusson 1978, *Astrophys. J.*, **219**, 753.
- Thorne, R. M. 1980, *Pure Appl. Geophys.*, **118**, 128.
- Van Hollebeke, M. A. I., and F. B. McDonald 1985, *Proc. 19th Internat. Cosmic Ray Conf. (La Jolla)*, **4**, 209.
- von Rosenvinge, T. T., et al. 1975, *Proc. 14th Internat. Cosmic Ray Conf. (Munich)*, **5**, 793.
- Wannier, P. G. 1980, *Ann. Rev. Astron. Astrophys.*, **18**, 399.
- Wiedenbeck, M. E. 1983, *Proc. 18th Internat. Cosmic Ray Conf. (Bangalore)*, **9**, 147.
- Wiedenbeck, M. E., and D. E. Greiner 1980, *Astrophys. J. (Letters)*, **239**, L139.
- Wiedenbeck, M. E., and D. E. Greiner 1981, *Astrophys. J. (Letters)*, **247**, L119.
- Wieler, R., H. Baur and P. Signer 1986, *Geochim. Cosmochim. Acta*, **50**, 1997.
- Woosley, S. E. and Thomas A. Weaver 1981, *Astrophys. J.*, **243**, 561.

**Appendix B**

**Collecting Power  
Comparison to Planned Experiments**

## Appendix B

### Comparison with Past and Planned Missions

Although there are currently *no* high resolution isotope spectrometers operating in space that are designed to measure solar or cosmic ray isotopes, there are previous and planned space flight instruments that have and will be providing such measurements. The characteristics of those instruments that have flown or are expected to fly prior to the SAMPEX mission are summarized below.

For those instruments that achieve sufficient mass resolution and background rejection to cleanly resolve isotopes, it is the *collecting power* of the instrument (geometry factor  $\times$  time integrated over the appropriate energy spectra) that ultimately determines the accuracy to which isotope abundances can be determined. In the following collecting power is estimated by taking into account the geometry factor, an appropriate spectrum integrated over the instrument's energy interval for isotope analysis, the duty cycle as determined by the orbit, and the actual or assumed time interval of measurement (lifetime). Figure B-1 and Tables B-1, B-2, and B-3 compare the collecting power of all such instruments that either have flown or are scheduled to fly prior to the SAMPEX mission. Note that for solar flare isotopes LEICA and MAST should provide about 1 to 2 orders of magnitude improvement in collecting power over all previous missions up to that time. Similarly, MAST can provide about an order of magnitude improvement for anomalous cosmic ray isotope studies. For galactic cosmic ray isotopes MAST will have comparable collecting power to the Ulysses and CRRES instruments.

In addition to the instruments listed, it is expected that instrumentation planned for the ISTP program and expected to be launched during the early to mid 1990's will provide comparable collecting power to that proposed for SAMPEX. Sources for the information in the following tables include the following: for the Caltech instrument on *ISEE 3*, Althouse *et al.* (1978) and Mewaldt, Spalding, and Stone (1984); for the UCB experiment on *ISEE-3*, Wiedenbeck and Greiner (1981); for CRIE and EHIC, Simpson, Wefel, and Zamow (1983); for Ulysses and CRRES, Garcia-Muñoz (1986).

**Table B-1**

Solar Energetic Particle Isotope Spectrometers

Mission or Instrument	Institution	Geometry Factor (cm <sup>2</sup> sr)	<sup>28</sup> Si Threshold (MeV/nuc)	Duty Cycle	Lifetime (years)	Relative Collecting Power <sup>a</sup>
ISEE-3	CIT	0.7	8.5	1.0	0.3	29
CRIE	Chicago	1.5	17	0.3 <sup>b</sup>	0.5	8
EHIC	Chicago	1.5	17	0.3 <sup>b</sup>	3	47
MAST	CIT/GSFC	14	19	0.3 <sup>b</sup>	3	350
LEICA	UMd	1.0	0.65	0.3 <sup>b</sup>	3	5000

<sup>a</sup> Collecting Power  $\equiv$  (Geometry Factor)  $\times$  (Duty Cycle)  $\times$  (Lifetime)  $\times$  ( $E/10$ )<sup>-2</sup>  $\times$  100, where  $E$  is the threshold for <sup>28</sup>Si analysis. For LEICA a long-term average solar-flare spectrum was used.

<sup>b</sup> Polar Orbit

**Table B-2**

Anomalous Cosmic Ray Spectrometers

Mission or Instr.	Inst.	Geometry Factor (cm <sup>2</sup> sr)	<sup>16</sup> O Threshold (MeV/n)	Spectral <sup>a</sup> Factor	Duty Cycle	Lifetime (years)	Relative Collecting Power <sup>b</sup>
ISEE-3	CIT	0.7	6.5	$\equiv$ 1.	1.0	0.3	21
CRIE	Chicago	1.5	12	0.5	0.4 <sup>c</sup>	0.5	15
EHIC	Chicago	1.5	12	0.5	0.4 <sup>c</sup>	3	90
MAST	CIT/GSFC	14	14	0.4	0.4 <sup>c</sup>	3	670

<sup>a</sup> Integrated flux of ACR O from threshold to 30 MeV/nuc.

<sup>b</sup> Collecting Power  $\equiv$  (Geom. Factor)  $\times$  (Spectral Factor)  $\times$  (Duty Cycle)  $\times$  (Lifetime)  $\times$  100.

<sup>c</sup> Assuming singly-charged <sup>16</sup>O and a polar orbit.

**Table B-3**

Galactic Cosmic Ray Isotope Spectrometers

Mission or Instrument	Institution	Geometry Factor (cm <sup>2</sup> sr)	<sup>28</sup> Si Energy Interval (MeV/nuc)	Duty Cycle	Lifetime (years)	Relative Collecting Power <sup>a</sup>
ISEE-3	CIT	0.7	8 - 200	1.0	0.3	40
ISEE-3	UCB	1.4	90 - 320	1.0	2	640
CRIE	Chicago	1.5	17 - 150	0.3 <sup>b</sup>	0.5	30
Ulysses	Chicago	6	90 - 300	1.0	3	3780
CRRES	Chicago	6	135 - 330	0.6 <sup>c</sup>	3	2110
EHIC	Chicago	1.5	17 - 150	0.3 <sup>b</sup>	3	180
MAST	CIT/GSFC	10	19 - 230	0.3 <sup>b</sup>	3	1900

<sup>a</sup> Collecting Power  $\equiv$  (Geometry Factor)  $\times$  (Energy Interval)  $\times$  (Duty Cycle)  $\times$  Lifetime

<sup>b</sup> Polar orbit

<sup>c</sup> Elliptical Earth orbit



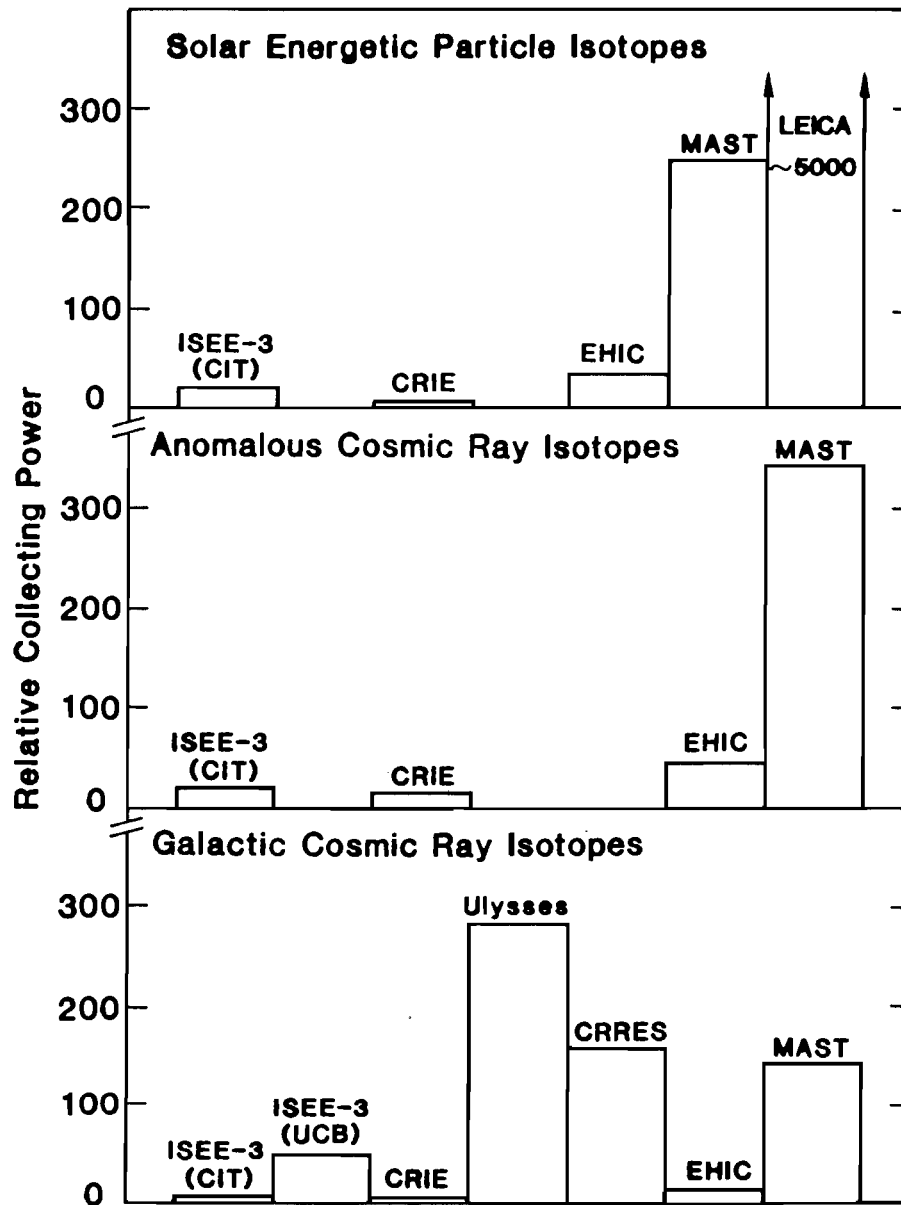


Fig. B-1 A comparison of the relative collecting power of past and planned isotope spectrometers up until the time of the SAMPEX Mission, taking into account the appropriate geometry factors, threshold and endpoint energies, and instrument duty-cycles and lifetimes. HILT, whose sensitivity exceeds MAST, is not shown since it does not resolve heavy isotopes.

**Appendix C**

**Instrumental Techniques and Performance**

## Appendix C

### Instrumental Techniques and Performance

#### a) MAST Measurement Technique and Expected Mass Resolution

The resolution of isotopes by MAST is accomplished by the standard technique of measuring a particle's energy loss  $\Delta E$  in a detector of thickness  $L_0$ , and its residual energy loss  $E'$ , in a thicker detector. For illustration, assume that the range  $R$  of a particle of mass  $M$ , charge  $Z$ , and kinetic energy  $E$  is given by

$$R = \frac{kM}{Z^2} \left( \frac{E}{M} \right)^a$$

where  $a \simeq 1.77$  for protons in silicon. Combining this with a similar equation for the range  $R - L$  of the particle with energy  $E'$  after traversing a thickness  $L$ , we can solve for the mass

$$M = \left( \frac{LZ^2}{k} \right)^{\frac{1}{1-a}} (E^a - E'^a)^{\frac{1}{1-a}}$$

The sources of uncertainty that affect the mass determination can be quantitatively evaluated by taking appropriate partial derivatives of this expression.

As is apparent in the above equation, the pathlength  $L$  of the particle through the  $\Delta E$  detector must be known in order to calculate the correct mass from the measured  $\Delta E$  and  $E'$ . For a particle that is incident at an angle  $\theta$  with respect to the normal to the  $\Delta E$  detector of thickness  $L_0$ , the pathlength is given by  $L = L_0 \sec \theta$ . The essential function of the position sensing detectors (PSDs) is to determine  $\theta$  for each incident particle.

Solid-state matrix detectors were used as active two-dimensional position sensing elements in the Caltech HIST instrument on *ISEE 3*, where the strips of two 24 x 24 matrix detectors were individually analyzed to provide 1 mm spatial resolution over a  $\sim 6 \text{ cm}^2$  area. The MAST PSDs will have 0.5 mm strip spacing over a  $\sim 20 \text{ cm}^2$  area. MAST uses a charge division scheme to determine position, thereby greatly simplifying the required electronics while preserving the necessary spatial resolution. In this scheme the charge collected on, e.g., the X strips on M1, is resistively divided between two charge sensitive preamps (X1, X2) at opposite ends of the X divider network so that the total energy loss in M1 is measured by (X1 + X2) while the X coordinate of the incident particle is determined by (X2-X1) / (X1+X2). We have tested this technique extensively in calibrations of these detectors with various beams at the Bevalac and find the spatial resolution to be as expected.

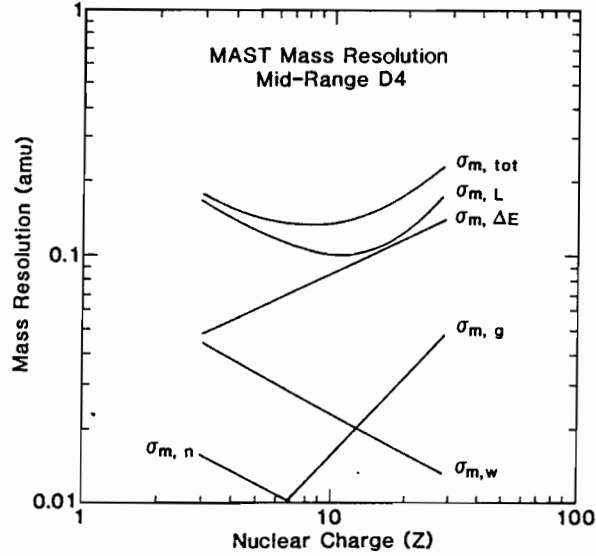
For high-Z particles that undergo large energy losses in the PSDs, this technique leads to a spatial resolution approaching that due to the strip spacing of 0.5 mm. For lighter particles, the preamplifier noise and PHA channel width contribute to the spatial resolution, so that in the worst case,  $\sigma_m = 0.3 \text{ amu}$  for  ${}^6\text{Li}$  stopping in D6.

Figure C-1 shows the contributions to the total mass resolution  $\sigma_m$  of MAST as a function of charge for the case of particles stopping midway through D4. Notice that  $\sigma_m$  is dominated by pathlength variations due to trajectory uncertainties ( $\sigma_{m.L(\theta)}$ ) and by ionization energy loss fluctuations ( $\sigma_{m.\Delta E}$ ). Figure C-2 shows the expected mass resolution for  ${}^{12}\text{C}$ ,  ${}^{28}\text{Si}$ , and  ${}^{58}\text{Ni}$  as a function of range in the detector stack, evaluated midway through the stopping detector. Although  $\sigma_{m.\Delta E}$  depends on how far the particle penetrates into the  $E'$  detector, its value at the midpoint is representative of the average resolution in each range.

The line labeled  $\sigma_{m.L(\theta)}$  in Figure C-1 represents the contribution of the uncertainty in the pathlength determined by the angle of incidence, evaluated at a typical angle of  $20^\circ$ . Three separate contributions to  $\sigma_{m.L(\theta)}$  can be identified:

$$\frac{\sigma_{m.pn}}{M} = 1.3\sqrt{2} \sin \theta \cos \theta \frac{X_{max}}{l_0} \frac{e_n C k}{\sqrt{rb} \Delta E}$$

$$\frac{\sigma_{m.w}}{M} = \frac{1.3}{\sqrt{6}} \sin \theta \cos \theta \frac{X_{max}}{l_0} \frac{w}{\Delta E}$$



**Fig. C-1** Contributions to the mass resolution of MAST evaluated for nuclei with nuclear charge  $3 \leq Z \leq 28$  that stop midway through D4 at a typical incidence angle of  $20^\circ$ . The various contributions include preamp noise (n); PHA channel width (cw); PHA gain stability (g); energy loss fluctuations in the  $\Delta E$  detectors ( $\Delta E$ ); and pathlength variations due to trajectory uncertainties ( $L(\theta)$ ). These are combined in quadrature to give the total mass resolution (tot). See text for more information.

$$\frac{\sigma_{m.sec\theta}}{M} = \frac{1.3}{\sqrt{6}} \sin \theta \cos \theta \frac{s}{l_o}$$

where:

- $w$  = analyzer channel width (MeV)
- $X_{max}$  = diameter of position sensing detector (cm)
- $l_o$  = M1, M3 separation = 3.6 cm.
- $e_n = 9 \times 10^{-10} V / \sqrt{HZ}$
- $C$  = detector capacitance (F)
- $k \sim 1.5$  (accounts for charge divider capacitance)
- $\tau \sim 10^{-6}$  sec
- $b \sim 4.44 \times 10^{-14}$  C/MeV
- $s$  = strip width (cm)
- $\Delta E$  = average energy loss in M1-M4 in MeV

In the limit  $\Delta E \rightarrow \infty$ , the position is determined to within one strip width ( $s$ ), and  $\sigma_{m.L(\theta)}$  depends only on the last term  $\sigma_{m.sec\theta}$ . For smaller values of  $\Delta E$ , there is a contribution due to the channel width of the PSD PHAs ( $\sigma_{m,w}$ ), and a contribution resulting from the PSD preamp noise ( $\sigma_{m,pn}$ ) due to detector capacitance. The MAST position sensing system has been designed so as to minimize the contribution of  $\sigma_{m.L(\theta)}$  to  $\sigma_m$ , without unnecessarily compromising the geometry factor of the instrument or increasing its electronic complexity.

The position information provided by the PSDs is also essential in minimizing the effect of response variations over the area of the  $\Delta E$  detectors  $\sigma_{m.L(t)}$ , due to thickness and charge collection non-uniformities. For the Caltech *ISEE 3* instrument we developed the technique of mapping the response of individual detectors using beams of relativistic  $^{40}\text{Ar}$  nuclei at the Bevalac and low energy protons from a tandem Van de Graaff. With these techniques it is possible to map detector response to an accuracy of  $\sim 0.1\%$ . Such

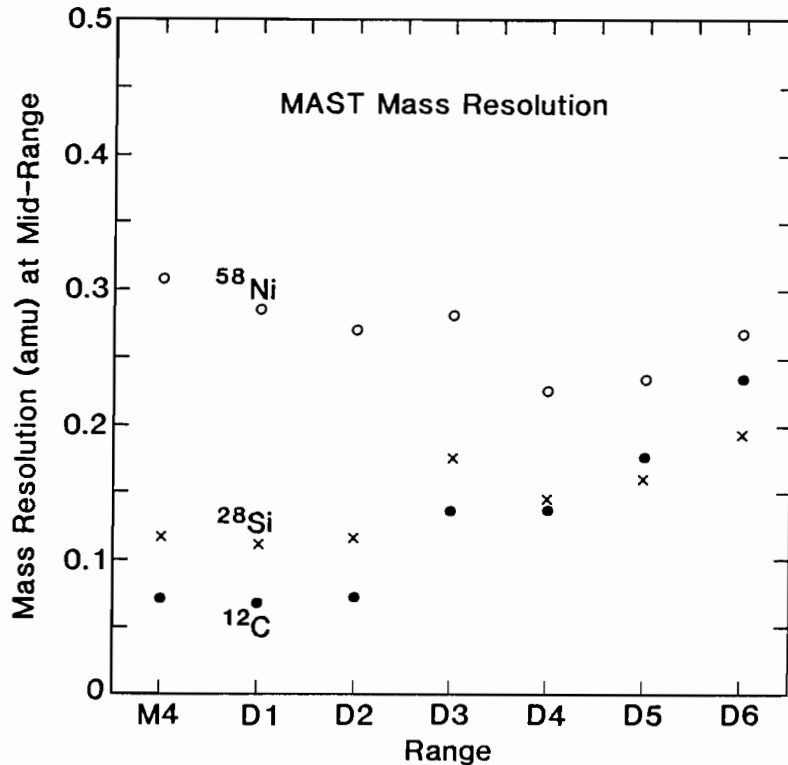


**Fig. C-2** Expected mass resolution ( $\sigma_{m,tot}$ ) in MAST for  $^{12}\text{C}$ ,  $^{28}\text{Si}$ , and  $^{58}\text{Ni}$  as a function of range within the telescope, evaluated midway through the last detector triggered at a typical incidence angle of  $20^\circ$ . The gradual increase in  $\sigma_{m,tot}$  deeper in the stack is a result of the gradual decrease in the energy deposited in the M1 and M4 (see above). The increase in  $\sigma_{m,tot}$  for  $^{58}\text{Ni}$  early in the stack is due to energy-loss fluctuations, taking into account the charge in the slope of the range-energy relationship of the heavy ions at low energies.

maps, in combination with the trajectory information, are used to correct the measured  $\Delta E$  pulse-heights in analyzing the flight data.

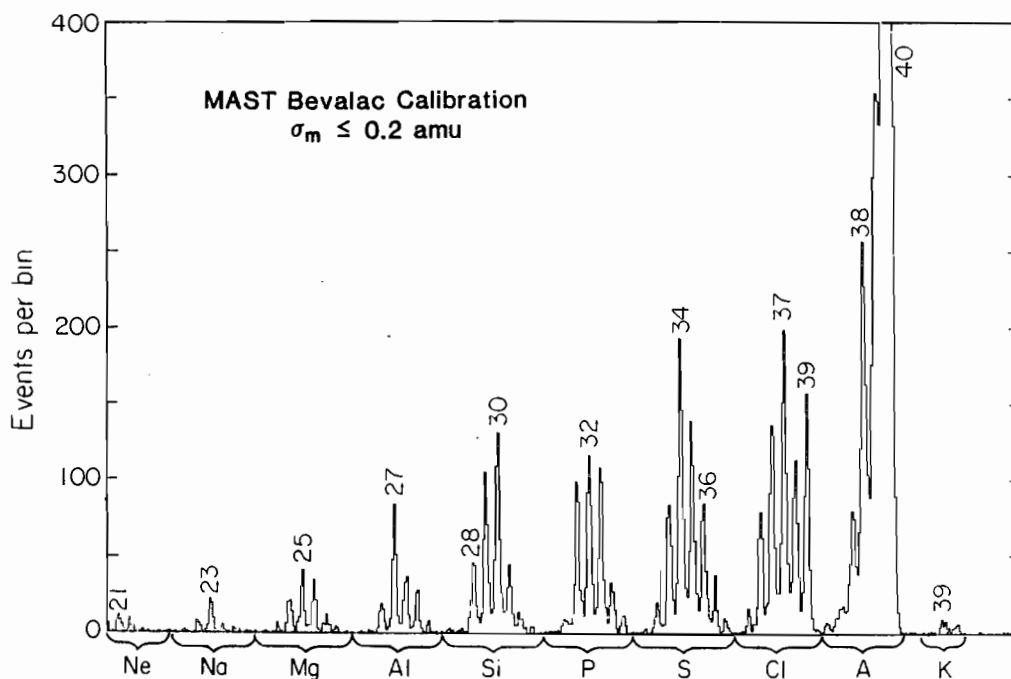
Note in Figure C-1 that electronic contributions to  $\sigma_m$ , such as  $\sigma_{m,n}$  and  $\sigma_{m,g}$  are negligible. MAST will achieve this performance by using the signal processing electronics technology originally developed for the Caltech EIS experiments (flown on IMPs 7 and 8) and further developed in thin-film hybrids for the Caltech HIST experiment on *ISEE 3*. The instrumentation consists of independent, parallel signal processing chains for each digitized parameter. Except for detector inputs, all signal interfaces with these chains are digital. Because these signal processors operate in a "normally open" linear gate mode, delay lines in the signal path are eliminated, along with their attendant non-linearity, poor temperature coefficient and weight. The 4095 channel analog-to-digital converters operate over a dynamic range of 1000:1 (full scale: threshold). Double integration, double differentiation, single pole RC shaping is used.

In MAST, background events due to nuclei that undergo nuclear interactions in the detector material are identified by comparing the redundant measurements of  $\Delta E$ . Note that there are always at least three such measurements in MAST, and in most cases more. Given sufficient event statistics, the MAST resolution should be sufficient to resolve all isotopes with  $Z < 30$ . For example, a mass resolution  $\sigma_m = 0.25$  amu is sufficient to resolve two adjacent isotopes whose relative abundance differs by a factor of  $\sim 100$  to 1.

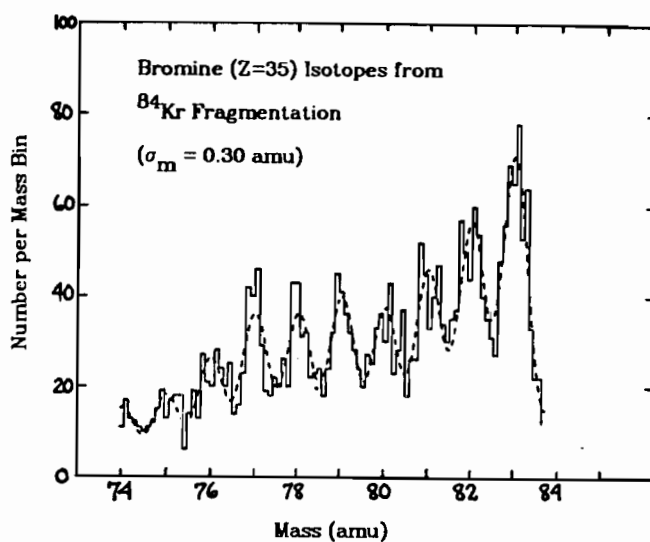
#### Mass Resolution Examples - MAST

In this section we present examples of the mass resolution that has been achieved using the Caltech HIST instrument flown on *ISEE-3* and the MAST detectors that were calibrated at the Bevalac in 1981 and

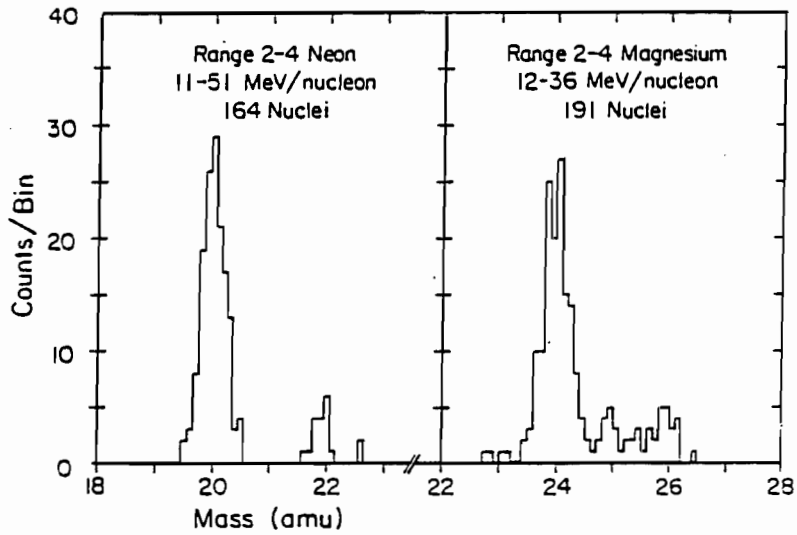
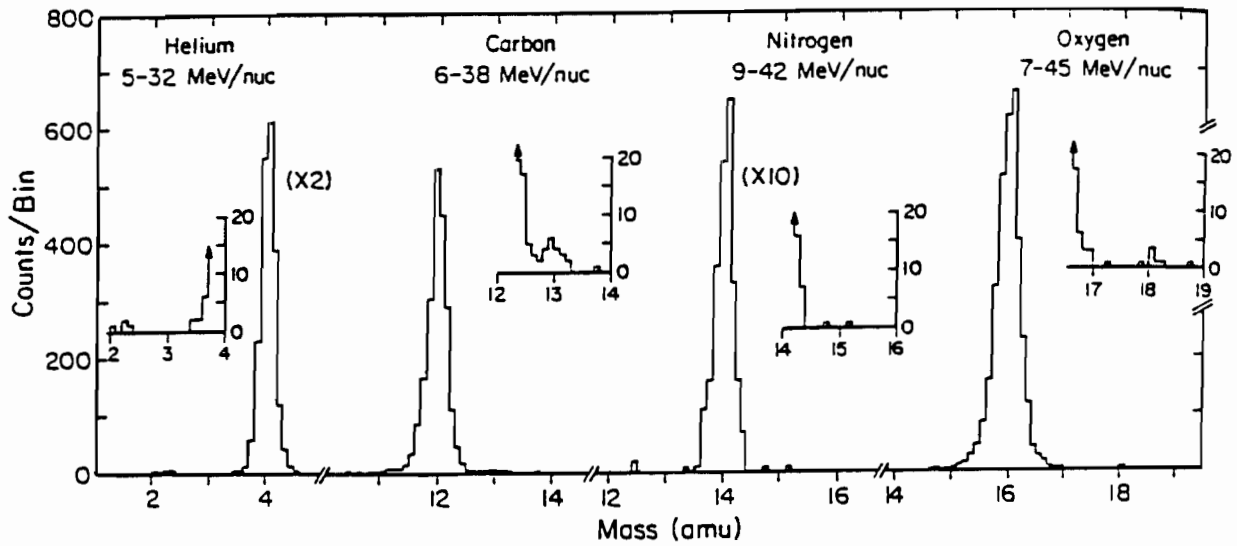
1984. The HIST and MAST telescopes are of similar design and use the same basic approach to identify isotopes as discussed above. The experimentally determined mass resolution in these examples is in basic agreement with the expected resolution based on the approach discussed above.



An example of the mass resolution achieved in Bevalac calibrations of the MAST detectors at the Bevalac. In this experiment a beam of  $^{40}\text{Ar}$  nuclei impinged on a  $\text{CH}_2$  target creating fragmentation products with typical energies of  $\sim 100$  MeV/nuc which then entered the MAST telescope. In the figure the relative yields of nuclei with  $10 \leq Z \leq 19$  are shown, with the dominant isotope of each isotope labeled. The  $^{40}\text{Ar}$  peak extends to  $>12,000$  events. On the abscissa, the isotopes of an individual element should be separated by  $\sim 14\%$  of the separation of the elements. The well resolved peaks show that the observed mass resolution is in all cases  $\leq 0.2$  amu, in agreement with the predicted resolution. Further improvement in the mass resolution can be expected when the response maps of the individual detectors are taken into account. These calibrations also tested and verified the position resolution capabilities of the MAST PSDs.

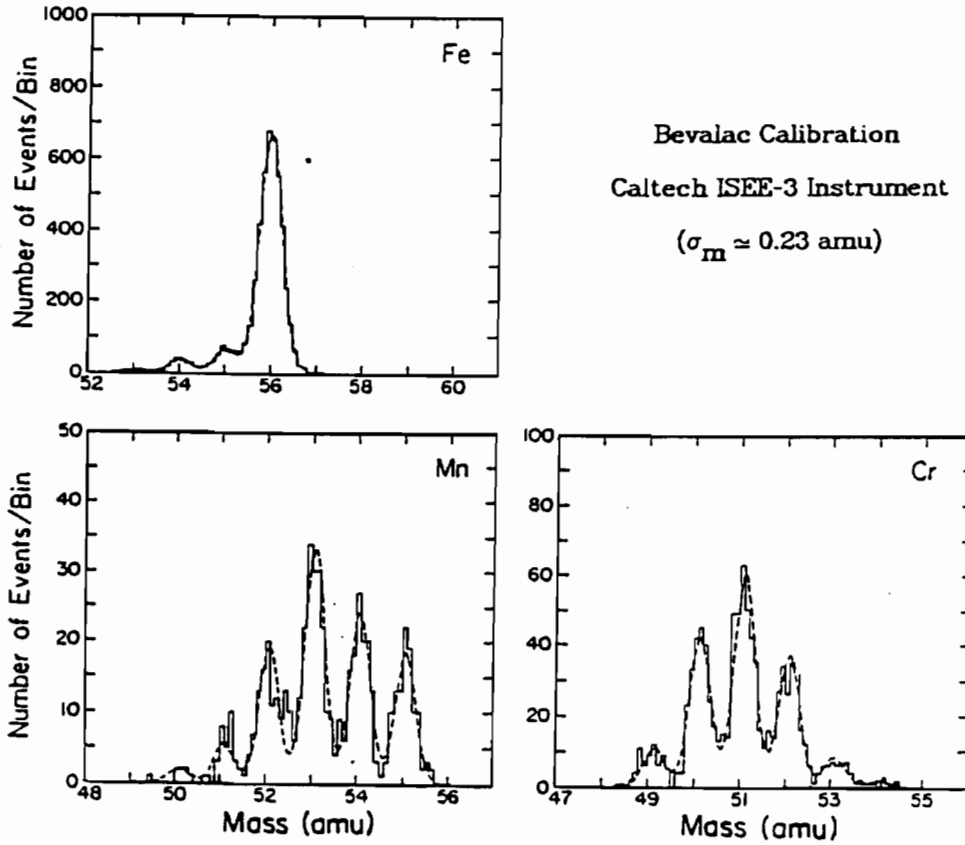


Mass histogram of Br (Z=35) isotopes obtained from a calibration of MAST detectors at the Bevalac. The Br isotopes, many of which are radioactive, were produced when a 300 MeV/nucleon Kr (Z=36) beam fragmented in a polyethylene target. The dashed line is a fit with  $\sigma_m = 0.30$  amu. The resolution is expected to improve somewhat when response maps are used to correct the  $\Delta E$  pulse heights.

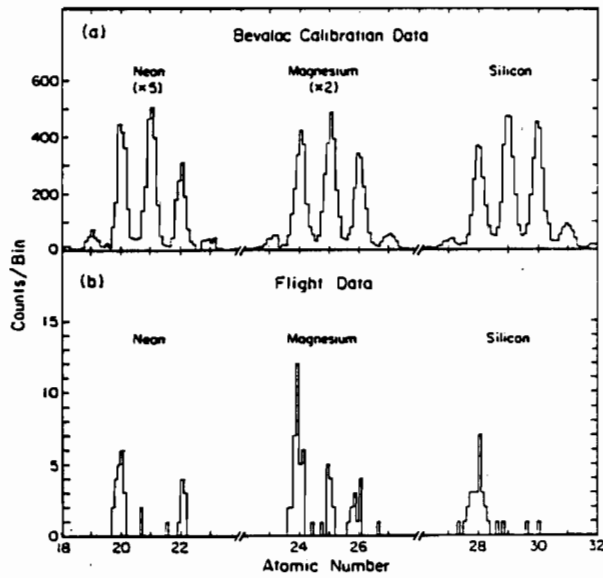


Mass distribution of He, C, N, O, Ne, and Mg isotopes obtained by the Caltech Heavy Isotope Spectrometer Telescope flown on ISEE-3. The observations were made during the large solar flare of 9/24/78.





Mass distributions of Cr, Mn, and Fe isotopes obtained in a Bevalac calibration of the Caltech Heavy Isotope Spectrometer Telescope that was launched on ISEE-3. The observed mass resolution is  $\sim 0.23$  amu.



Mass histograms of 30-180 MeV/nuc Ne, Mg, and Si isotopes from the Bevalac and from flight data, obtained with the Caltech ISEE-3 instrument. The galactic cosmic ray and Bevalac data were analyzed in exactly the same manner using identical instrument calibrations. The mass resolution in both cases is 0.2 amu.

## b) LEICA Instrument

### *LEICA performance*

The Low Energy Ion Composition Analyzer (LEICA) is virtually identical to the Solar Energetic Particle composition instrument developed at the University of Maryland for flight on a Space Shuttle Get-Away-Special (GAS) mission in 1988/1989. LEICA thus benefits from a four-year design and development effort at Maryland, which has produced a flight instrument. The GAS flight instrument was calibrated in our laboratory with alpha sources, and has been exposed to heavy ion beams at the Brookhaven Tandem Van de Graaff in January 1988. Figure C-3 shows the excellent timing resolution on the GAS flight instrument for 1.25 MeV/nucleon  $^4\text{He}$ , where a  $\sigma = 277$  psec was achieved. Figures C-4 and C-5 show the mass resolution for  $^{16}\text{O}$  and  $^4\text{He}$  obtained with the GAS instrument. For LEICA, we anticipate improved mass resolution over the GAS instrument that will be achieved by more efficient coupling to the MCPs, which will improve timing signal-to-noise ratios.

Figure C-6 shows a Monte-Carlo simulation of LEICA observations during the moderately large November 1977 solar particle event. The simulation took account of LEICA telemetry allocation, timing accuracy, trajectory determination error, FWHM due to non-ionizing collisions in the solid state detectors, electronic noise, and fraction of time spent by SAMPEX in the polar regions accessible to low energy solar particles. The relative abundances of major species in the figure are based on solar energetic particle observations, while for all the minor ions meteoritic abundances were used. It is clear from the figure that high resolution alone will not allow meaningful measurements of rare species: a large geometrical factor is also needed in order to detect a significant number of rarer ions. We note that although LEICA measures particle mass only, and not atomic number, there is no significant case of ambiguity of element type for particles of mass up to Fe.

### *LEICA modes of operation*

LEICA operates in its normal mode continuously except for about one hour/week when an on-board calibrator is activated by ground command. The multiparameter measurements returned by LEICA for each ion allow for self-calibration of the instrument in space: any shifts in detector response will result in a shift of particle tracks in the time-vs-energy data, which can be easily detected and corrected for. If necessary, there is a provision for uploading new look-up tables for the species rates to take account of possible drifts. The ability to adjust detector and MCP bias and four-fold redundancy in the solid state detector array helps protect against a wide range of possible drifts and malfunctions. LEICA uses no expendibles and employs space qualified or proven parts with which the investigator team has long experience. In LEICA, these parts are configured in a novel manner to achieve unprecedented measurements of suprathermal and energetic ions.

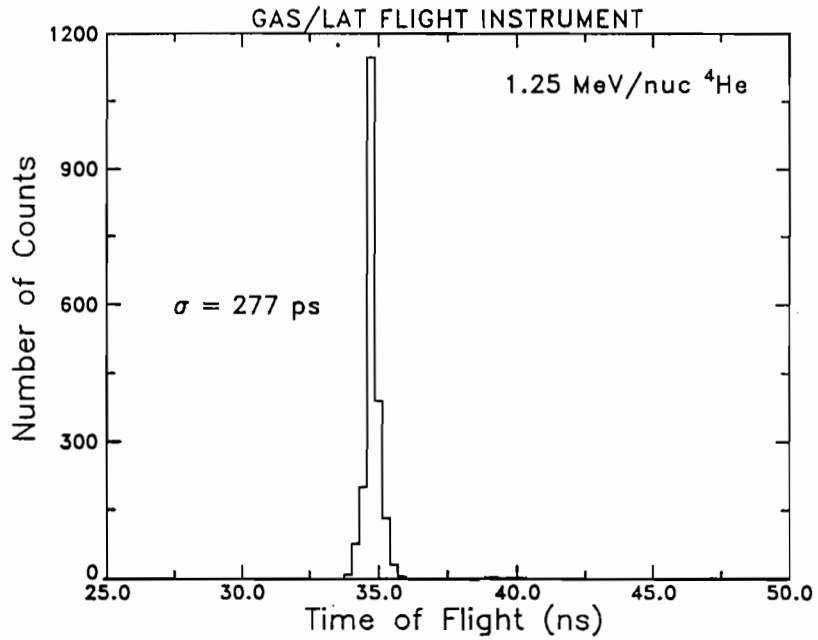


Fig. C-3 Prototype LEICA telescope timing resolution

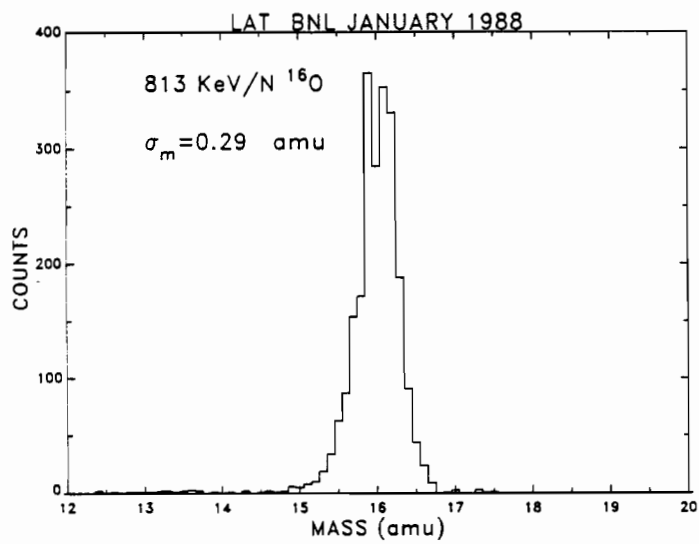


Fig. C-4 Prototype LEICA telescope mass resolution for  $^{16}\text{O}$ .

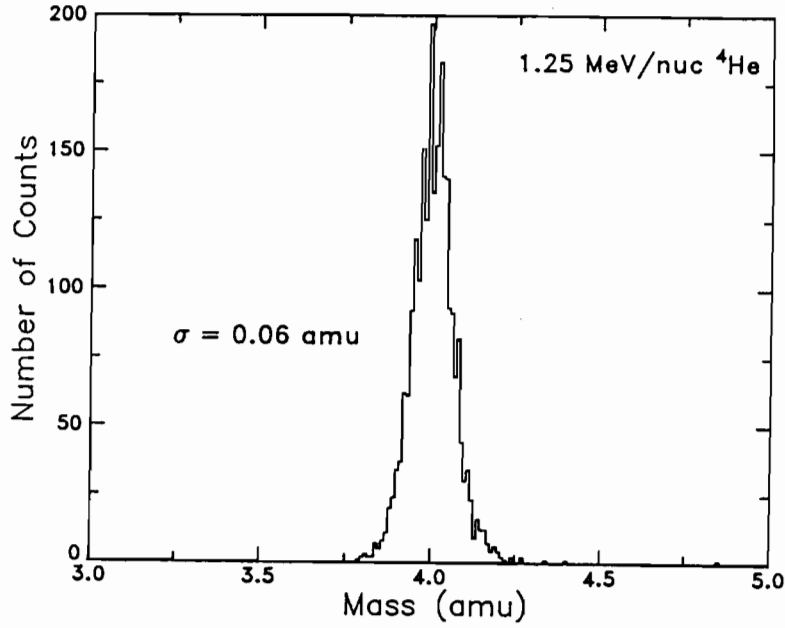


Fig. C-5 Prototype LEICA telescope alpha particle mass resolution.

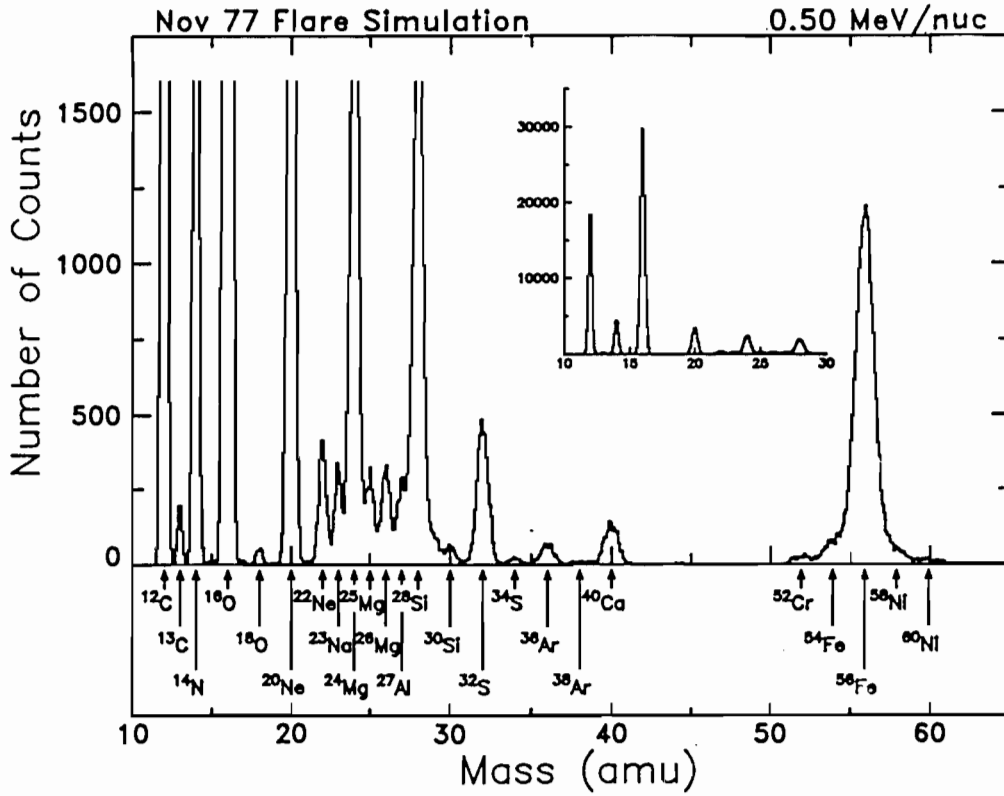


Fig. C-6 LEICA telescope simulated mass histogram for November 22, 1977 solar particle event.

### c) HILT Performance

The HILT sensor is designed to measure heavy ions from He to Fe in the energy range from 8 to 310 MeV/nucleon (for oxygen). In preparation of a STS flight of this sensor as part of a Get-Away-Special payload extensive calibration measurements at the Hahn Meitner Cyclotron (Berlin) have been made. Figure C-7 shows results from a calibration run, where reaction products produced by scattering a 800 MeV  $S^{32}$  beam on a thick Ni target have been measured with the sensor. The figure shows as an example a matrix of the ionization chamber versus SSD energy signal and demonstrates the high mass resolution and low background of the system. In this low energy range all low Z elements (He, Li, Be, B, C, N, and O) can easily be separated. For the elements between Ne and Fe this is true for the more abundant even Z elements. At low Z (He-B) the resolution is sufficient to also identify individual isotopes.

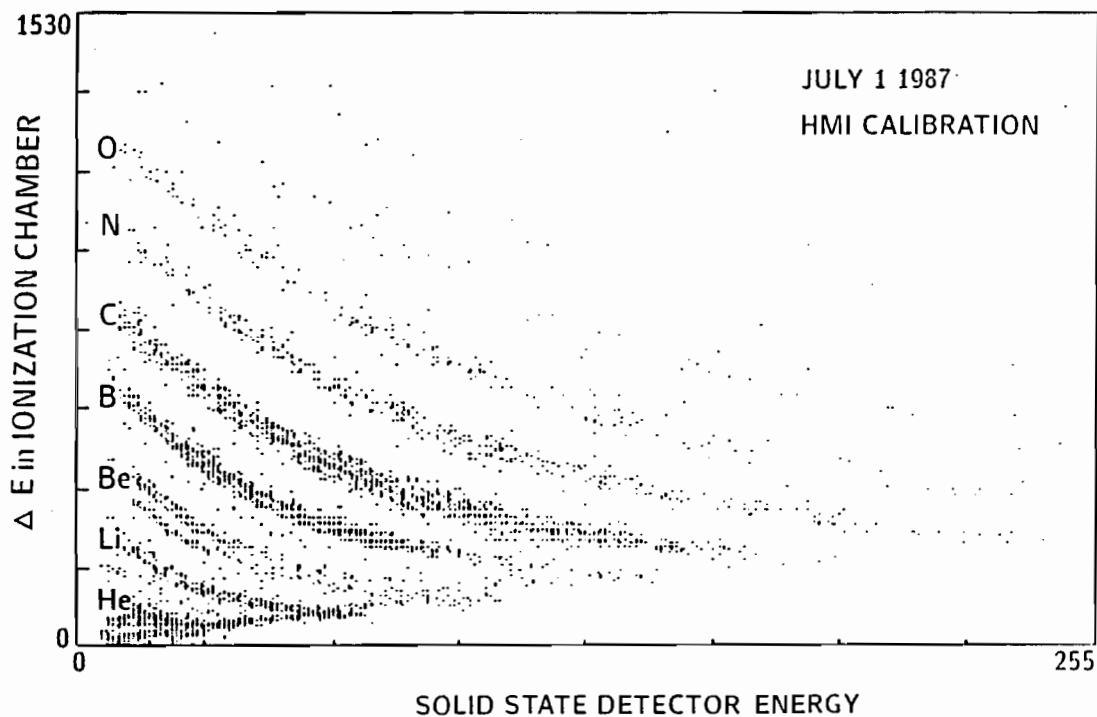


Fig. C-7 HILT heavy ion calibration data

**Appendix D**

**HILT Micrometeoroid Protection**

## Appendix D

### HILT Micrometeoroid Protection

The entrance window of the HILT ionization chamber (IC)-proportional counter (PC) system is subject to bombardment by micrometeoroids. If the mass of a micrometeoroid exceeds a certain critical mass, the impact of the micrometeoroid will create a pinhole in the foil. Gas leakage through these pinholes may give rise to the loss of the gas supply and therefore to the failure of the IC-PC system. In this appendix the probability of the failure of the IC-PC system of HILT due to the impact of micrometeoroids will be discussed. It will be shown that this probability is less than 8% in the first 2 years of operation.

The penetration limit of thin foils by micrometeoroids has been studied in great detail for sensors measuring interplanetary dust particles (e.g., Pailer and Grün 1980, and references therein). The critical thickness of the foil is increasing in general with projectile density and perpendicular velocity. In the velocity range under consideration ( $\sim 10$  km/s), however, to a good approximation particles with diameter  $d$  larger than the foil thickness will penetrate and create a hole of diameter  $D$  comparable to  $d$  (Grün and Rauser 1969). Upon penetration the micrometeoroids burst into many fragments (Pailer and Grün 1980). It is therefore possible to increase the effective thickness of the window by having a multi-layered structure. With two  $40 \mu$  Al foils a factor of 3-6 increase in the effective thickness can be realized, dependent on the bulk density of the micrometeoroids.

The mass spectrum and flux of micrometeoroids in the neighborhood of the earth is reasonable well known (e.g., McDonnell 1971, and references therein). The flux of micrometeoroids penetrating Al foils of equivalent thickness of  $400 \mu$  has been measured by several spacecraft (McDonnell 1971) and is about

$$F_m = 5 \cdot 10^{-8} (m^2 s 2\pi sr)^{-1}$$

This gives a mean time between penetrating impacts of 25 years. This in turn implies a 92% probability of 2 years of successful operation for the proposed instrumentation.

Finally, we point out that the assumption that all particles are vertically incident on the foil is implicit in the above considerations. If the angular distribution is taken into account, then the pathlength of particles will be increased and the perpendicular velocity decreased. Both effects will increase the critical mass and therefore a significant increase in the mean time between penetrating impacts can be expected. The above value of 92% for the probability of 2 years of successful operation can therefore be regarded as a lower limit.

**Appendix E**

**Spacecraft Accomodations/Requirements**



## Appendix E

### Spacecraft Accomodations/Requirements

SAMPEX is intended to be flown on a NASA supplied spacecraft such as those described in Appendix A of the Small-Class Explorer A.O. (OSSA 2-88). The experiment objectives require a zenith-nadir pointing spacecraft in a low altitude near-polar orbit. However, the spacecraft described in Appendix A of the A.O. generally have much greater capabilities than is required by SAMPEX. The configuration we need would use the basic spacecraft structure for the Small-Class Explorers, but would not have all the options (such as 3-axis stabilization and pointing) and so would be simpler, lighter, and less costly. A lighter spacecraft has the advantage of allowing a longer mission life, which directly benefits the scientific returns of SAMPEX. Below we examine some considerations involved with accomodating SAMPEX on the Small-Class Explorer spacecraft.

#### a) Mass

Consider the 132 kg zenith-nadir 3-axis stabilized spacecraft described in the A.O. in Appendix A, Table 1 (page A-9). This spacecraft has solar paddles and provides 81 W to the science instrument. The configuration needed for SAMPEX is considerably lighter since it does not need the pointing system, the solar paddles, or as large a power system. From informal discussions with Mr. R. Pincus (GSFC Code 740.2), it appears that the a Small-Class Explorer spacecraft configured to meet SAMPEX requirements would have a  $\approx 110$  kg mass. With this spacecraft mass, we can achieve our desired orbital inclination and lifetime as shown below.

Our detailed orbital lifetime analysis (Appendix F.a) shows that with body mounted solar cells (to reduce drag), a 3-year lifetime will be achieved for 580 km altitude under solar maximum conditions. A near polar orbit of  $82^\circ$  inclination is considered here for the nominal mission since it gives adequate coverage of different cutoff rigidities, and it increases the payload mass by about 7 kg compared to a  $90^\circ$  orbit (see Appendix F.b). Using the "payload mass" data in the A.O. for polar orbit, this results in a 168 kg payload for the  $82^\circ$  orbit at the required height. Thus, there is  $168 - 110 = 58$  kg available for SAMPEX, thus allowing some margin over the 54.5 kg mass of the instrument.

The low altitude orbit of SAMPEX has the additional advantage that the total radiation exposure over a three year mission is small (see Appendix F.c)

#### b) Experiment Power Requirements

Assume a quasi-cylindrical spacecraft 38 inches in diameter and 60 inches long:

$$\text{Total Area} = 2\pi rh + 2\pi r^2 = 2\pi \times 19 \times 60 + 2\pi \times (19)^2 = 9431 \text{ square inches}$$

$$\text{Ave. pwr} = A \times \epsilon \times (.067 \text{ watts/sq in}) = 79 \text{ watts}$$

where  $\epsilon \approx 1/8$  is the typical correction for the random incidence direction of sunlight on the solar cells.

We have assumed "garden variety" solar cells. Higher performance cells could be used. Of course some space on the surface will be required for instrument apertures, antennas, attitude sensors, etc. However the zenith orientation of the spacecraft will tend to provide a larger average illuminated surface than the random assumption.

We now consider the required power using the Ball Scout Satellite Model. Table E-1 summarizes power allocation during data acquisition mode (SAMPEX experiments on, RF off), and data dump mode (SAMPEX experiments off, RF on). Data acquisition mode has the larger power needs, totalling 47.5 W, but this is much less than the roughly 79 W available from the above simple calculation. Thus a substantial power margin exists. The maximum shadow is approximately 36% of an orbit.

$$(79 \text{ watts}) (1 - .36) = 51 \text{ watts}$$

Thus sufficient power is available even during maximum shadow.

**Table E-1 Power Allocation**

<b>Data Acquisition Mode</b>	
GSTN Transponder	3.0 watts
antenna switch	0.1
battery shunt regulator	4.0
CMD and data	15.0
heaters	6.0
magnetometer	0.7
single axis gyro	2.0
SAMPEX experiments	16.7
<b>TOTAL:</b>	<b>47.5 watts</b>

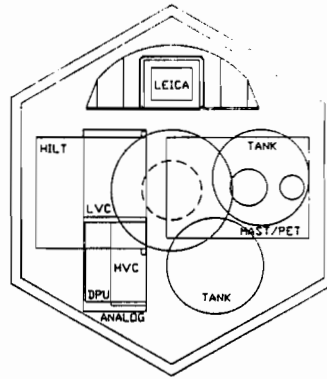
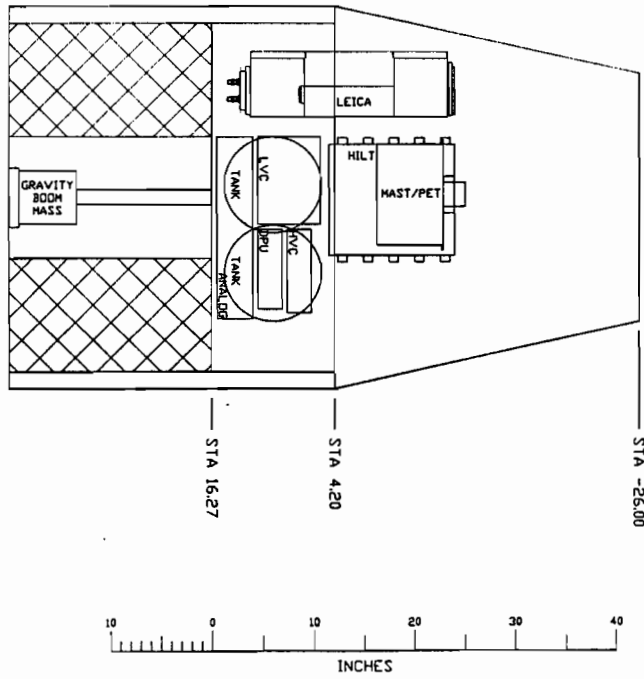
<b>Data Dump Mode</b>	
As above	47.5
minus experiments	-16.7
RF Amplifier	8.1
<b>TOTAL:</b>	<b>38.9 watts</b>

**Reference:**

J. R. Stuart, Capabilities of a Current Technology Low-Cost Lightweight Satellite Design, AIAA/DARPA LightSat Meeting Paper AIAA 87-3028.

**c) Experiment Layout in Available Volume**

Appendix A of the Small-Class Explorer AO shows the space available for the science payload (Figure 6 of the AO Appendix). The SAMPEX instruments can be easily accommodated within the available volume as shown in Figures E-1 and E-2. The figures show the size and typical locations for LEICA, MAST/PET, and HILT, along with the supporting electronics and isobutane tanks. Ample spacing has been left between the components to allow for support structure. In the figure, the gravity boom mass shown in the central part of the S/C bus is of the size used on Oscar/Transit satellites — this space is available to SAMPEX since the optional propulsion system is not needed. The gravity boom would extend towards the nadir, while the centers of the instrument FOVs all point towards the zenith. Stabilization could also be done with a single axis gyro and the choice between this or gravity gradient would be determined later.



SMALL EXPLORER LAYOUT  
REF: FIG 6 of App A/NASA Announcement of Opportunity  
UNIVERSITY OF MARYLAND  
SPACE PHYSICS GROUP/SPST  
COLLEGE PARK, MARYLAND 20742  
Scale: approx 1/8 16 SEP 1988

**Fig. E-1** Side and front views showing SAMPEX subsystem typical layout in the space available space. Spacecraft, station values, etc., are taken from Figure 6 in Appendix A of the Small-Class Explorer A.O.

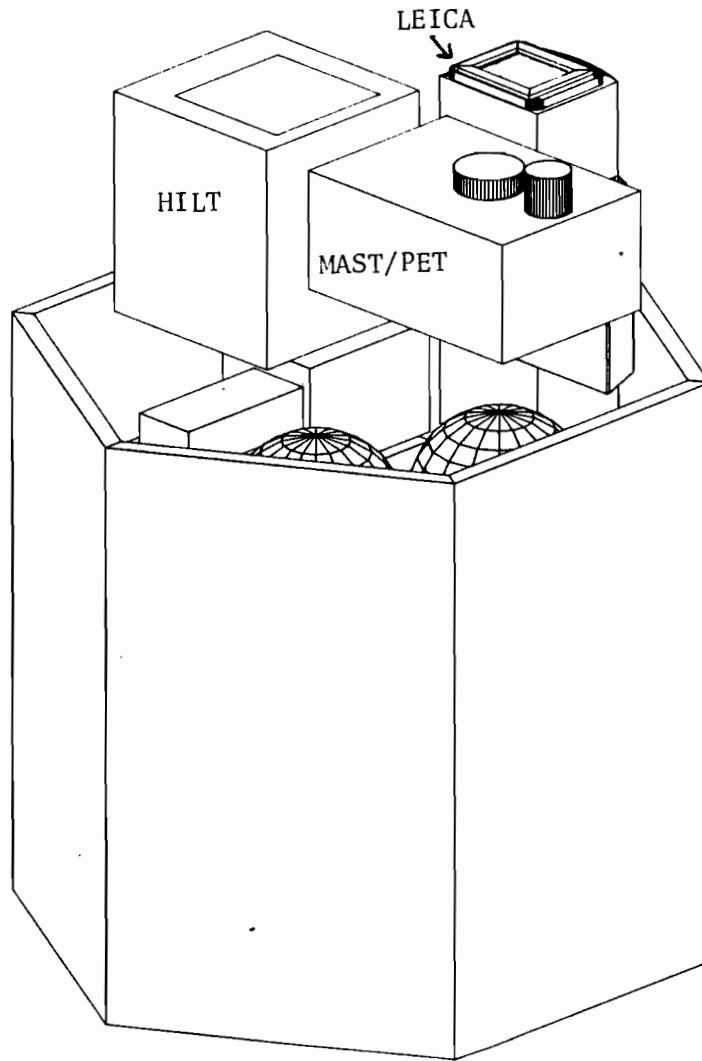


**Fig. E-2** Perspective view of SAMPEX subsystems, from figure E-1. Solar cells are assumed to be body mounted to reduce drag and thereby extend the orbital lifetime (see Appendix F.a).

**Appendix F**

**Spacecraft Orbital Lifetime, Inclination and Radiation Dose Analysis**

**a) Orbital Lifetime**

A study was carried out to determine the minimum orbital altitude necessary for the SAMPEX in order to have a three-year minimum lifetime. The calculations were performed for solar maximum and for two spacecraft configurations-with and without extended solar panels. Without extended panels the required initial altitude is 583 km. The study follows.

**Reference:**

Bayliss, S. S., "A program to determine lifetime in a circular orbit", The Aerospace Corporation, ATM 75(5901-03)-23, January 17, 1975.

## I. Introduction

The purpose of this study was to determine the minimum circular orbit altitudes required to obtain orbital lifetimes on the order of three to four years for an experiment satellite. Two configurations were considered, the satellite with and without extended solar panels. In addition, the lifetimes were examined for the worst case, solar maximum condition.

## II. Analysis and Results

This study utilizes the cross-sectional area of the satellite, the mass of the satellite, an orbit propagator and the ARDC 1959 atmospheric model (ref. 1) to perform lifetime studies. The satellite is assumed to have a coefficient of drag of 2.5 and the 1959 model which provides atmospheric drag during maximum solar activity is used in propagating the orbit. The ARDC 1959 model was developed partially based on data obtained in the vicinity of a solar maximum period and although it is a static model, the results obtained using it compare well with the results obtained using the Jacchia 64 model for launches on October 1990 and April 1992. In order to determine the altitudes necessary to obtain the desired lifetimes, an analysis is performed varying altitude between 400 and 1000 km for the satellite with and without extended solar panels.

The satellite is composed of a cone, a cylinder and a set of extended or conformal (non-extended) solar panels. The configuration consists of the truncated cone mounted on top of the cylinder with the base of the cone and the top of the cylinder interfacing and the solar panels attached to booms extending out of the sides of the cylinder. The cylinder is 36 inches in diameter and 36 inches in height. The truncated cone is 36 inches in diameter at the base, 24 inches in diameter at the truncated end and 30 inches in height. The extended panels have a cross-sectional area of 32.28 square feet. The satellite's cross-section is 15.25 square feet without extended panels and 47.4 square feet with extended panels. The mass of the satellite is 12.3 slugs.

The effects of varying the initial altitude for the satellite with and without extended solar panels on the orbit lifetime are shown in Figure 1. Selected points along each curve are given in Table 1. In addition, Figure 2 is provided showing greater resolution along

the lifetime axis. Table 2 shows the indicated altitudes required to achieve orbit lifetimes of 3 and 4 years.

#### **IV Conclusions**

The purpose of this study was to determine the altitudes required to obtain given orbit lifetimes for the satellite described above. The included figures and tables provide this information for the satellite with and without extended solar panels during solar maximum conditions. The required altitude for a 3 year lifetime was found to be 669 km with extended solar panels and 583 km without extended solar panels.



**TABLE 1. Satellite Orbital Lifetimes for Various Initial  
Circular Orbit Altitudes (ARDC 1959,  $C_D = 2.5$ )**

Altitude (km)	Lifetime (days)	
	Extended Panels	No Extended Panels
400	26	74
500	125	352
600	480	1347
700	1553	4356
800	4403	12350
900	11214	31453
1000	26134	73301

**TABLE 2. Minimum Initial Circular Orbit Altitudes  
to Achieve Three and Four Year Orbit Lifetimes**

Lifetime (years)	Altitude (km)	
	Extended Panels	No Extended Panels
3	669.0	583.4
4	694.6	606.5

FIGURE 1

# Satellite Orbital Lifetime Versus Initial Circular Orbit Altitude

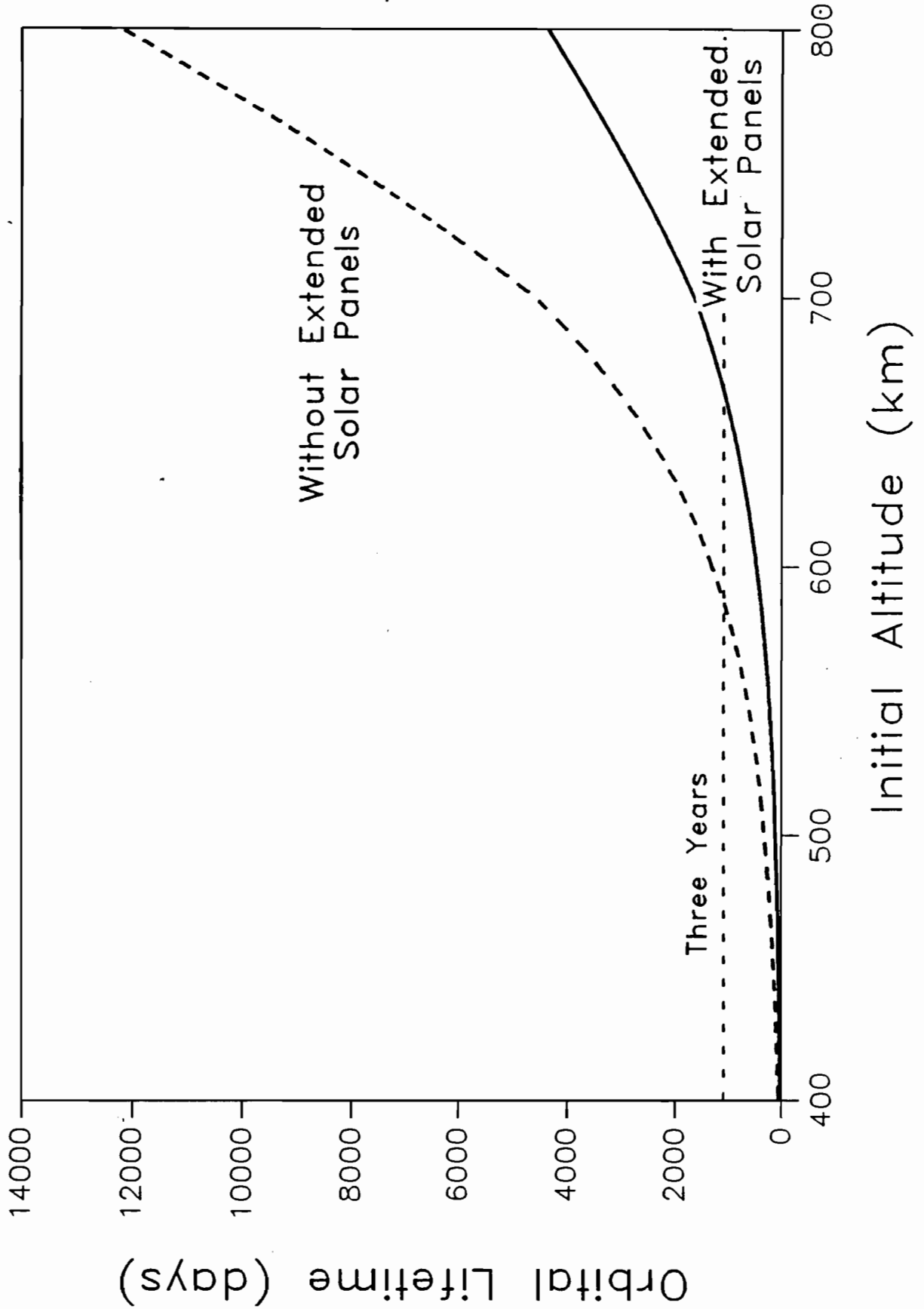
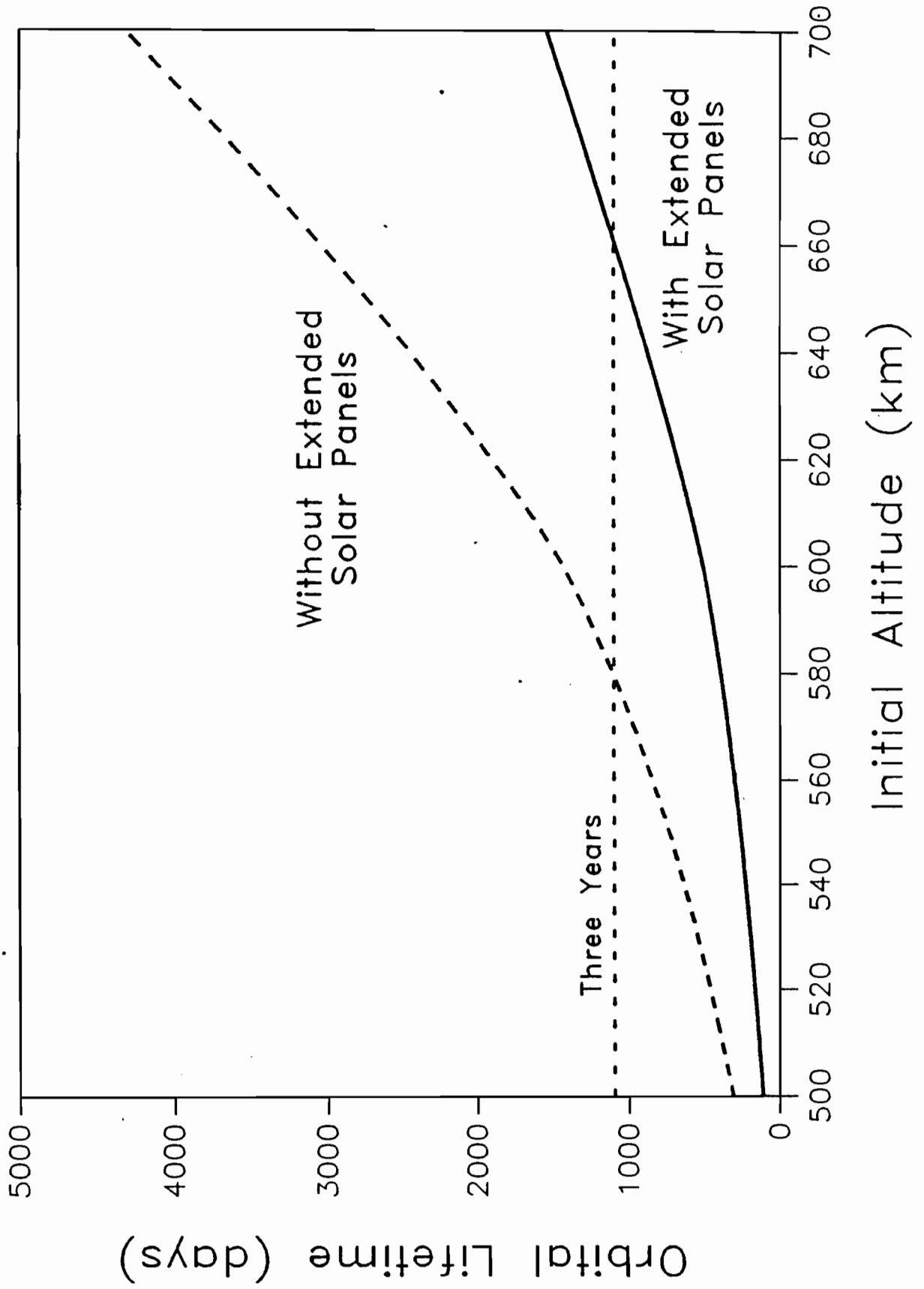


FIGURE 2

# Satellite Orbital Lifetime Versus Initial Circular Orbit Altitude



**TABLE 1. Solar Maximum Period Orbit Lifetimes for  $W/C_D A = 12.0$   
Satellite Using Jacchia 1964 Atmospheric Density Model**

PERIGEE (km)	APOGEE (km)	LAUNCH (Mo/Day/Yr)	LIFETIME (days)
250	800	4/19/1990	106
250	2000	12/23/1989	486
300	2000	12/10/1988	1214

### b) Orbital Inclination Analysis

Figure F-1 shows the payload inclination relationship for a Vandenberg launch for three circular orbits, relative to a 90° inclination. (Note that the payload declines below 76° inclination because of the necessity of a "dog-leg" launch.) This figure shows a payload increase of 7.9 kg for a 300 km orbit and 5.9 kg for a 700 km orbit. An interpolation suggests a gain of 7 kg by reducing the inclination from 90° to 82° for a nominal mission orbit of 500 km. The tradeoff between payload weight and time spent above the cutoff as a function of orbital inclination will be assessed during the study phase of this project.

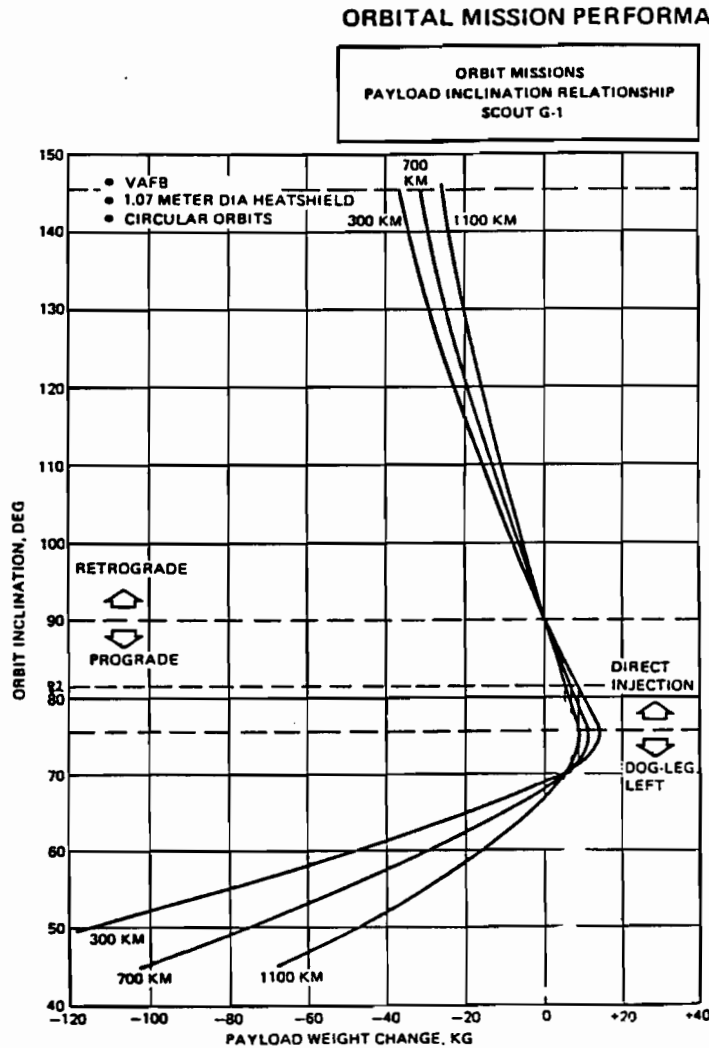


Fig. F-1 Payload inclination relationship - Vandenberg AFB

### c) Radiation Dose

The low orbit required by the SAMPEX mission results in a very low radiation exposure. Figure F-2 is a plot of the dose in rads (Si)/yr vs Al shield thickness for 400, 500, 600 km circular orbits. The calculations used the NASA AE-8 and AP-8 environments and the Shieldose radiation transport code. It can be seen that the dose is low for components behind the incidental spacecraft and box shielding; the total dose for a 3-yr mission would be under 1500 rads.

Very large solar proton events can give a significant dose - the so-called anomalously large events. There were two such events in Solar Cycle 19 (July 1959 and November 1960) and one in Solar Cycle 20 (August 1972). None occurred in Solar Cycle 21. The solar proton radiation environment is usually treated in a stochastic fashion, cf. King (1973). The estimated probability of the solar proton fluence above 25 MeV exceeding  $10^{10}/\text{cm}^2$  over the mission life in a low proton orbit is at most a few percent. (An energy of 25 MeV has been chosen as a threshold energy where penetration into the electronics can occur.)

$$10^{10} \text{ p/cm}^2 \times 2.5 \times 10^{-7} \text{ rads (Si)/p} = 2500 \text{ rads.}$$

Thus the total dose could be dominated by solar particles albeit at low probability. Suffice to say we can use parts with hardnesses in the 5 to 10 K rad range and avoid the cost and delivery impact of the "usual" rad-hard parts.

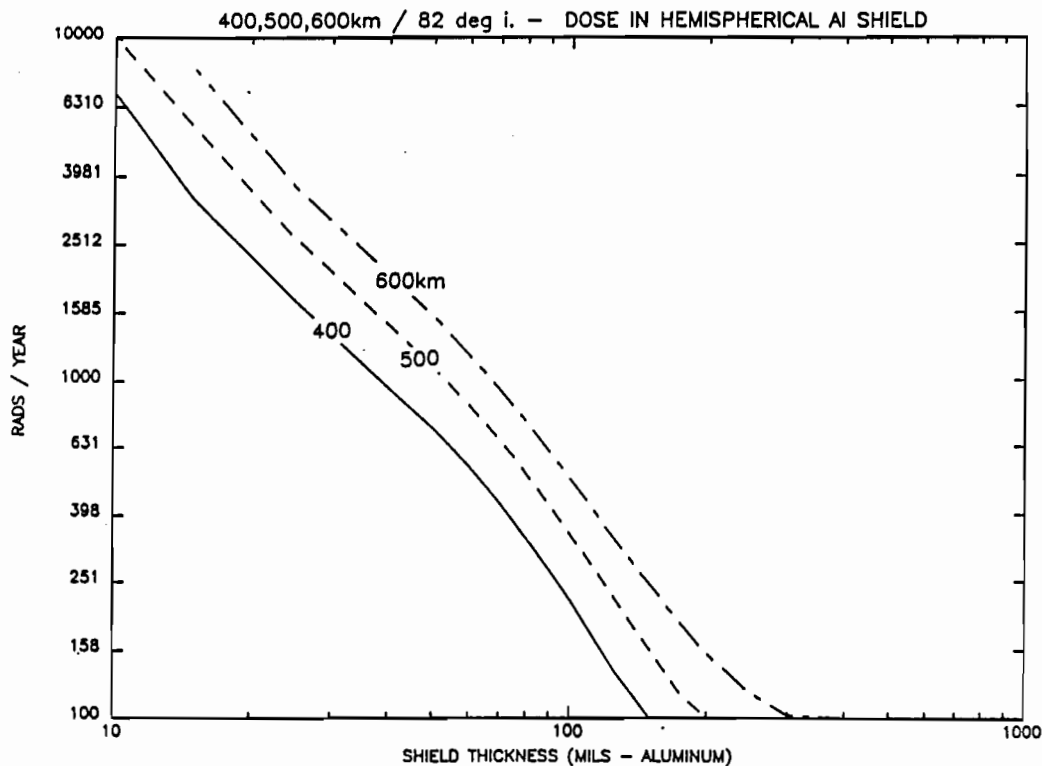


Fig. F-2 Radiation doses for SAMPEX mission

**Appendix G**  
**Biographical Information**



Brief Biographical Sketch

**Daniel N. Baker**

EDUCATION: University of Iowa, B.A., 1969; M.S., 1973; Ph.D. 1974

PROFESSIONAL EXPERIENCE:

1974-1975 Research Associate, Dept. of Physics and Astronomy (U. of Iowa)  
1975-1977 Research Fellow, Div. of Physics, Mathematics, and Astronomy  
(California Institute of Technology)  
1977-1981 Staff Member, Los Alamos Scientific Laboratory  
1981-1987 Group Leader, Space Plasma Physics  
Earth and Space Science Division, Los Alamos National Laboratory  
1987-Present Laboratory Chief, Laboratory for Extraterrestrial Physics  
Space and Earth Sciences Directorate, Goddard Space Flight Center

D. N. Baker has done research in spacecraft instrumental design and calibration, space physics data analysis, and magnetospheric modeling. He has studied plasma physical and energetic particle phenomena in the magnetospheres of Jupiter and Mercury, and he has studied extensively the plasma sheet and magnetopause boundary regions of the earth's magnetosphere. His recent experience has been in the analysis of large data sets from spacecraft at geostationary orbit, in the analysis of data in the region of Jupiter, the deep magnetotail, and comets, in the study of solar wind-magnetospheric energy coupling, and theoretical modeling of the possible role of heavy ions in the development of magnetotail instabilities. His present interests include extensive work on the problem of magnetosphere-atmosphere coupling. He is the author or co-author of approximately 170 scientific papers in refereed journals in the area of space research. He has served on numerous NASA and NSF committees, and many other positions such as Magnetospheric Section Secretary for the AGU, and Associate Editor of *Geophysical Research Letters*.

Selected publications:

- Near-equatorial high-resolution measurements of electron precipitation at  $L \simeq 6.6$ , D. N. Baker, P. Stauning, E. W. Hones, Jr., P. R. Higbie, and R. D. Belian, *J. Geophys. Res.*, **86**, 2295, 1981.
- Multiple spacecraft and correlated riometer study of magnetospheric substorm phenomena, D. N. Baker, E. W. Hones, Jr., R. D. Belian, P. R. Higbie, R. P. Lepping, and P. Stauning, *J. Geophys. Res.*, **87**, 6121, 1982.
- Substorms in the magnetosphere, D. N. Baker, S. I. Akasofu, W. Baumjohann, J. W. Bieber, D. H. Fairfield, E. W. Hones, Jr., B. H. Mauk, R. L. McPherron, and T. E. Moore, Chapter 8 of *Solar Terrestrial Physics - Present and Future*, NASA Pub. 1120, Washington, D. C., 1984.
- Highly relativistic magnetospheric electrons: A role in coupling to the middle atmosphere?, D. N. Baker, J. B. Blake, D. J. Gorney, P. R. Higbie, R. W. Klebesadel, and J. H. King, *Geophys. Res. Lett.*, **14**, 1027, 1987.

## Brief Biographical Sketch

### J. Bernard Blake

J. B. Blake received a B.S. Degree in Engineering Physics in 1957, a M.S. Degree in Physics in 1958, and a Ph.D. in Physics in 1962 from the University of Illinois. He was a Research Associate at the University of Illinois from January 1962 to September 1962 when he joined the Space Sciences Laboratory of The Aerospace Corporation as a Member of the Technical Staff. He is presently Head of the Space Particles and Fields Department. Scientific activity has included research in beta decay, the Mossbauer effects, magnetospheric, auroral and cosmic-ray physics, and nuclear astrophysics. He has been an experimenter on several Air Force, NASA and European satellites over the last 25 years including OV3-3, ATS-1, OV1-19, ATS-6, SCATHA and VIKING.

#### Selected publications:

- D. N. Baker, J. B. Blake, D. J. Gorney, P. R. Higbie, R. W. Klebesadel and J. H. King, Highly Relativistic Magnetospheric Electrons: A Role in Coupling to the Middle Atmosphere? , *Geophys. Res. Lett.*, **14**, 1027, 1987.
- D. N. Baker, R. D. Belian, P. R. Higbie, R. W. Klebesadel and J. B. Blake, Deep Dielectric Charging Effects Due to High-Energy Electrons in Earth's Outer Magnetosphere, *J. Electrostatics*, **20** 3, 1987.
- D. S. P. Dearborn and J. B. Blake, Possible Contributions by Wolf-Rayet Stars to the Proto-Solar Nebula: Extinct Radioactivities, or Grains of Truth From Wolf-Rayet Stars? , *Astrophys. J.*, **302**, 305, 1988.
- J. B. Blake and J. E. Cox, The Radiation Dose in a Molniya-Type Orbit, *Proceedings of the 1987 CHERBS Conf.*, in press, 1988.
- J. B. Blake and D. S. P. Dearborn, a Local Source of  $^{26}\text{Al}$  Gamma Rays, *Astrophys. J. (Letters)*, in press, 1988.
- J. B. Blake and R. Mandel, On-Orbit Observations of Single-Event Upset in Harris HM-6508 RAMs: An Update, *Proceedings of the 1987 CHERBS Conf.*, American Institute of Physics, in press, 1988.
- J. B. Blake, R. D. Belian, D. R. Croley, J. F. Fennell, G. Gloeckler, D. C. Hamilton and D. N. Baker, The 8 February Magnetospheric Compression Event: Observations of Simultaneous Magnetospheric Leakage and Specularly Reflected Solar Wind Ions, *Space Research*, in press, 1988.
- F. Soraas, K. Bronstad, M. Havag, J. E. Espelid, R. Studanes, W. Studemann, B. Wilken, g. Kremser, A. Korth, D. Hall, D. Bryant, J. F. Fennell, J. B. Blake, R. Koga, T. A. Fritz and R. Lundin, Energy and Pitch Angle Distribution of Ring Current Ions as Observed by the MICS Instrument on the VIKING Satellite, *Space Research*, in press, 1988.

## Brief Biographical Sketch

### Linwood (Lin) B. Callis

#### Education:

M. S. Aerospace Engineering, Cornell University, 1962.

B. S. Aerospace Engineering, Virginia Polytechnic Institute and State University, 1959.

Linwood Callis is a senior research scientist in the Theoretical Studies Branch, Atmospheric Sciences Division, at the NASA-Langley Research Center. He has extensive experience in theoretical model development (one- and two-dimensional photochemical models of the atmosphere, radiative transfer codes, atmospheric radiative-convective codes, and constant pressure trajectory and meridional diabatically diagnosed trajectory models), satellite data analysis, and the use of theoretical capabilities in conjunction with satellite data for both the stratosphere and the lower mesosphere. Past studies have been directed toward a wide range of atmospheric, environmental, and climate studies. Among these are the study of: (1) the importance of atmospheric scattering to atmospheric photochemistry; (2) the role of thermal coupling in the study of stratospheric phenomena; (3) the effect of atmospheric chemistry on the Earth-atmosphere thermal balance; (4) the effect of solar variability on the state of the middle atmosphere; (5) the consistency of photochemical calculations and stratospheric observations; (6) the odd nitrogen levels of the middle atmosphere; and (7) phenomena related to Antarctic ozone depletion. Mr. Callis serves as a member of the Working Group on Solar-Terrestrial Relationships under the auspices of the International Commission on the Meteorology of the Upper Atmosphere (ICMUA). He also serves on the Committee on the Middle Atmosphere, a committee of the American Meteorological Society. He is a member of the American Geophysical Union.

#### Selected publications:

Callis, L. B., R. E. Boughner, and J. D. Lambeth, The Stratosphere: Climatologies of the Radiative Heating and Cooling Rates and the Diabatically Diagnosed Net Circulation Fields, *J. Geophys. Res.*, **92**, 5585-5607, 1987.

Callis, L. B. and M. Natarajan, Ozone and Nitrogen Dioxide Changes in the Stratosphere During 1979-84, *Nature*, **323**, 772-777, 1986.

Callis, L. B. and M. Natarajan, The Antarctic Ozone Minimum: Relationship to Odd Nitrogen, Odd Chlorine, the Final Warming, and the 11-Year Solar Cycle, *J. Geophys. Res.*, **91**, 10,771-10,796, 1986.

Callis, L. B., M. Natarajan, R. E. Boughner, J. M. Russell III, and J. D. Lambeth, Stratospheric Photochemical Studies Using Nimbus 7 Data 2. Development of Inferred Trace Species Distributions, *J. Geophys. Res.*, **91**, 1167-1197, 1986.

Callis, L. B., M. Natarajan, and R. E. Boughner, On the Relationship Between the Greenhouse Effect, Atmospheric Photochemistry, and Species Distribution, *J. Geophys. Res.*, **88**, 1401-1426, 1983.

Brief Biographical Sketch

**Douglas C. Hamilton**

Douglas C. Hamilton received his A.B. in Physics and Mathematics from the University of Kansas in 1969 and his Ph.D. in Physics from the University of Chicago in 1977. He served as Research Associate at the Laboratory for Astrophysics and Space Research at the University of Chicago from 1976-78. At Chicago he studied the interplanetary propagation of solar energetic particles and Jovian electrons using data from the Pioneer 10 and Pioneer 11 spacecraft. Dr. Hamilton came to the University of Maryland in 1978, and he is now Assistant Professor jointly in the Department of Physics and Astronomy and the Institute for Physical Science and Technology. His research interests include the propagation and composition of solar energetic particles and the compositions and dynamics of energetic ions in the magnetospheres of Earth and the outer planets. He is involved in the development of improved charged particle instruments for both interplanetary and magnetospheric applications. He is co-investigator on experiments flown on the Voyager 1, Voyager 2, and AMPTE spacecraft.

Selected publications:

Ring current development during the great geomagnetic storm of February 1986, D. C. Hamilton, G. Gloeckler, F. M. Ipavich, W. Stuedemann, B. Wilken, G. Kremser, *J. Geophys. Res.*, in press, 1988.

A multi-spacecraft study of the injection and transport of solar energetic particles, J. Beeck, G. M. Mason, D. C. Hamilton, G. Wibberenz, H. Kunow, D. Hovestadt, and B. Klecker, *Astrophys. J.*, **322**, 1052, 1987.

Energetic atomic and molecular ions in Saturn's magnetosphere, D. C. Hamilton, G. Gloeckler, S. M. Krimigis, and L. J. Lanzerotti, *J. Geophys. Res.*, **88**, 8905, 1983.

Composition of nonthermal ions in the Jovian magnetosphere, D. C. Hamilton, G. Gloeckler, S. M. Krimigis, and L. J. Lanzerotti, *J. Geophys. Res.*, **86**, 8301, 1981.

The radial transport of energetic solar flare particles from 1 to 6 AU, D. C. Hamilton, *J. Geophys. Res.*, **82**, 2157, 1977.

## Brief Biographical Sketch

### Dietrich Hovestadt

Head of Energetic Particle Group, Max-Planck-Institut für Physik und Astrophysik.

EDUCATION: Diploma in Physics (Nuclear Physics), University of Hamburg, 1960, Ph.D. (Nuclear Physics), Technical University Munich, 1964.

RELEVANT EXPERIENCE: research on physics of energetic particles near earth and in interplanetary space; origin and composition of magnetospheric, interplanetary and solar particles, solar wind; development of instruments for elemental and ionic charge state composition for solar wind and solar energetic particles.

PRINCIPAL INVESTIGATOR: (1) radiation belt composition experiment on GRS-1/AZUR; (2) solar energetic particle experiment on ESRO 4; (3) energetic particle experiment on ISEE-1 and ISEE-3; (4) low energy particle composition experiment SULEICA on AMPTE-IRM; (5).charge composition experiment on Shuttle GETAWAYSPECIAL.

CO-INVESTIGATOR: (1) Ions and Electron experiment on IMP-7 and IMP-8; (2) EPAC experiment on ULYSSES.

#### Selected publications:

Hovestadt et al. 1973, Anomalous energy spectrum of Oxygen between 2.4 and 20 MeV/N, *Phys. Rev. Letters*, **31**, 650.

Hovestadt et al. 1978, Evidence for solar wind origin of heavy ions in the radiation belt, *Geophys. Res. Lett.*, **1**, 55.

Hovestadt et al. 1984, Ionic charge state measurements during He<sup>+</sup> rich solar particle events, *Astrophys. J.*, **281**, 463.

Klecker et al., 1984, Direct determination of the ionic charge distribution of helium and iron in <sup>3</sup>He-rich solar energetic particle events, *Astrophys. J.*, **281**, 458.

Hovestadt et al., 1986, Pick-up ions in the solar wind as a source of suprathermal particles, in *The Sun and the Heliosphere in Three Dimensions*, ed. R. Marsden, Reidel Publ. Co., page 413.

Brief Biographical Sketch

**Berndt Klecker**

Berndt Klecker received his Diploma in Physics from the Technical University Munich (TUM) in 1973 and his Ph.D. in Physics from the TUM in 1978. Since 1976 he is Staff Member of the Max-Planck-Institute fuer extraterrestrische Physik, Garching. His research work involved experimental and theoretical cosmic ray and magnetospheric physics. He was collaborator on the energetic particle experiments E1-88 on GRS-A AZUR, the energetic particle experiment S-103 on ESRO-IV, and the experiment MAE/ULET on IMP-7 and -8. He has been co-investigator on the Low Energy Particle Composition experiments on ISEE-1 and -3 (ICE), on the time-of-flight spectrometer SULEICA on AMPTE / IRM and on the experiment ALPHA-X for the surface analysis of the marsian moon PHOBOS. He is currently working on instrumentation for a space shuttle flight that is designed to extend cosmic ray composition and charge state measurements to higher energies than has been possible to date.

Selected publications:

- Klecker, B., *et al.*, Discovery of energetic molecular ions ( $\text{NO}^+$  and  $\text{O}_2^+$ ) in the storm time ring current, *Geophys. Res. Lett.*, **13**, 632-635, 1986.
- Klecker, B. *et al.*, Direct determination of the ionic charge distribution of helium and iron in  $^3\text{He}$ -rich solar energetic particle events, *Astrophys. J.*, **281**, 458-462, 1984.
- Klecker, B., *et al.*, Spectral and compositional variations of low energy ions during an energetic storm particle event, *Astrophys. J.*, **251**, 393-401, 1981.
- Klecker, B., Hovestadt, D., Gloeckler, G., Fan, C.Y., On the charge state of the anomalous oxygen component, *Geophys. Res. Lett.*, **7**, 1033-1036, 1980.

## Brief Biographical Sketch

### Glenn M. Mason

Glenn M. Mason received his A.B. in Physics from Harvard College in 1965, and his Ph.D. in Physics from the University of Chicago in 1971. He served as Research Associate and then Senior Research Associate from 1971-1977 at the Laboratory for Astrophysics and Space Research at the University of Chicago. During this period his research work involved the elemental and isotopic composition of galactic cosmic rays, and solar modulation of galactic cosmic rays. At Chicago he was co-investigator on the IMP 6, 7 and 8 satellite experiments, and worked on the development of high resolution cosmic ray telescopes which, for example, performed the first measurements of the cosmic ray age by measuring the abundance of the radioactive isotope  $^{10}\text{Be}$ . Dr. Mason came to the University of Maryland in 1977, and he is now Associate Professor jointly in the Department of Physics and Astronomy and the Institute for Physical Science and Technology. At Maryland he has worked on the development of novel instrumentation that allows determination of the mass composition of solar and interplanetary particles in previously unexplored energy ranges. He was co-investigator on the NASA Solar Polar missions, and is currently constructing a low energy particle telescope for space shuttle flight. His research work at Maryland has concentrated on the composition of solar energetic particles, and the acceleration and transport of particles both in the solar atmosphere and in the interplanetary medium.

#### Selected publications:

Impulsive acceleration and scatter-free transport of  $\sim 1$  MeV per nucleon ions in  $^3\text{He}$ -rich solar particle events, G. M. Mason, C. K. Ng, B. Klecker, and G. Green, *Astrophys. J.*, in press, 1989.

The Composition of galactic cosmic rays and solar energetic particles, G. M. Mason, *Rev. Geophys. Space. Phys.*, **25**, 685, 1987.

The heavy ion compositional signature in  $^3\text{He}$ -rich solar particle events, G. M. Mason, D. V. Reames, B. Klecker, D. Hovestadt, and T. T. von Rosenvinge, *Astrophys. J.*, **303**, 849, 1986.

Temporal variation for nucleonic abundances in solar flare energetic particle events. II. Evidence for large scale shock acceleration, G. M. Mason, G. Gloeckler, and D. Hovestadt, *Astrophys. J.*, **280**, 902, 1984.

A survey of  $\sim 1$  MeV nucleon $^{-1}$  solar flare particle abundances  $1 \leq Z \leq 26$  during the 1973-1977 solar minimum period, G. M. Mason, L. A. Fisk, G. Gloeckler, and D. Hovestadt, *Astrophys. J.*, **239**, 1070, 1980.

Brief Biographical Sketch

Richard A. Mewaldt

Richard Mewaldt received his B.A. in Physics from Lawrence University in 1965 and his M.A. (1967) and Ph.D. (1971) from Washington University in St. Louis. He came to Caltech as a Research Fellow in physics in 1971, where he was subsequently appointed Senior Research Fellow (1975) and Senior Research Associate (1981). His research interests have centered on the study of energetic electrons and nuclei accelerated in solar flares, in interplanetary space, and in galactic cosmic rays, and on the development and testing of high resolution spaceflight and balloon-borne instrumentation to measure these particles. He has been a co-investigator on experiments flown on the IMP-7, IMP-8, and ISEE-3 spacecraft, and on an experiment planned for the NASA Solar Polar Mission. This work has recently concentrated on measuring the isotopes of energetic nuclei observed in space, and has led to the first high resolution measurements of the isotopic composition of heavy solar flare nuclei; the discovery that galactic cosmic ray and solar system magnesium have a different isotopic composition; and to improved measurements of the isotopic composition of a variety of cosmic ray elements from H to Fe. He has also collaborated on several balloon-borne cosmic ray instruments, and is currently working on instrumentation designed to extend cosmic ray isotope measurements to higher energies than has been possible to date.

Selected publications:

Isotope Abundances of Solar Coronal Material Derived from Solar Energetic Particle Measurements, R.A. Mewaldt and E.C. Stone, to be published in *Astrophys. J.*, February 15, 1989.

A High Resolution Study of the Isotopes of Solar Flare Nuclei, R.A. Mewaldt, J.D. Spalding, and E.C. Stone, *Astrophys. J. (Letters)*, **280**, 892, 1984.

The Isotopic Composition of the Anomalous Low-Energy Cosmic Rays, R.A. Mewaldt, J.D. Spalding, and E.C. Stone, *Astrophys. J.*, **283**, 450, 1984.

The Elemental and Isotopic Composition of Galactic Cosmic Ray Nuclei, R.A. Mewaldt, *Rev. Geophys. Space. Phys.*, **21**, No. 2, 295, 1983.

High-Resolution Measurements of Galactic Cosmic Ray Nuclei, R.A. Mewaldt, J.D. Spalding, E.C. Stone, and R.E. Vogt, *Astrophys. J. (Letters)*, **235**, L95, 1980.



Brief Biographical Sketch

**Manfred Scholer**

M. Scholer: Scientific Staff Member, Max-Planck-Institut für extraterr. Physik, since 1970

Education: University Munich, Diploma (1965), Technical University Munich, PhD (1969)

Experience: Theoretical work in magnetospheric and ionospheric physics, on waves in the interplanetary medium, and on modulation and acceleration of cosmic rays in interplanetary space. Computer simulations of magnetospheric MHD problems. Data analysis and interpretation of energetic particle experiments, with emphasis on the behavior of energetic solar flare particles in interplanetary space and on the entry of these particles into the earth's magnetosphere.

Collaborator on AZUR GRS-1, ESRO IV, IMP-7 and -8. Co-Investigator on ISEE-1, ISEE-3, and AMPTE-IRM. Co-Investigator on the planned space missions SOHO and CLUSTER.

Selected publications:

- G. Morfill, M. Scholer, Uneven illumination of the polar caps by solar protons: Comparison of different particle entry models, *J. Geophys. Res.*, **78**, 5449, 1973
- G. Morfill, M. Scholer, Study of the magnetosphere using energetic solar particles, *Space Sci. Rev.*, **15**, 267, 1973.
- M. Scholer, Energetic solar particle access into the geomagnetic tail, in: Correlated Interplanetary and Magnetospheric Observations, D. Reidel, p. 419, 1974.
- M. Scholer, G. Morfill, On the topology of the geomagnetic field, in: Magnetospheric Physics, D. Reidel, p. 61, 1974.
- M. Scholer, Transport of energetic solar particles on closed magnetospheric field lines, *Space Sci. Rev.*, **17**, 3, 1975.
- M. Scholer, Energetic solar particle behaviour in the magnetosphere, in: Solar Terrestrial Prediction Proceedings, **2**, p. 446, 1979.

Brief Biographical Sketch

Edward C. Stone

After receiving his master's degree (1959) and Ph.D. (1964) from the University of Chicago, Professor Stone came to Caltech as a Research Fellow in Physics. He was subsequently appointed Senior Research Fellow (1967), Assistant Professor (1967), Associate Professor (1971), Professor (1976), and Chairman, Division of Physics, Mathematics and Astronomy (1983). He also held a Sloan Foundation Fellowship (1971-1973) and since 1972 has served as the Project Scientist for the Voyager Mission which is being conducted by Caltech's Jet Propulsion Laboratory. He is a member of the Board of Directors of the California Association for Research in Astronomy which will build and operate the Keck Observatory. Since his first cosmic ray experiments on Discoverer satellites in 1961, he has investigated the isotopic and elemental composition of galactic cosmic rays and solar flare particles, studied planetary magnetospheres and the interplanetary medium, and coordinated the Voyager investigations of the outer solar system. He has been a principal investigator on eight NASA spacecraft and a co-investigator on three others and has received the NASA medal for Exceptional Scientific Achievement, the NASA Distinguished Service Medal, the AIAA Dryden Medal, the AIAA Space Science Award, and the NASA Distinguished Public Service Medal. He is a member of the National Academy of Sciences, a fellow of the American Physical Society and the American Geophysical Union, an associate fellow of the American Institute of Aeronautics and Astronautics, and a member of the American Astronomical Society, the International Academy of Astronautics, and the International Astronomical Union.

Selected publications:

Evidence for Anomalous Cosmic Ray Hydrogen, E.R. Christian, A.C. Cummings and E.C. Stone, to be published in *Astrophys. J. (Letters)*, 1988.

Solar Coronal and Photospheric Abundances from Solar Energetic Particle Measurement, H.H. Breneman and E.C. Stone, *Astrophys. J. (Letters)*, **299**, L57, 1985.

Evidence that the Anomalous Cosmic-Ray Component is Singly Ionized, A.C. Cummings, E.C. Stone, and W.R. Webber, *Astrophys. J. (Letters)*, **287**, L99, 1984.

Cosmic-Ray Abundances of Elements with Atomic Number  $26 \leq Z \leq 40$  Measured on HEAO-3, W.R. Binns, R.K. Fickle, T.L. Garrard, M.H. Israel, J. Klarmann, E.C. Stone, and C.J. Waddington, *Astrophys. J. (Letters)*, **247**, L115, 1981.

The Isotopic Composition of Galactic Cosmic-Ray Iron Nuclei, R.A. Mewaldt, J.D. Spalding, E.C. Stone, and R.E. Vogt, *Astrophys. J. (Letters)*, **236**, L121, 1980.

Brief Biographical Sketch

Tycho T. von Rosenvinge

DATE OF BIRTH: April 18, 1942

PRESENT POSITION: Head, Low Energy Cosmic Ray Group  
High Energy Astrophysics Division  
NASA/Goddard Space Flight Center

EDUCATION: B.A.-1963-Amherst College, Amherst, MA  
Ph.D.-1970-University of Minnesota

NASA PROJECTS: OGO 5; IMPS 6,7,8; ISEE-3; ISPM; ISTP;  
Rapidly Moving Telescope.  
Project Scientist: ISEE-3 (1972-1983)  
Project Scientist: International Cometary Explorer (1984- )

RESEARCH: Concentrated on understanding the acceleration, composition, and transport of energetic interplanetary particles, including solar flare particles, shock accelerated particles, the anomalous component, and galactic cosmic rays. Project Scientist for the first spacecraft ever to encounter a comet.

SELECTED PAPERS: "Satellite Measurements of the Charge Composition of Solar Cosmic Rays in the  $6 \leq Z \leq 26$  Interval", B.J. Teegarden, T.T. von Rosenvinge, and F.B. McDonald, *Ap. J.*, 180, 571, 1973.

"The Interplanetary Acceleration of Energetic Nucleons", F.B. McDonald, B.J. Teegarden, J.H. Trainor, T.T. von Rosenvinge and W.R. Webber, *Ap. J.*, 203, 149, 1976.

"Interplanetary Particle Observations Associated with Solar Flare Gamma-Ray Line Emission", T.T. von Rosenvinge, R. Ramaty, and D.V. Reames, *Proc. 17th Int. Cosmic Ray Conf.*, 3, 28, 1981.

"Solar  $^3\text{He}$ -rich events and Non-Relativistic Electron Events: A New Association", D.V. Reames, T.T. von Rosenvinge, and R.P. Lin, *Ap. J.*, 292, 716, 1985.

"The Composition of Solar Energetic Particles", R.E. McGuire, T.T. von Rosenvinge, and F.B. McDonald, *Ap. J.*, 301, 938, 1986.

"The International Cometary Explorer Mission to Comet Giacobini-Zinner", T.T. von Rosenvinge, J.C. Brandt, and R.W. Farquhar, *Science*, 232, 353, 1986.